PACIFIC EARTHQUAKE ENGINEERING
RESEARCH CENTER

NGA-West2 Campbell-Bozorgnia Ground Motion Model for the Horizontal Components of PGA, PGV, and 5%-Damped Elastic Pseudo-Acceleration Response Spectra for Periods Ranging from 0.01 to 10 sec

Kenneth W. Campbell
EQECAT, Inc.
Beaverton, Oregon

Yousef Bozorgnia
Pacific Earthquake Engineering Research Center
University of California, Berkeley

PEER 2013/06
MAY 2013

NGA-West2 Campbell-Bozorgnia Ground Motion Model for the Horizontal Components of PGA, PGV, and 5%-Damped Elastic Pseudo-Acceleration Response Spectra for Periods Ranging from 0.01 to 10 sec

Kenneth W. Campbell
EQECAT, Inc.
Beaverton, Oregon

Yousef Bozorgnia
Pacific Earthquake Engineering Research Center
University of California, Berkeley

PEER Report 2013/06
Pacific Earthquake Engineering Research Center
Headquarters at the University of California, Berkeley

May 2013

ABSTRACT

This report summarizes the development of the NGA-West2 Campbell-Bozorgnia empirical ground motion prediction equation (GMPE). This GMPE updates and supersedes the GMPE developed by Campbell and Bozorgnia (2008) as part of the NGA-West1 Project (Power et al. 2008). We used the extensive and expanded PEER NGA-West2 ground motion database recorded from shallow crustal earthquakes in active tectonic domains to develop a GMPE for the "average" (RotD50) horizontal components of peak ground acceleration (PGA), peak ground velocity (PGV), and 5%-damped elastic pseudo-absolute acceleration response spectral ordinates (PSA) at 21 periods ranging from 0.01 to 10 sec. As in our NGA-West1 GMPE, we included terms and predictor variables that modeled magnitude scaling, geometric attenuation, style of faulting, hanging-wall effects, shallow linear and nonlinear site response, and basin response. In our NGA-West2 model we added several new terms and predictor variables, including a new hanging-wall model and related parameters; hypocentral depth; rupture dip, regionally dependent linear shallow site and basin response; regionally dependent anelastic attenuation; and magnitude-dependent between-event and within-event standard deviations. Our new GMPE is considered valid for estimating ground motions from shallow continental earthquakes occurring worldwide in active tectonic domains for magnitudes ranging from 3.3 to as large as 8.5, depending on the style of faulting, and distances as far as 300 km from the source.

ACKNOWLEDGMENTS

This study was sponsored by the Pacific Earthquake Engineering Research Center (PEER) and funded by the California Earthquake Authority, California Department of Transportation, and the Pacific Gas & Electric Company. Any opinions, findings, and conclusions or recommendations expressed in this material are those of the authors and do not necessarily reflect those of the sponsoring agencies. We greatly benefitted from continuous and constructive interactions among the NGA researchers, including (in alphabetical order by last name): Norm Abrahamson, Linda Al Atik, Tim Ancheta, Gail Atkinson, Jack Baker, Annemarie Baltay, Dave Boore, Brian Chiou, Bob Darragh, Steve Day, Jennifer Donahue, Rob Graves, Nick Gregor, Tom Hanks, I.M. Idriss, Ronnie Kamai, Tadahiro Kishida, Albert Kottke, Sanaz Rezaeian, Badie Rowshandel, Emel Seyhan, Shrey Shahi, Tom Shantz, Walt Silva, Paul Spudich, Jon Stewart, Jennie Watson-Lamprey, Katie Wooddell, and Bob Youngs. A key strength of the NGA projects has been such a productive interaction. Partial support of the first author was provided by EQECAT, Inc., Oakland, California. Claire Johnson's dedidcation in editing the report is gratefully appreciated.

ERRATA
PEER Report No. 2013-06

NGA-West2 Campbell-Bozorgnia Ground Motion Model for the Horizontal Components of PGA, PGV, and 5%-Damped Elastic Pseudo-Acceleration Response Spectra for Periods Ranging from 0.01 to 10 sec

July 15, 2013

PAGE 2, PARAGRAH 3, LINES 6 & 7:

The phrase "… *strike-normal (SN), strike-parallel (SP), and …*" should be deleted.

PAGE 4, PARAGRAH 2, LINE 14:

The equation "*(* $R_{RUP} \leq 80$ *km)*" should be deleted.

PAGE 12, SECTION 3.3.10, BULLET 4, LINE 2:

The phrase "… *, where* R_X *is negative in the footwall direction and positive in the hanging-wall direction*" should be added before the reference "*(Ancheta et al. 2013)*".

PAGE 15, SECTION 3.4.2, PARAGRAPH 2, LINE 8:

The word "*NGA-West*" should be replaced with "*NGA-West2*".

PAGE 15, SECTION 3.4.2, PARAGRAPH 2:

This paragraph should be deleted. The arbitrary horizontal component was not revised as part of the study.

PAGE 22, TABLE 3.4:

The columns labeled ϕ_c and σ_{ARB} should be deleted. The arbitrary horizontal component was not revised as part of the study. The values in the column labeled $\rho_{\ln PGA,\ln Y}$ should be replaced with the following values (from top to bottom): 1.000, 0.998, 0.986, 0.938, 0.887, 0.870, 0.876, 0.870, 0.850, 0.819, 0.743, 0.684, 0.562, 0.467, 0.364, 0.298, 0.234, 0.202, 0.184, 0.176, 0.154, 1.000, and 0.684, which are valid for $\mathbf{M} \geq 5$ events. The magnitude-dependence of this correlation coefficient will be addressed in a separate study.

PAGE 57, PARAGRAPH 2, LAST LINE:

Replace the phrase "… *use in PSHA…*" with "… *estimating spectral displacement and PGD…*".

PAGE 62, PARAGRAH 3, LINE 1:

The term "Z_{HYP}" should be deleted. The same term at the beginning of Line 2 should be retained.

PAGE 62, EQUATION (6.7):

Equation (6.7) should be corrected as follows: $W = \min\left(\sqrt{10^{(\mathbf{M}-4.07)/0.98}}, (Z_{BOT} - Z_{TOR})/\sin(\delta)\right)$.

CONTENTS

LIST OF FIGURES

LIST OF TABLES

1 Introduction

1.1 SCOPE OF THE PEER NGA-WEST2 PROJECT

The PEER Next Generation of Ground Motion Attenuation Phase 2 Project (the "PEER NGA-West2 Project") is a multidisciplinary research initiative coordinated by the Pacific Earthquake Engineering Research Center (PEER) to extend the original NGA Project, now the NGA-West1 Project, to develop next generation ground motion models for shallow crustal earthquakes in active tectonic regions. According to Bozorgnia et al. (2012), an objective of the PEER NGA-West2 Project is to update the NGA-West1 horizontal empirical ground motion prediction equations (GMPEs) (a.k.a., ground motion models or attenuation relationships) through a comprehensive and highly interactive research program.

The NGA-West2 model development was composed of the following technical topics: (1) updating the NGA-West1 models for moderate-to-large magnitude data recorded through 2011: (2) extending the NGA-West1 models to magnitudes as small as **M**3.0: (3) developing GMPEs for the vertical component: (4) developing a model for scaling 5%-damped response-spectral amplitudes for damping values between 0.5% and 30%: (5) exploring the effects of source directivity: (6) developing models for adjusting the "average" horizontal component for component polarization (directionality): (7) developing models for incorporating epistemic uncertainty: and (8) updating the linear and nonlinear site-response models. As part of the supporting research projects conducted as part of the NGA-West2 Project, there was also an effort to derive a hanging-wall model from ground motion simulations to aid the NGA-West2 ground motion model developers in evaluating the hanging-wall terms in their NGA-West1 models. An overview of the PEER NGA-West2 Project components, process, and products is presented in Bozorgnia et al. (2012).

1.2 SCOPE OF NGA-WEST2 GROUND MOTION MODEL DEVELOPMENT

Under the auspices of the PEER NGA-West2 Project, updated empirical GMPEs were developed for shallow crustal earthquakes for applicability in active tectonic regions around the world, such as the western United States, through a comprehensive and highly interactive research program that involved the following components: (1) development of separate sets of ground motion models by five teams (the "developers"); (2) development of an updated and expanded PEER ground motion database to provide the recorded ground motion data and the supporting metadata on the causative earthquakes, source-to-site travel paths, and local site conditions needed by the GMPE developers for their empirical regression analyses and model-development activities; (3)

a number of supporting research projects including numerical simulations of rock motions and soil site response to provide an improved scientific basis for evaluating functional forms and determining constraints on the GMPEs; and (4) a series of workshops, working group meetings, GMPE developer meetings, and external reviews that provided input to the project and review of project results by both the scientific research community and the engineering user community.

The GMPE developers of the five previous NGA-West1 empirical GMPEs participated in the concurrent update of their models. These developers, along with the reference to their NGA-West1 peak ground acceleration (PGA), peak ground velocity (PGV), and spectral acceleration models, are listed alphabetically as follows: (1) Abrahamson and Silva (2007, 2008), (2) Boore and Atkinson (2007, 2008), (3) Campbell and Bozorgnia (2007, 2008), (4) Chiou and Youngs (2008a, 2008b), and (5) Idriss (2008). In addition, we also used the NGA-West1 database to develop GMPEs for inelastic response spectra (Bozorgnia et al. 2006, 2010), cumulative absolute velocity (Campbell and Bozorgnia 2010), Japan Meterological Agency (JMA) instrumental seismic intensity (Campbell and Bozorgnia 2011a), standardized cumulative absolute velocity (Campbell and Bozorgnia 2011b), and Arias intensity (Campbell and Bozorgnia 2012a). We also developed correlation equations between cumulative absolute velocity and seismic intensity (Campbell and Bozorgnia 2012b).

To meet the needs of the earthquake engineering community, all of the NGA-West2 models were required to be applicable to the following conditions: (1) they should include the ground motion intensity measures PGA, PGV, and 5%-damped elastic pseudo-absolute response-spectral acceleration (PSA) for a minimum set of periods ranging from 0–10 sec; (2) they should model the average horizontal component defined by the median rotated direction RotD50 (Boore 2010), as well as horizontal components in the strike-normal (SN), strike-parallel (SP), and maximum rotated (RotD100) directions, although this latter requirement was covered by the NGA-West2 Directionality Working Group (Baker and Shahi 2013); (3) they should be valid for shallow crustal earthquakes with strike-slip, reverse, and normal mechanisms in active tectonic regions; (4) they should be valid for moment magnitudes ranging from 3.0 to 8.5; (5) they should be valid for distances ranging from 0 to 200 km; and (6) they should incorporate the time-averaged shear-wave velocity in the top 30 m of the site (V_{S30}) as a site parameter, although no specific range of V_{S30} values was specified.

The terms that were addressed by Campbell-Bozorgnia NGA-West2 empirical GMPE include: (1) hanging-wall effects; (2) style of faulting; (3) rupture or hypocentral depth; (4) rupture dip; (5) regionally dependent shallow linear site amplification; (6) nonlinear soil response; (7) three-dimensional (3D) sedimentary basin amplification; (8) regionally dependent anelastic attenuation; (9) magnitude-dependent between-event (inter-event) and within-event (intra-event) standard deviations; and (10) standard deviations that depend on nonlinear site response. The remainder of this report documents the development of the Campbell-Bozorgnia NGA-West2 empirical GMPE. The other NGA-West2 models and supporting projects are documented in a series of companion PEER reports.

2 GROUND MOTION DATABASE

The ground motion database used in this study is a subset of the PEER ground motion database that was updated as part of the PEER NGA-West2 Project (Ancheta et al. 2012, 2013). An electronic version of the PEER NGA-West2 database can be accessed from the PEER website. The NGA-West2 database includes over 21,000 three-component recordings from worldwide earthquakes with moment magnitudes ranging from 3.0 to 7.9. The database includes recordings that for the most part represent free-field site conditions. In order to increase the reliability of our selected database, we applied the following additional criteria for deciding whether a recording should be used: (1) the earthquake should be within the shallow seismogenic continental lithosphere (crust) in a region considered to be tectonically active; (2) the recording should be located at or near ground level with no known embedment effects; (3) the earthquake should have enough recordings to reliably represent the mean ground motion, although this criterion was relaxed for larger earthquakes in order to retain these important recordings; and (4) the earthquake metadata and recording should be reliable (see below for earthquakes and recordings that were excluded because of reliability issues).

We excluded from the larger PEER NGA-West2 database the following earthquakes, recordings, or seismic stations in order to meet our general selection criteria and project requirements: (1) recordings having only one horizontal component or only a vertical component, which precludes calculating the RotD50 horizontal component; (2) recording sites with no measured or estimated value of V_{S30}, which precludes modeling shallow site effects; (3) earthquakes with no rake or focal mechanism, which precludes modeling style-of-faulting effects; (4) earthquakes with the hypocenter or a significant amount of the fault rupture located in the lower crust (below about 20 km), in an oceanic plate, or in a stable continental region (SCR), which are not consistent with the desired tectonic domain; (5) the Lamont Doherty Geologic Observatory recordings from the 1999 Düzce, Turkey, earthquake, which are considered to be unreliable because of their odd spectral shapes; (6) recordings from instruments designated quality D from the 1999 Chi-Chi, Taiwan, earthquake according to the quality designation of Lee et al. (2001), which are considered to be unreliable because of their poor quality; (7) "aftershocks" located in the immediate vicinity of the inferred mainshock rupture plane and defined as a "Class 2" event with $CR_{JB} < 10$ km according to criteria given in Ancheta et al. (2012, 2013) and Wooddell (2012), which are potentially considered to have below-average stress drops; (8) rupture distances (R_{RUP}) within 80 km to isolate the effects of apparent geometric attenuation; however, to model apparent anelastic attenuation we used a separate database with recordings at distances as far as 500 km; (9) an earthquake considered to be poorly recorded according to the criteria (a) $\mathbf{M} < 5.5$ and $N < 5$ or (b) $5.5 \le \mathbf{M} < 6.5$ and $N < 3$ (i.e., note

that singly recorded events with large magnitudes are included), where $\mathbf{M}$ is moment magnitude and N is the number of recordings with $R_{RUP} \leq 80$ km; (10) a seismic station not representative of free-field site conditions, which we define as an instrument that is: (a) in the basement of a building, (b) embedded more than a few meters below the ground surface, or (c) on a dam crest, embankment, or toe (note that abutment recordings were included if sited on rock in order to supplement the limited number of firm and hard rock sites in the database); and (11) recordings from the Pacoima Dam upper-left abutment and the Tarzana Cedar Hill Nursery that have been shown to exhibit strong topographic effects.

The application of the above criteria, as described further below, resulted in selecting a total of 15,521 recordings from 322 earthquakes. This includes 7208 near-source ($R_{RUP} \leq 80$ km) recordings from 282 California and worldwide earthquakes. The remainder events are primarily California earthquakes. We used the same selection critiera, except for criterion 9 in the previous paragraph, to include an additional 8313 far-source ($80 < R_{RUP} \leq 500$ km) recordings from 276 earthquakes with magnitudes ranging from $3.0 \leq \mathbf{M} \leq 7.9$ for the purpose of constraining the apparent anelastic attenuation term. Most of these earthquakes are the same ones included in the near-source database. This compares to 1561 recordings from 64 earthquakes of $4.3 \leq \mathbf{M} \leq 7.9$ used to develop our NGA-West1 model. Significant additional earthquakesthat we have included in our selected database are the 2003 Bam, Iran ($\mathbf{M}$6.6); 2004 Parkfield, California ($\mathbf{M}$6.0); 2008 Wenchuan, China ($\mathbf{M}$7.9); 2009 L'Aquila, Italy ($\mathbf{M}$6.3); 2010 El Mayor-Cucapah, Mexico ($\mathbf{M}$7.0); 2010 Darfield, New Zealand ($\mathbf{M}$7.0); and 2011 Christchurch, New Zealand ($\mathbf{M}$6.2) events. The distribution of the recordings with respect to magnitude and distance is shown in Figure 2.1 for the near-source and far-source databases ($R_{RUP} \leq 80$ km) used to develop our GMPE (CB13). A list of the selected earthquakes and recording sites is given in Appendix A for the near-source database and in Appendix B for the far-source database.

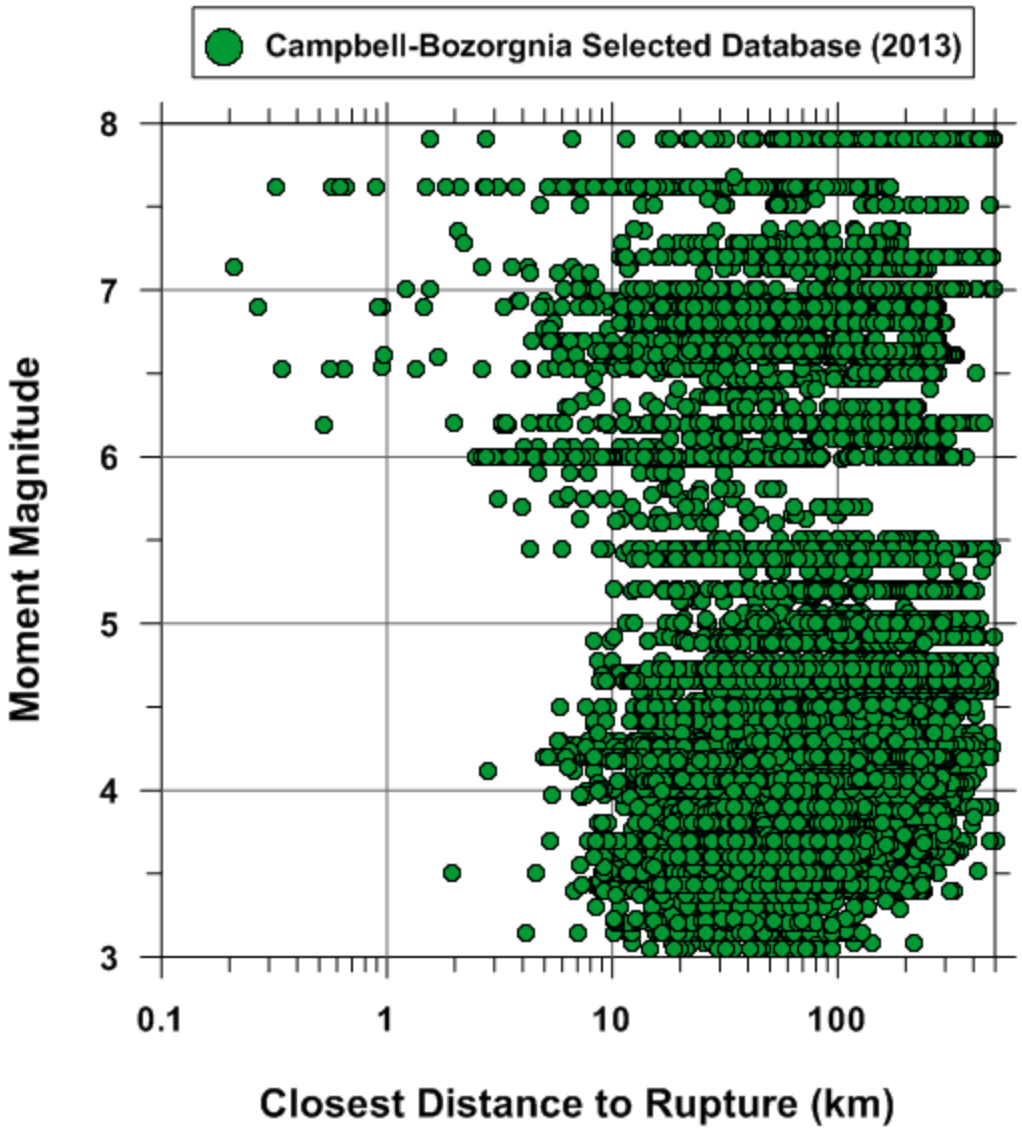

Figure 2.1 **Distribution of recordings with magnitude and distance for the CB13 database.**

3 Ground Motion Model

The functional forms for the mathematical terms used in our NGA-West2 GMPE were developed or confirmed using data exploration techniques such as analysis of residuals. Candidate functional forms were developed or selected through numerous iterations to capture the observed trends in the recorded ground motion data. We primarily updated and modified the functional forms used in our NGA-West1 model. Our hanging-wall term was updated in part with the hanging-wall model developed by Donahue et al. (2013) using ground motion simulations and constrained empirically. The GMPE includes new terms for rupture dip and hypocentral depth that were developed from an analysis of residuals. Final functional forms were chosen based on the following general criteria: (1) their simplicity, although this was not an overriding factor; (2) their sound seismological basis; (3) their unbiased residuals; and (4) their ability to be extrapolated to values of magnitude, distance, and other predictor variables that are important to engineering applications such as probabilistic seismic hazard analysis (PSHA). To satisfy item 4, theoretical constraints were also used based on the supporting research projects conducted as part of the PEER NGA-West1 and NGA-West2 Projects.

3.1 REGRESSION ANALYSIS APPROACH

The model development was done in two phases. In the first phase the near-source database was used to develop a GMPE that captured near-source effects, including the "apparent" geometric attenuation term. This is not "geometric attenuation" as defined in seismology but the apparent geometric attenuation of response spectral ordinates. The same is true for the "apparent" anelastic attenuation term. In the remainder of this report the word "apparent" in front of these terms will be dropped for simplicity. The emphasis on near-scource distances ($R_{RUP} \leq 80$ km) is due to the importance of such distances in seismic hazard analysis. The use of the near-source database also avoided the trade-off between the geometric and anelastic attenuation terms that occur when both are attempted to be fit simultaneously. During the development of the functional forms the regression analysis using the near-source database was performed in two steps using a subset of spectral periods and the two-stage weighted regression procedure of Boore et al. (1993, 1994) and Joyner and Boore (1993). The only exception to this procedure was that the analysis used nonlinear rather than linear regression. In Stage 1, all of the mathematical terms involving individual recordings were fit by the method of nonlinear least squares using all of the selected recordings. Each earthquake was constrained to have a zero mean residual by including a "source" (a.k.a, between-event, inter-event or simply event) term for each earthquake. The terms included in Stage 1 were f_{dis}, f_{hng}, f_{site} and f_{sed} in the GMPE presented

in the next section. In Stage 2 all of the mathematical terms involving the earthquake source were fit by the method of weighted least squares using the source terms from Stage 1. Each source term was assigned a weight that was inversely proportional to its variance from Stage 1. The Stage 2 terms included f_{mag}, f_{flt}, f_{hyp} and f_{dip} in the GMPE presented in the next section.

The two-stage analysis allowed us to clearly investigate the within-event and between-event terms and associated residuals, and helped stabilize the regression analysis; thus allowing us to better evaluate and model magnitude-scaling effects at small and large magnitudes. Once the functional forms of all of the mathematical terms were established, a final regression analysis was performed for the entire range of spectral periods using random-effects regression (Abrahamson and Youngs 1992). After the near-source GMPE was developed, we used random effects-regression in conjunction with the far-source database to develop a regionally-dependent anelastic attenuation term. Finally, we did a limited amount of smoothing of the coefficients in order to remove roughness in predicted response spectra.

3.2 STRONG MOTION INTENSITY MEASURES

The strong motion intensity measure (IM) used in our GMPE and the PEER NGA-West2 Project is not the traditional geometric mean of the two as-recorded horizontal components that was used in our pre-NGA models (Campbell 1997, 2000, 2001; Campbell and Bozorgnia, 1994, 2003a, 2003b, 2003c, 2004) or the GMRotI50 "geometric mean" horizontal component (Boore et al. 2006) used in the NGA-West1 models (Campbell and Bozorgnia 2008). The original as-recorded geometric mean was calculated as the square root of the product (or, alternatively, the mean of the logarithms) of the peak and spectral ground motion parameters of the two as-recorded orthogonal horizontal components. This geometric mean is dependent on the orientation of the sensors as installed in the field. This means that the ground motion measure could differ for the same 3D wave field depending on the orientation of the sensors. Such a dependence on sensor orientation is most pronounced for strongly correlated ground motions that often occur at oscillator periods of one second and longer.

The PEER NGA-West1 Project opted to use an alternative definition of the ground motion IM that is independent of sensor orientation. It is based on a set of geometric means computed from the orthogonal horizontal motions after rotating them through a non-redundant angle of 90° (Boore et al. 2006). A single period-independent rotation is used in which a single angle is chosen that minimizes the spread of the rotation-dependent geometric means over the usable range of spectral periods. Period-independence ensures that the proper correlation between spectral ordinates is maintained. There is a distribution of geometric means to choose from using this approach (one for each of the 90 discrete rotation angles). The PEER NGA-West1 Project selected the 50th-percentile, or what is called GMRotI50 by Boore et al. (2006), as being the most appropriate for engineering use.

In 2009 the U.S. National Earthquake Hazards Reduction Program (NEHRP) provisions adopted the maximum rotated horizontal component to develop seismic design maps (BSSC 2009). This lead Boore (2010) to propose a simpler version of GMRotI50 that is defined to be consistent with this newly defined ground motion IM and that does not require the calculation of a geometric mean. Boore generically refers to this parameter as RotDnn. One difference between this parameter and GMRotI50 is that rather than using the median (50th-percentile) value of the

geometric means of the two rotated horizontal components, he recommends using the median of the IM obtained from the single combined rotated horizontal component, which he calls RotD50. The maximum rotated horizontal component used in BSSC (2009) is simply the largest (100th-percentile) of the IMs obtained from the combined rotated horizontal component, which Boore (2010) calls RotD100. The other difference is the use of the median (or maximum) rotated horizontal component that is period-dependent ("D") rather than period-independent ("I"). Boore (2010) notes that, while RotI50 may still be an adequate measure of the median motion, the conceptual simplicity of the relation between the different fractal levels is lost for the period-independent rotation-angle measures.

The IMs addressed in this study are the RotD50 components of PGA, PGV, and PSA at 21 oscillator periods (T) ranging from 0.01 to 10 sec. The specific spectral periods are 0.01, 0.02, 0.03, 0.05, 0.075, 0.1, 0.15, 0.2, 0.25, 0.3, 0.4, 0.5, 0.75, 1, 1.5, 2, 3, 4, 5, 7.5 and 10 sec. The consensus of the NGE-West2 GMPE developers was to exclude peak ground displacement (PGD) as an IM because of its strong dependence on the low-pass filter used to process the strong-motion recordings. Methods for estimating values of PGD that attempt to overcome its dependence on the low-pass filter corner frequency were explored by Campbell and Bozorgnia (2007). Scaling spectral values to damping values ranging from 0.5% to 30% can be obtained from the spectral value at 5% damping using the spectral damping factors developed by Rezaeian et al. (2012, 2013).

3.3 MEDIAN GROUND MOTION MODEL

The natural logarithm of the RotD50 horizontal ground motion component of PGA (g), PGV (cm/sec), and PSA (g) is given by the equation

$$\ln Y = \begin{cases} \ln \text{PGA}; & Y < \text{PGA},\ T < 0.25 \\ f_{mag} + f_{dis} + f_{flt} + f_{hng} + f_{site} + f_{sed} + f_{hyp} + f_{dip} + f_{atn}; & \text{Otherwise} \end{cases} \tag{3.1}$$

where the terms represent the scaling of ground motion with respect to earthquake magnitude, (apparent) geometric attenuation, style of faulting, hanging-wall geometry, shallow site response, basin response, hypocentral depth, rupture dip, and (apparent) anelastic attenuation. Note that PGA is the true value of peak ground acceleration and is not equivalent to PSA at $T = 0.01$ sec as was the case in our NGA-West1 model, although the two have very similar amplitudes. Note also that there are some combinations of predictor variable values, especially at large distances, for which the calculated value of PSA at periods of $T < 0.25$ sec can fall below the value of PGA. Since this is an artifact of the numerical analysis and is not possible given the definition of pseudo-absolute acceleration, the calculated value of PSA is set equal to the value of PGA when this occurs.

3.3.1 Magnitude Term

$$f_{mag} = \begin{cases} c_0 + c_1\mathbf{M}; & \mathbf{M} \le 4.5 \\ c_0 + c_1\mathbf{M} + c_2(\mathbf{M} - 4.5); & 4.5 < \mathbf{M} \le 5.5 \\ c_0 + c_1\mathbf{M} + c_2(\mathbf{M} - 4.5) + c_3(\mathbf{M} - 5.5); & 5.5 < \mathbf{M} \le 6.5 \\ c_0 + c_1\mathbf{M} + c_2(\mathbf{M} - 4.5) + c_3(\mathbf{M} - 5.5) + c_4(\mathbf{M} - 6.5); & \mathbf{M} > 6.5 \end{cases} \tag{3.2}$$

3.3.2 Geometric Attenuation Term

$$f_{dis} = (c_5 + c_6\mathbf{M}) \ln\left(\sqrt{R_{RUP}^2 + c_7^2}\right) \tag{3.3}$$

3.3.3 Style-of-Fautling Term

$$f_{flt} = f_{flt,F} f_{flt,M} \tag{3.4}$$

$$f_{flt,F} = c_8 F_{RV} + c_9 F_{NM} \tag{3.5}$$

$$f_{flt,M} = \begin{cases} 0; & \mathbf{M} \le 4.5 \\ \mathbf{M} - 4.5; & 4.5 < \mathbf{M} \le 5.5 \\ 1; & \mathbf{M} > 5.5 \end{cases} \tag{3.6}$$

3.3.4 Hanging-Wall Term

$$f_{hng} = c_{10} f_{hng,R_X} f_{hng,R_{RUP}} f_{hng,M} f_{hng,Z} f_{hng,\delta} \tag{3.7}$$

$$f_{hng,R_X} = \begin{cases} 0; & R_X < 0 \\ f_1(R_X); & 0 \le R_X < R_1 \\ \max[f_2(R_X), 0]; & R_X \ge R_1 \end{cases} \tag{3.8}$$

$$f_1(R_X) = h_1 + h_2(R_X / R_1) + h_3(R_X / R_1)^2 \tag{3.9}$$

$$f_2(R_X) = h_4 + h_5\left(\frac{R_X - R_1}{R_2 - R_1}\right) + h_6\left(\frac{R_X - R_1}{R_2 - R_1}\right)^2 \tag{3.10}$$

$$R_1 = W\cos(\delta) \tag{3.11}$$

$$R_2 = 62\mathbf{M} - 350 \tag{3.12}$$

$$f_{hng,R_{RUP}} = \begin{cases} 1; & R_{RUP} = 0 \\ (R_{RUP} - R_{JB}) / R_{RUP}; & R_{RUP} > 0 \end{cases} \tag{3.13}$$

$$f_{hng,M} = \begin{cases} 0; & \mathbf{M} \le 5.5 \\ (\mathbf{M} - 5.5)[1 + a_2(\mathbf{M} - 6.5)]; & 5.5 < \mathbf{M} \le 6.5 \\ 1 + a_2(\mathbf{M} - 6.5); & \mathbf{M} > 6.5 \end{cases} \tag{3.14}$$

$$f_{hng,Z} = \begin{cases} 1 - 0.06\, Z_{TOR}; & Z_{TOR} \le 16.66 \\ 0; & Z_{TOR} > 16.66 \end{cases} \tag{3.15}$$

$$f_{hng,\delta} = (90 - \delta) / 45 \tag{3.16}$$

3.3.5 Shallow Site Response Term

$$f_{site} = f_{site,G} + S_J f_{site,J} \tag{3.17}$$

$$f_{site,G} = \begin{cases} c_{11} \ln\left(\frac{V_{S30}}{k_1}\right) + k_2 \left\{ \ln\left[A_{1100} + c\left(\frac{V_{S30}}{k_1}\right)^n \right] - \ln\left[A_{1100} + c\right] \right\}; & V_{S30} \le k_1 \\ (c_{11} + k_2 n) \ln\left(\frac{V_{S30}}{k_1}\right); & V_{S30} > k_1 \end{cases} \tag{3.18}$$

$$f_{site,J} = \begin{cases} (c_{12} + k_2 n)\left[\ln\left(\frac{V_{S30}}{k_1}\right) - \ln\left(\frac{200}{k_1}\right) \right]; & V_{S30} \le 200 \\ (c_{13} + k_2 n) \ln\left(\frac{V_{S30}}{k_1}\right); & \text{All } V_{S30} \end{cases} \tag{3.19}$$

3.3.6 Basin Response Term

$$f_{sed} = \begin{cases} (c_{14} + c_{15} S_J)(Z_{2.5} - 1); & Z_{2.5} \le 1 \\ 0; & 1 < Z_{2.5} \le 3 \\ c_{16} k_3 e^{-0.75}[1 - \exp(-0.25(Z_{2.5} - 3)]; & Z_{2.5} > 3 \end{cases} \tag{3.20}$$

3.3.7 Hypocentral Depth Term

$$f_{hyp} = f_{hyp,H} f_{hyp,M} \tag{3.21}$$

$$f_{hyp,H} = \begin{cases} 0; & Z_{HYP} \le 7 \\ Z_{HYP} - 7; & 7 < Z_{HYP} \le 20 \\ 13; & Z_{HYP} > 20 \end{cases} \tag{3.22}$$

$$f_{hyp,M} = \begin{cases} c_{17}; & \mathbf{M} \le 5.5 \\ [c_{17} + (c_{18} - c_{17})(\mathbf{M} - 5.5)]; & 5.5 < \mathbf{M} \le 6.5 \\ c_{18}; & \mathbf{M} > 6.5 \end{cases} \tag{3.23}$$

3.3.8 Rupture Dip Term

$$f_{dip} = \begin{cases} c_{19}\delta; & \mathbf{M} \le 4.5 \\ c_{19}(5.5 - \mathbf{M})\delta; & 4.5 < \mathbf{M} \le 5.5 \\ 0; & \mathbf{M} > 5.5 \end{cases} \tag{3.24}$$

3.3.9 Anelastic Attenuation Term

$$f_{atn} = \begin{cases} (c_{20} + \Delta c_{20})(R_{RUP} - 80); & R_{RUP} > 80 \\ 0; & R_{RUP} \le 80 \end{cases} \tag{3.25}$$

3.3.10 Definitions of Predictor Variables

The definitions of the predictor variables appearing in the equations given in the previous sections are defined as follows:

- $\mathbf{M}$ is moment magnitude
- R_{RUP} (km) is closest distance to the coseismic rupture plane
- R_{JB} (km) is closest distance to the surface projection of the coseismic rupture plane (Joyner-Boore distance)
- R_X (km) is closest distance to the surface projection of the top edge of the coseismic rupture plane measured perpendicular to its average strike (Ancheta et al. 2013)
- W (km) is the down-dip width of the rupture plane
- λ (°) is rake defined as the average angle of slip measured in the plane of rupture between the strike direction and the slip vector (e.g., Ancheta et al. 2013; Lay and Wallace 1995]
- F_{RV} is an indicator variable representing reverse and reverse-oblique faulting where $F_{RV} = 1$ for $30° < \lambda < 150°$ and $F_{RV} = 0$ otherwise

- F_{NM} is an indicator variable representing normal and normal-oblique faulting where $F_{NM}=1$ for $-150° < \lambda < -30°$ and $F_{NM}=0$ otherwise
- Z_{TOR} (km) is the depth to the top of the coseismic rupture plane
- δ (°) is the average dip of the rupture plane
- V_{S30} (m/sec) is the time-averaged shear-wave velocity in the top 30 m of the site
- A_{1100} (g) is the median predicted value of PGA on rock with $V_{S30}=1100$ m/sec (rock PGA)
- S_J is an indicator variable representing regional site effects where $S_J=1$ for sites located in Japan and $S_J=0$ otherwise
- $Z_{2.5}$ (km) is depth to the 2.5 km/sec shear-wave velocity horizon beneath the site (sediment depth)
- Z_{HYP} (km) is the hypocentral depth of the earthquake

3.3.11 Model Coefficients

The coefficients appearing in the equations given in the previous sections are defined as follows:

- c and n are period-independent, theoretically constrained model coefficients
- a_2, h_i and k_i are period-dependent, theoretically constrained model coefficients
- c_i and Δc_{20} are empirically derived model coefficients (see Section 3.5)

3.3.12 Treatment of Missing Values

When predictor variables for selected recordings were missing from the PEER database, they were either estimated using proxies or the regression analysis involving the terms that included those variables was performed using only the recordings for which values were available. Sediment depth ($Z_{2.5}$) was the only predictor variable that had missing values and no credible proxies to substitute for the missing values. When values of V_{S30} were missing, they were replaced with proxy values derived from surface geological units, geotechnical site categories, ground slope, geomorphology, or elevation based on relationships given in Stewart et al. (2012) and Ancheta et al. (2012, 2013). When finite rupture models were not available, the distance variables R_{RUP}, R_{JB}, and R_X and the source variables W, Z_{HYP}, and δ were derived from focal mechanism or moment tensor information and source dimension versus magnitude relationships (Ancheta et al. 2012, 2013). These predictor variables are defined in Section 3.3.10.

3.4 ALEATORY VARIABILITY MODEL

Aleatory variability is defined in terms of both the RotD50 and arbitrary horizontal components of motion.

3.4.1 RotD50 Horizontal Component

Consistent with the random-effects regression analysis used to derive the median value of *Y*, the aleatory variability model for the RotD50 horizontal component is defined by the equation

$$y_{ij} = Y_{ij} + \eta_i + \varepsilon_{ij} \tag{3.26}$$

where η_i is the between-event (inter-event) residual for event *i* and y_{ij}, Y_{ij}, and ε_{ij} are the observed value, predicted value, and within-event (intra-event) residual for recording *j* of event *i*, respectively. The independent normally distributed variables η_i and ε_{ij} have zero means and estimated between-event and within-event standard deviations on reference rock ($V_{S30} = 1100$ m/sec) or on soil represented by linear site response, $\tau_{\ln Y}$ and $\phi_{\ln Y}$, given by the magnitude-dependent equations

$$\tau_{\ln Y} = \begin{cases} \tau_1; & \mathbf{M} \le 4.5 \\ \tau_2 + (\tau_1 - \tau_2)(5.5 - \mathbf{M}); & 4.5 < \mathbf{M} < 5.5 \\ \tau_2; & \mathbf{M} \ge 5.5 \end{cases} \tag{3.27}$$

$$\phi_{\ln Y} = \begin{cases} \phi_1; & \mathbf{M} \le 4.5 \\ \phi_2 + (\phi_1 - \phi_2)(5.5 - \mathbf{M}); & 4.5 < \mathbf{M} < 5.5 \\ \phi_2; & \mathbf{M} \ge 5.5 \end{cases} \tag{3.28}$$

where τ_i and ϕ_i are empirically derived standard deviations.

The final model standard deviations that incorporate the effects of nonlinear soil response are given by the equations

$$\tau = \sqrt{\tau_{\ln Y_B}^2 + \alpha^2 \tau_{\ln PGA_B}^2 + 2\alpha\rho_{\ln PGA,\ln Y}\tau_{\ln Y_B}\tau_{\ln PGA_B}} \tag{3.29}$$

$$\phi = \sqrt{\phi_{\ln Y_B}^2 + \phi_{\ln AF}^2 + \alpha^2\phi_{\ln PGA_B}^2 + 2\alpha\rho_{\ln PGA,\ln Y}\phi_{\ln Y_B}\phi_{\ln PGA_B}} \tag{3.30}$$

where $\tau_{\ln Y_B} = \tau_{\ln Y}$ and $\tau_{\ln PGA_B} = \tau_{\ln PGA}$ are the between-event standard deviations for the IM of interest and PGA at the base of the site profile; $\phi_{\ln Y_B} = (\phi_{\ln Y}^2 - \phi_{\ln AF}^2)^{1/2}$ and $\phi_{\ln PGA_B} = (\phi_{\ln PGA}^2 - \phi_{\ln AF}^2)^{1/2}$ are the within-event standard deviations for the IM of interest and PGA at the base of the site profile; $\phi_{\ln AF}$ is the estimated standard deviation of the logarithm of the site amplification factor f_{site} for linear site response; $\rho_{\ln PGA,\ln Y}$ is the correlation coefficient between the within-event

residuals of the intensity measure of interest and PGA; and α is the linearized functional relationship between f_{site} and $\ln A_{1100}$, which is calculated from the partial derivative

$$\alpha = \frac{\partial f_{site}}{\partial \ln A_{1100}} = \begin{cases} k_2 A_{1100} \left\{ \left[A_{1100} + c\left(\frac{V_{S30}}{k_1} \right)^n \right]^{-1} - \left[A_{1100} + c \right]^{-1} \right\} & V_{S30} < k_1 \\ 0 & V_{S30} \geq k_1 \end{cases} \tag{3.31}$$

The total aleatory standard deviation is given by combining the between-event and within-event standard deviations by square-root of sum of squares (SRSS) by the equation

$$\sigma = \sqrt{\tau^2 + \phi^2} \tag{3.32}$$

3.4.2 Arbitrary Horizontal Component

We define the arbitrary horizontal component as the expected value of the peak amplitude from the two as-recorded orthogonal horizontal components (Baker and Cornell 2006). Although this expected value (taken with respect to its logarithm) is identical to the geometric mean of the as-recorded horizontal components and virtually identical to the median rotated horizontal component (Boore 2010), its standard deviation is not. Baker and Cornell (2006) point out that many engineering applications require a probabilistic estimate of the arbitrary horizontal component and not the geometric mean or median horizontal components. In such a case, even though no adjustment of the median is required, the larger standard deviation associated with the arbitrary horizontal component will lead to a larger probabilistic estimate of ground motion.

Boore et al. (1997) and Boore (2005) show that the aleatory variance of the arbitrary horizontal component, which they call the component-to-component variability, can be calculated from the equation

$$\phi_c^2 = \frac{1}{4N} \sum_{j=1}^{N} (\ln y_{1j} - \ln y_{2j})^2 \tag{3.33}$$

where the subscripts 1 and 2 refer to the two individual as-recorded horizontal components of motion, *j* is an index representing the recording number, and *N* is the total number of recordings. We used this equation to calculate the values of ϕ_c associated with the selected PEER database we used to develop our NGA-West model. The total standard deviation corresponding to this component is given by the equation

$$\sigma_{Arb} = \sqrt{\sigma^2 + \phi_c^2} \tag{3.34}$$

where σ is the total RotD50 standard deviation given by Equation (3.32).

3.5 RESULTS

The model coefficients k_i and $c_0 - c_{19}$ are listed in Table 3.1 and the hanging-wall model coefficients h_i are listed in Table 3.2. Table 3.3 lists the anelastic attenuation coefficients c_{20} and Δc_{20}, where the latter captures the regional differences in anelastic attenuation for those regions where sufficient data are available to determine a separate anelastic attenuation coefficient. The base region used to derive c_{20} includes California, Taiwan, the Middle East and similar active tectonic regions. The regions used to derive Δc_{20} include Japan and Italy as one region (JP) and eastern China as another region (CH). The aleatory standard deviations τ_i and ϕ_i and the correlation coefficients $\rho_{\ln PGA,\ln Y}$ are listed in Table 3.4. Note that the coefficients $c = 1.88$ and $n = 1.18$ are the same for all spectral periods as indicated in the footnote to Table 3.1.

In order to evaluate the validity of the median GMPE, it is useful to plot the between-event and within-event residuals as defined in Abrahamson and Youngs (1992). Residual plots for PGA, PGV, and PSA at spectral periods of 0.2, 1, 3, and 5 sec are shown in Figures 3.1 to 3.10. In these plots a positive residual indicates under-prediction by the model and a negative residual indicates over-prediction by the model. Figures 3.1 to 3.4 show between-event residuals as a function of magnitude, hypocentral depth, rake, and rupture dip. Figures 3.5 to 3.10 show within-event residuals as a function of magnitude, rupture distance, horizontal distance from the top edge of the rupture plane for sites located directly over the rupture plane (hanging-wall effects), 30-m shear-wave velocity, rock PGA, and sediment depth. The plots show that there are no systematic trends or biases in the residuals that would indicate that the model is inconsistent with the data.

Figures 3.11 to 3.19 present a series of plots that show how our median ground motion model scales with rupture distance, magnitude, site effects, and spectral period. The values of the predictor variables used to calculate the ground motions are listed in the title at the top of each plot. Figure 3.11 shows the scaling of PGA with distance (attenuation) for magnitudes of 3.5, 4.5, 5.5, 6.5, and 7.5 for a strike-slip fault. Figure 3.12 shows similar plots comparing our NGA-West2 model (CB13) with our NGA-West1 model (CB08). This figure shows that the two GMPEs predict similar amplitudes except at $\mathbf{M} = 4.5$ where CB13 is now better constrained due to the inclusion of the large number of small magnitude recordings in the NGA-West2 database. It also shows that CB13 predicts stronger geometric attenuation characteristics than CB08 at small magnitudes. The stronger large-distance attaenuation in CB13 is mainly due to the inclusion of an anelastic attenuation term. Figure 3.13 shows similar plots to Figure 3.12 for PSA at $T = 1$ sec with similar conclusions, except that the difference at large distances is not as significant. Figure 3.14 shows scaling of PGA with distance for sites over the hanging-wall of a reverse fault. The small-magnitude bias of CB08 is somewhat larger in this case. Hanging-wall effects are stronger for CB13 because of the new hanging-wall model that predicts the largest effects over the bottom edge of the rupture plane.

Figure 3.15 shows the scaling of PGA with magnitude for rupture distances of 5, 10, 40, and 80 km for a strike-slip fault. This figure shows that magnitude scaling for $\mathbf{M} \geq 5.5$ is similar for CB08 and CB13 except at the largest distances where the small-magnitude bias of CB08 becomes noticeable even above this magnitude. The stronger magnitude scaling at smaller magnitudes exhibited by CB13 is the result of including the small-magnitude recordings in the

development of our NGA-West2 GMPE. Figure 3.16 shows similar plots for PSA at $T = 1$ sec. In this case, the two models have similar amplitudes down to around $\mathbf{M} = 5$ below which the small-magnitude bias of CB08 becomes evident.

Figure 3.17 shows the scaling of PSA with magnitude for rupture distances of 5, 10, 40, and 80 km. There is a clear shift in the peak of the spectra from spectral periods of about 0.08 sec to 0.15 sec at short distances as magnitude increases from around 3.5 to 5.5, where the peak becomes relatively constant. There is also a noticeable shift at larger distances where the spectral peak shifts to longer periods at small magnitudes and broadens considerably at large magnitudes. Figure 3.18 shows how PSA behaves as the median estimate of rock PGA (A_{1100}) increases from $0.1g$ to $0.7g$ for NEHRP site categories B ($V_{S30} = 1070$ m/sec), C ($V_{S30} = 525$ m/sec), D ($V_{S30} = 255$ m/sec), and E ($V_{S30} = 150$ m/sec). All predictor variables are held constant except for A_{1100}. This figure clearly shows the strong shift in the spectral peak to longer periods and the associated reduction in spectral amplitude for the softer site conditions (NEHRP D and E) as rock PGA increases. This phenomenon is the result of nonlinear soil effects.

Figure 3.19 compares the between-event, within-event, and total aleatory standard deviations between CB08 and CB13. The largest difference is for $\mathbf{M} < 4.5$ where the short-period PSA standard deviations for CB13 are larger than for CB08 because of the inclusion of the small-magnitude data. However, we are somewhat surprised that the CB13 within-event standard deviations are actually smaller at longer periods. We surmise that this might be due to the availability of high-quality broadband recordings from a similar region (California) and the fact that these spectral periods correspond to the constant displacement part of the spectrum, which is largely controlled by moment magnitude. There is a relatively constant increase in the CB13 between-event standard deviations of about 0.1 for the larger magnitudes that we believe is the result of including earthquakes with larger numbers of recordings from a more geographically diverse active tectonic regions. The within-event standard deviations are more similar to CB08. The result is that the total standard deviation increases by about 0.07. For both magnitude ranges, the large increase in standard deviations at $T > 5$ sec found by CB08 is not observed in CB13 due to an increase in the number of high-quality digital recordings.

Table 3.1 Median ground motion model coefficients.

T (sec)	c_0	c_1	c_2	c_3	c_4	c_5	c_6	c_7	c_8	c_9	c_{10}	c_{11}
0.010	-4.292	0.977	0.533	-1.485	-0.499	-2.773	0.248	6.753	0	-0.214	0.720	1.094
0.020	-4.271	0.976	0.549	-1.488	-0.501	-2.772	0.247	6.502	0	-0.208	0.730	1.149
0.030	-3.963	0.931	0.628	-1.494	-0.517	-2.782	0.246	6.291	0	-0.213	0.759	1.290
0.050	-3.475	0.887	0.674	-1.388	-0.615	-2.791	0.240	6.317	0	-0.244	0.826	1.449
0.075	-3.293	0.902	0.726	-1.469	-0.596	-2.745	0.227	6.861	0	-0.266	0.815	1.535
0.10	-3.666	0.993	0.698	-1.572	-0.536	-2.633	0.210	7.294	0	-0.229	0.831	1.615
0.15	-4.866	1.267	0.510	-1.669	-0.490	-2.458	0.183	8.031	0	-0.211	0.749	1.877
0.20	-5.411	1.366	0.447	-1.750	-0.451	-2.421	0.182	8.385	0	-0.163	0.764	2.069
0.25	-5.962	1.458	0.274	-1.711	-0.404	-2.392	0.189	7.534	0	-0.150	0.716	2.205
0.30	-6.403	1.528	0.193	-1.770	-0.321	-2.376	0.195	6.990	0	-0.131	0.737	2.306
0.40	-7.566	1.739	-0.020	-1.594	-0.426	-2.303	0.185	7.012	0	-0.159	0.738	2.398
0.50	-8.379	1.872	-0.121	-1.577	-0.440	-2.296	0.186	6.902	0	-0.153	0.718	2.355
0.75	-9.841	2.021	-0.042	-1.757	-0.443	-2.232	0.186	5.522	0	-0.090	0.795	1.995
1.0	-11.011	2.180	-0.069	-1.707	-0.527	-2.158	0.169	5.650	0	-0.105	0.556	1.447
1.5	-12.469	2.270	0.047	-1.621	-0.630	-2.063	0.158	5.795	0	-0.058	0.480	0.330
2.0	-12.969	2.271	0.149	-1.512	-0.768	-2.104	0.158	6.632	0	-0.028	0.401	-0.514
3.0	-13.306	2.150	0.368	-1.315	-0.890	-2.051	0.148	6.759	0	0	0.206	-0.848
4.0	-14.020	2.132	0.726	-1.506	-0.885	-1.986	0.135	7.978	0	0	0.105	-0.793
5.0	-14.558	2.116	1.027	-1.721	-0.878	-2.021	0.140	8.538	0	0	0	-0.748
7.5	-15.509	2.223	0.169	-0.756	-1.077	-2.179	0.178	8.468	0	0	0	-0.664
10.0	-15.975	2.132	0.367	-0.800	-1.282	-2.244	0.194	6.564	0	0	0	-0.576
PGA	-4.346	0.984	0.537	-1.499	-0.496	-2.773	0.248	6.768	0	-0.212	0.720	1.090
PGV	-2.895	1.510	0.270	-1.299	-0.453	-2.466	0.204	5.837	0	-0.168	0.305	1.713

Table 3.1 Continued.

T (sec)	c_{12}	c_{13}	c_{14}	c_{15}	c_{16}	c_{17}	c_{18}	c_{19}	k_1	k_2	k_3
0.010	2.191	1.416	-0.0070	-0.207	0.390	0.0981	0.0334	0.00755	865	-1.186	1.839
0.020	2.189	1.453	-0.0167	-0.199	0.387	0.1009	0.0327	0.00759	865	-1.219	1.840
0.030	2.164	1.476	-0.0422	-0.202	0.378	0.1095	0.0331	0.00790	908	-1.273	1.841
0.050	2.138	1.549	-0.0663	-0.339	0.295	0.1226	0.0270	0.00803	1054	-1.346	1.843
0.075	2.446	1.772	-0.0794	-0.404	0.322	0.1165	0.0288	0.00811	1086	-1.471	1.845
0.10	2.969	1.916	-0.0294	-0.416	0.384	0.0998	0.0325	0.00744	1032	-1.624	1.847
0.15	3.544	2.161	0.0642	-0.407	0.417	0.0760	0.0388	0.00716	878	-1.931	1.852
0.20	3.707	2.465	0.0968	-0.311	0.404	0.0571	0.0437	0.00688	748	-2.188	1.856
0.25	3.343	2.766	0.1441	-0.172	0.466	0.0437	0.0463	0.00556	654	-2.381	1.861
0.30	3.334	3.011	0.1597	-0.084	0.528	0.0323	0.0508	0.00458	587	-2.518	1.865
0.40	3.544	3.203	0.1410	0.085	0.540	0.0209	0.0432	0.00401	503	-2.657	1.874
0.50	3.016	3.333	0.1474	0.233	0.638	0.0092	0.0405	0.00388	457	-2.669	1.883
0.75	2.616	3.054	0.1764	0.411	0.776	-0.0082	0.0420	0.00420	410	-2.401	1.906
1.0	2.470	2.562	0.2593	0.479	0.771	-0.0131	0.0426	0.00409	400	-1.955	1.929
1.5	2.108	1.453	0.2881	0.566	0.748	-0.0187	0.0380	0.00424	400	-1.025	1.974
2.0	1.327	0.657	0.3112	0.562	0.763	-0.0258	0.0252	0.00448	400	-0.299	2.019
3.0	0.601	0.367	0.3478	0.534	0.686	-0.0311	0.0236	0.00345	400	0.000	2.110
4.0	0.568	0.306	0.3747	0.522	0.691	-0.0413	0.0102	0.00603	400	0.000	2.200
5.0	0.356	0.268	0.3382	0.477	0.670	-0.0281	0.0034	0.00805	400	0.000	2.291
7.5	0.075	0.374	0.3754	0.321	0.757	-0.0205	0.0050	0.00280	400	0.000	2.517
10.0	-0.027	0.297	0.3506	0.174	0.621	0.0009	0.0099	0.00458	400	0.000	2.744
PGA	2.186	1.420	-0.0064	-0.202	0.393	0.0977	0.0333	0.00757	865	-1.186	1.839
PGV	2.602	2.457	0.1060	0.332	0.585	0.0517	0.0327	0.00613	400	-1.955	1.929

Note: $c = 1.88$ and $n = 1.18$ for all spectral periods.

Table 3.2 Constrained hanging-wall coefficients.

T (sec)	a_2	h_1	h_2	h_3	h_4	h_5	h_6
0.010	0.168	0.242	1.471	-0.714	1.000	-0.336	-0.270
0.020	0.166	0.244	1.467	-0.711	1.000	-0.339	-0.263
0.030	0.167	0.246	1.467	-0.713	1.000	-0.338	-0.259
0.050	0.173	0.251	1.449	-0.701	1.000	-0.338	-0.263
0.075	0.198	0.260	1.435	-0.695	1.000	-0.347	-0.219
0.10	0.174	0.259	1.449	-0.708	1.000	-0.391	-0.201
0.15	0.198	0.254	1.461	-0.715	1.000	-0.449	-0.099
0.20	0.204	0.237	1.484	-0.721	1.000	-0.393	-0.198
0.25	0.185	0.206	1.581	-0.787	1.000	-0.339	-0.210
0.30	0.164	0.210	1.586	-0.795	1.000	-0.447	-0.121
0.40	0.160	0.226	1.544	-0.770	1.000	-0.525	-0.086
0.50	0.184	0.217	1.554	-0.770	1.000	-0.407	-0.281
0.75	0.216	0.154	1.626	-0.780	1.000	-0.371	-0.285
1.0	0.596	0.117	1.616	-0.733	1.000	-0.128	-0.756
1.5	0.596	0.117	1.616	-0.733	1.000	-0.128	-0.756
2.0	0.596	0.117	1.616	-0.733	1.000	-0.128	-0.756
3.0	0.596	0.117	1.616	-0.733	1.000	-0.128	-0.756
4.0	0.596	0.117	1.616	-0.733	1.000	-0.128	-0.756
5.0	0.596	0.117	1.616	-0.733	1.000	-0.128	-0.756
7.5	0.596	0.117	1.616	-0.733	1.000	-0.128	-0.756
10.0	0.596	0.117	1.616	-0.733	1.000	-0.128	-0.756
PGA	0.167	0.241	1.474	-0.715	1.000	-0.337	-0.270
PGV	0.596	0.117	1.616	-0.733	1.000	-0.128	-0.756

Table 3.3 Regional anelastic attenuation coefficients.

T (sec)	c_{20}	Δc_{20}		
		CA	**JP**	**CH**
0.010	-0.0055	0	-0.0035	0.0036
0.020	-0.0055	0	-0.0035	0.0036
0.030	-0.0057	0	-0.0034	0.0037
0.050	-0.0063	0	-0.0037	0.0040
0.075	-0.0070	0	-0.0037	0.0039
0.10	-0.0073	0	-0.0034	0.0042
0.15	-0.0069	0	-0.0030	0.0042
0.20	-0.0060	0	-0.0031	0.0041
0.25	-0.0055	0	-0.0033	0.0036
0.30	-0.0049	0	-0.0035	0.0031
0.40	-0.0037	0	-0.0034	0.0028
0.50	-0.0027	0	-0.0034	0.0025
0.75	-0.0016	0	-0.0032	0.0016
1.0	-0.0006	0	-0.0030	0.0006
1.5	0	0	-0.0019	0
2.0	0	0	-0.0005	0
3.0	0	0	0	0
4.0	0	0	0	0
5.0	0	0	0	0
7.5	0	0	0	0
10.0	0	0	0	0
PGA	-0.0055	0	-0.0035	0.0036
PGV	-0.0017	0	-0.0006	0.0017

Note: CA represents California and similar active tectonic domains, JP represents Japan and Italy, and CH represents eastern China (Wenchuan earthquake).

Table 3.4 Aleatory variability model standard deviations and correlation coefficients.

T (sec)	τ_1	τ_2	ϕ_1	ϕ_2	$\phi_{\ln AF}$	ϕ_c	**M** ≤ 4.5		**M** ≥ 5.5		$\rho_{\ln PGA,\ln Y}$
							σ	σ_{ARB}	σ	σ_{ARB}	
0.010	0.404	0.325	0.734	0.492	0.300	0.166	0.838	0.854	0.590	0.613	1.000
0.020	0.417	0.326	0.738	0.496	0.300	0.166	0.848	0.864	0.594	0.617	0.999
0.030	0.446	0.344	0.747	0.503	0.300	0.165	0.870	0.886	0.609	0.631	0.989
0.050	0.508	0.377	0.777	0.520	0.300	0.162	0.928	0.942	0.642	0.662	0.963
0.075	0.504	0.418	0.782	0.535	0.300	0.158	0.930	0.943	0.679	0.697	0.922
0.10	0.445	0.426	0.769	0.543	0.300	0.170	0.888	0.904	0.690	0.711	0.898
0.15	0.382	0.387	0.769	0.543	0.300	0.180	0.859	0.878	0.667	0.691	0.890
0.20	0.339	0.338	0.761	0.552	0.300	0.186	0.833	0.854	0.647	0.673	0.871
0.25	0.340	0.316	0.744	0.545	0.300	0.191	0.818	0.840	0.630	0.658	0.852
0.30	0.340	0.300	0.727	0.568	0.300	0.198	0.803	0.827	0.642	0.672	0.831
0.40	0.356	0.264	0.690	0.593	0.300	0.206	0.776	0.803	0.649	0.681	0.785
0.50	0.379	0.263	0.663	0.611	0.300	0.208	0.764	0.792	0.665	0.697	0.735
0.75	0.430	0.326	0.606	0.633	0.300	0.221	0.743	0.775	0.712	0.746	0.628
1.0	0.470	0.353	0.579	0.628	0.300	0.225	0.746	0.779	0.720	0.754	0.534
1.5	0.497	0.399	0.541	0.603	0.300	0.222	0.735	0.768	0.723	0.756	0.411
2.0	0.499	0.400	0.529	0.588	0.300	0.226	0.727	0.761	0.711	0.746	0.331
3.0	0.500	0.417	0.527	0.578	0.300	0.229	0.726	0.761	0.713	0.749	0.289
4.0	0.543	0.393	0.521	0.559	0.300	0.237	0.753	0.789	0.683	0.723	0.261
5.0	0.534	0.421	0.502	0.551	0.300	0.237	0.733	0.770	0.693	0.732	0.200
7.5	0.523	0.438	0.457	0.546	0.300	0.271	0.695	0.746	0.700	0.751	0.174
10.0	0.466	0.438	0.441	0.543	0.300	0.290	0.642	0.704	0.698	0.756	0.174
PGA	0.409	0.322	0.734	0.492	0.300	0.166	0.840	0.856	0.588	0.611	1.000
PGV	0.317	0.297	0.655	0.494	0.300	0.190	0.728	0.752	0.576	0.607	0.691

Note: All standard deviations are in natural logarithmic units and are for linear site conditions.

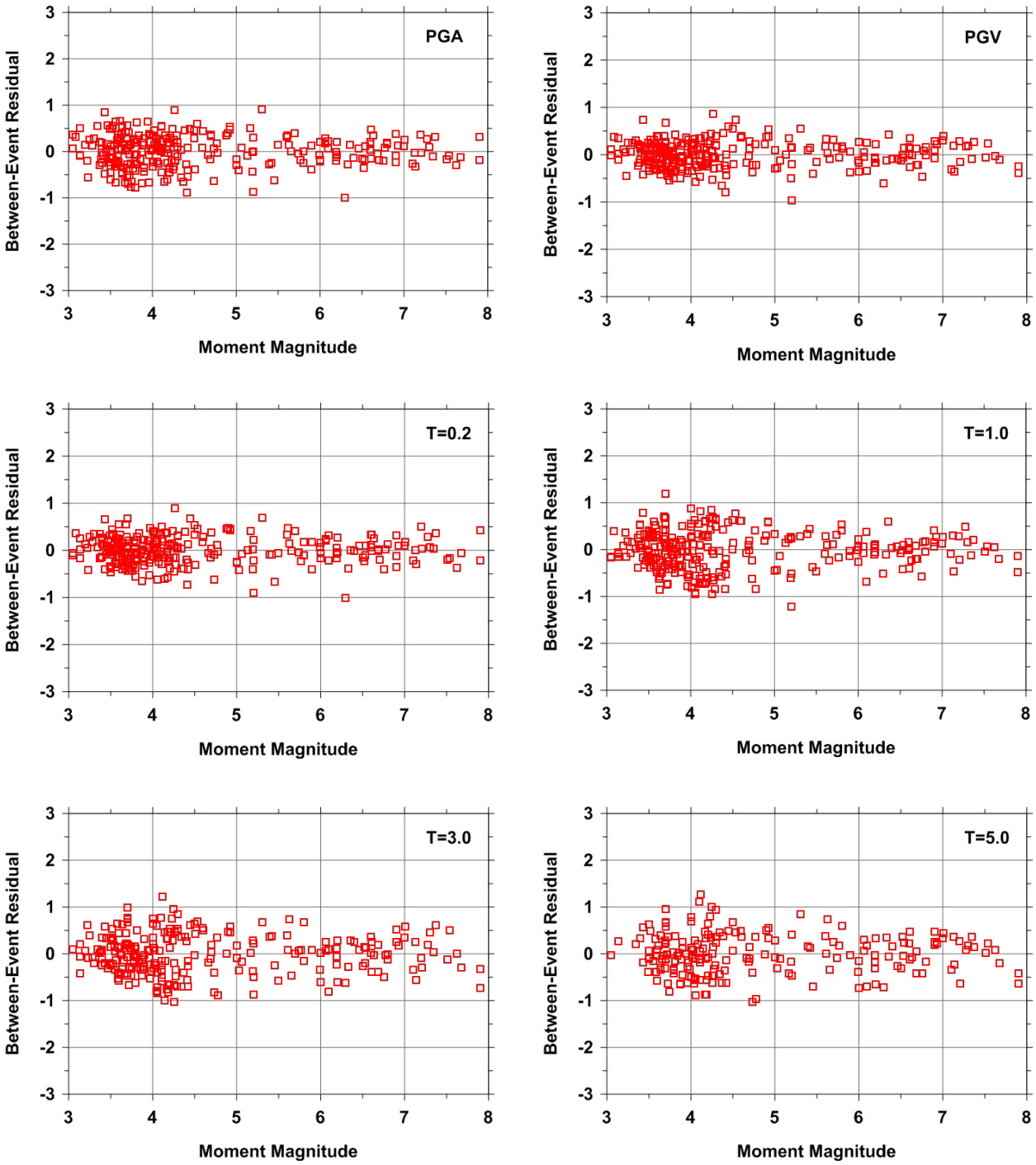

Figure 3.1 Dependence of between-event residuals on earthquake magnitude.

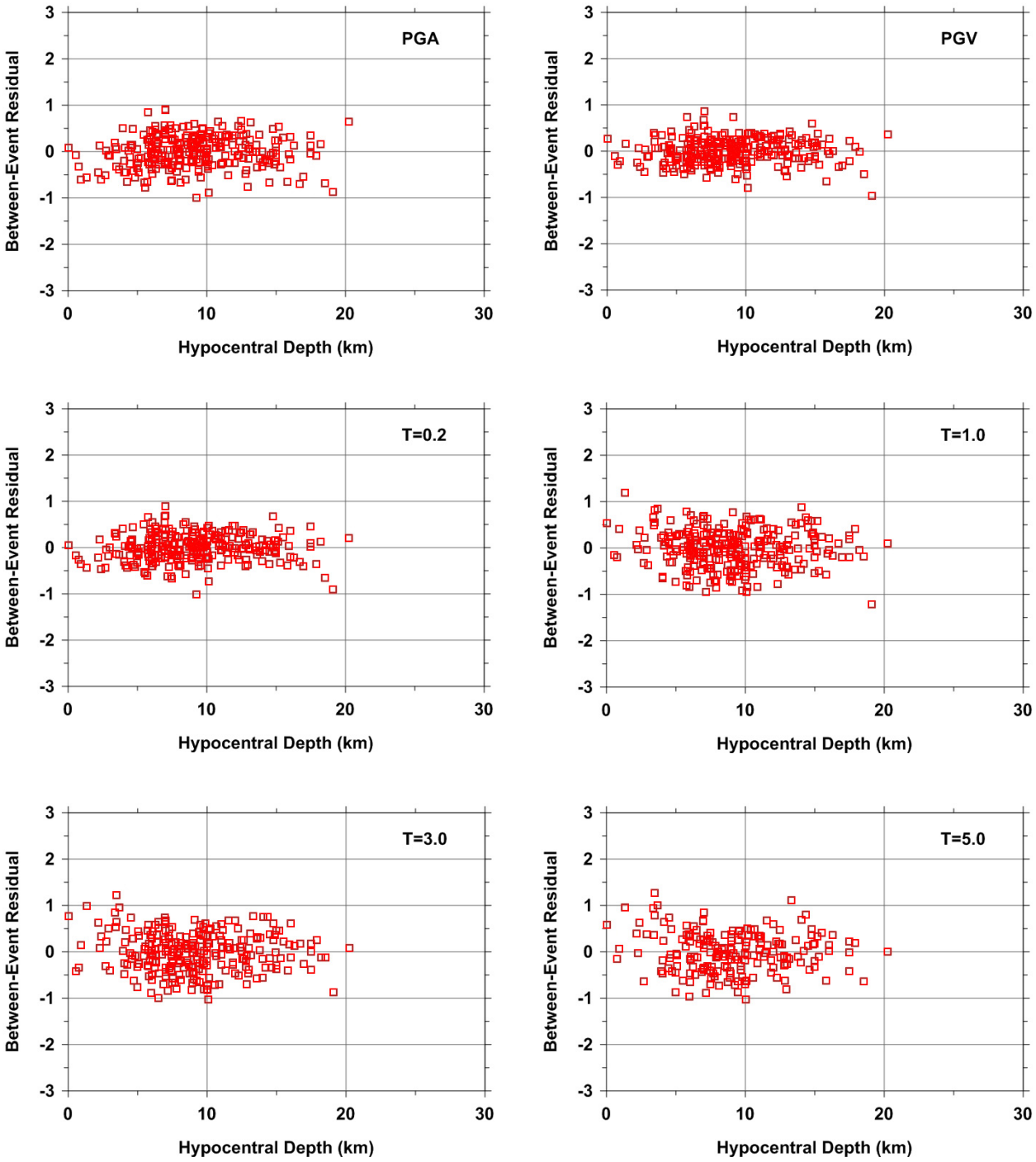

Figure 3.2 Dependence of between-event residuals on hypocentral depth.

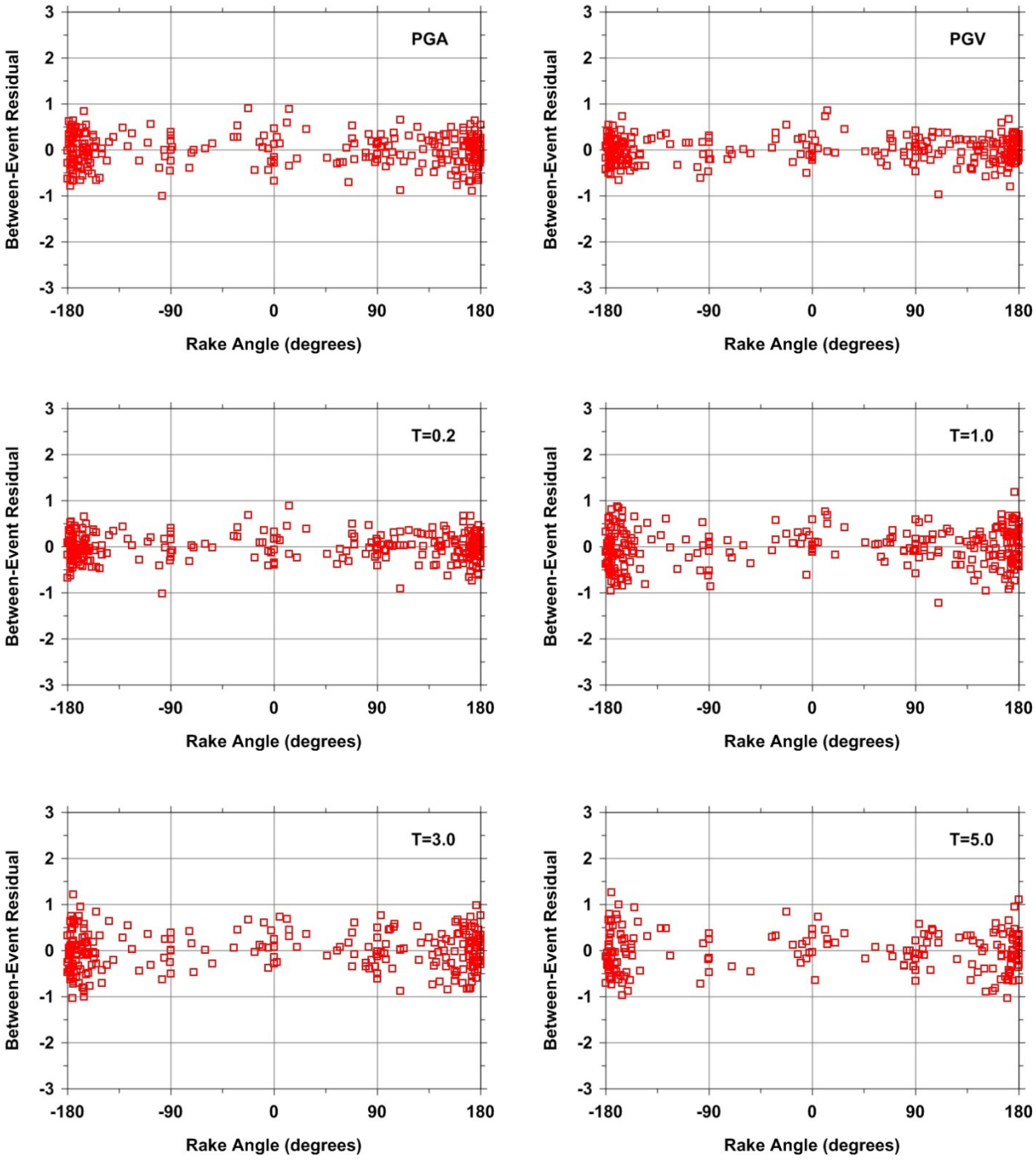

Figure 3.3 Dependence of between-event residuals on rake.

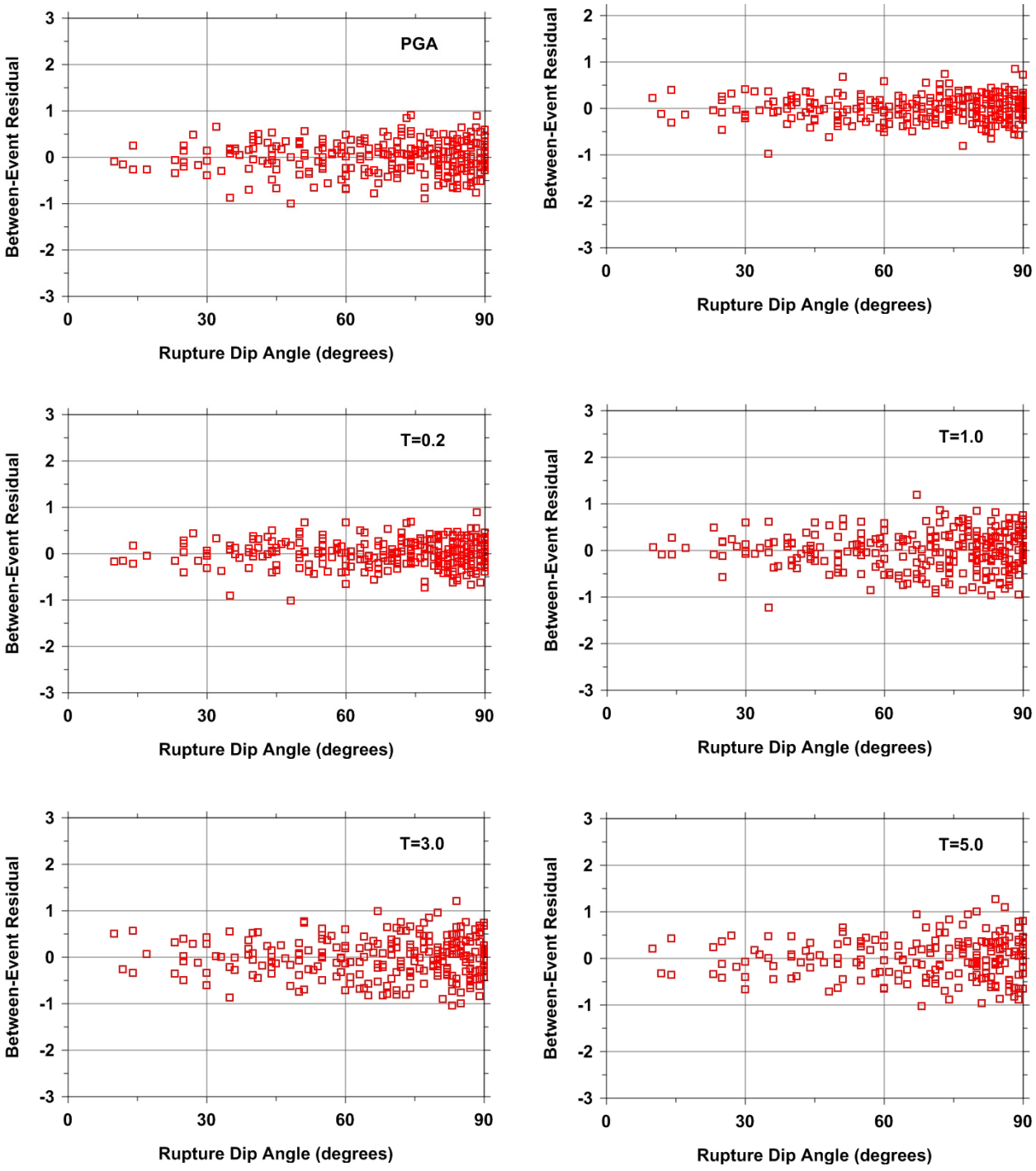

Figure 3.4 Dependence of between-event residuals on rupture dip.

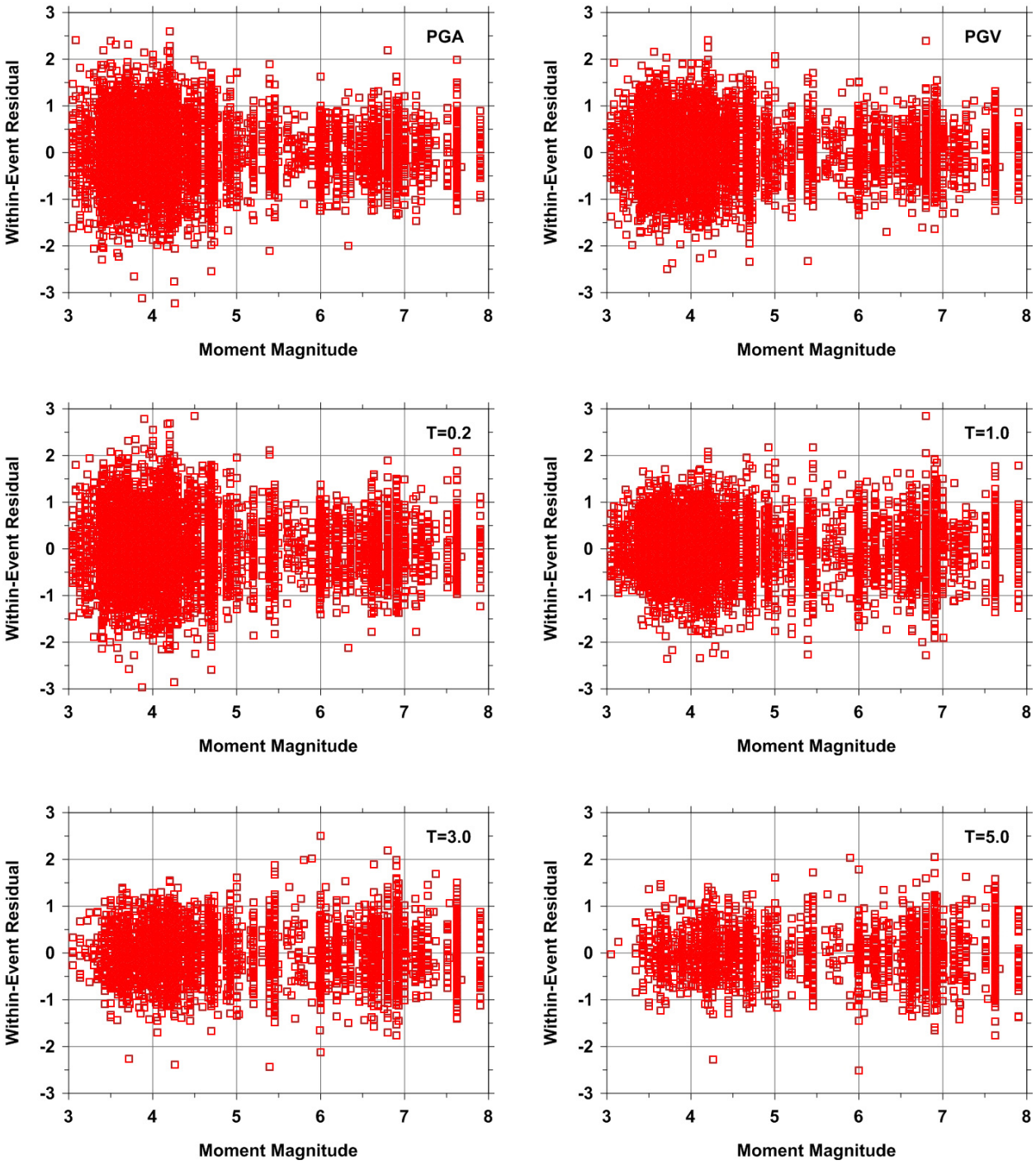

Figure 3.5 Dependence of within-event residuals on earthquake magnitude.

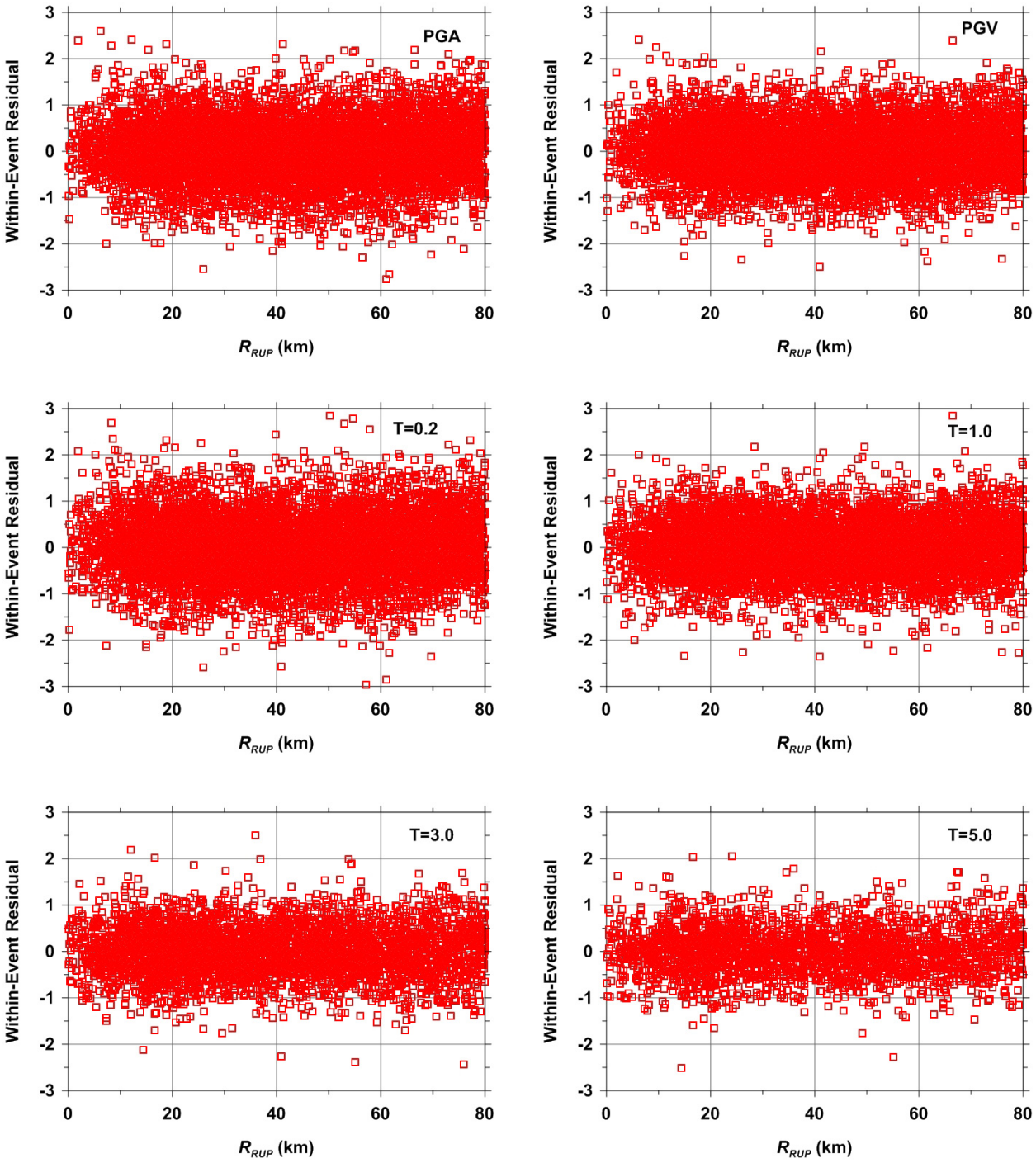

Figure 3.6(a) **Dependence of within-event residuals on rupture distance for distances ranging from 0 to 80 km.**

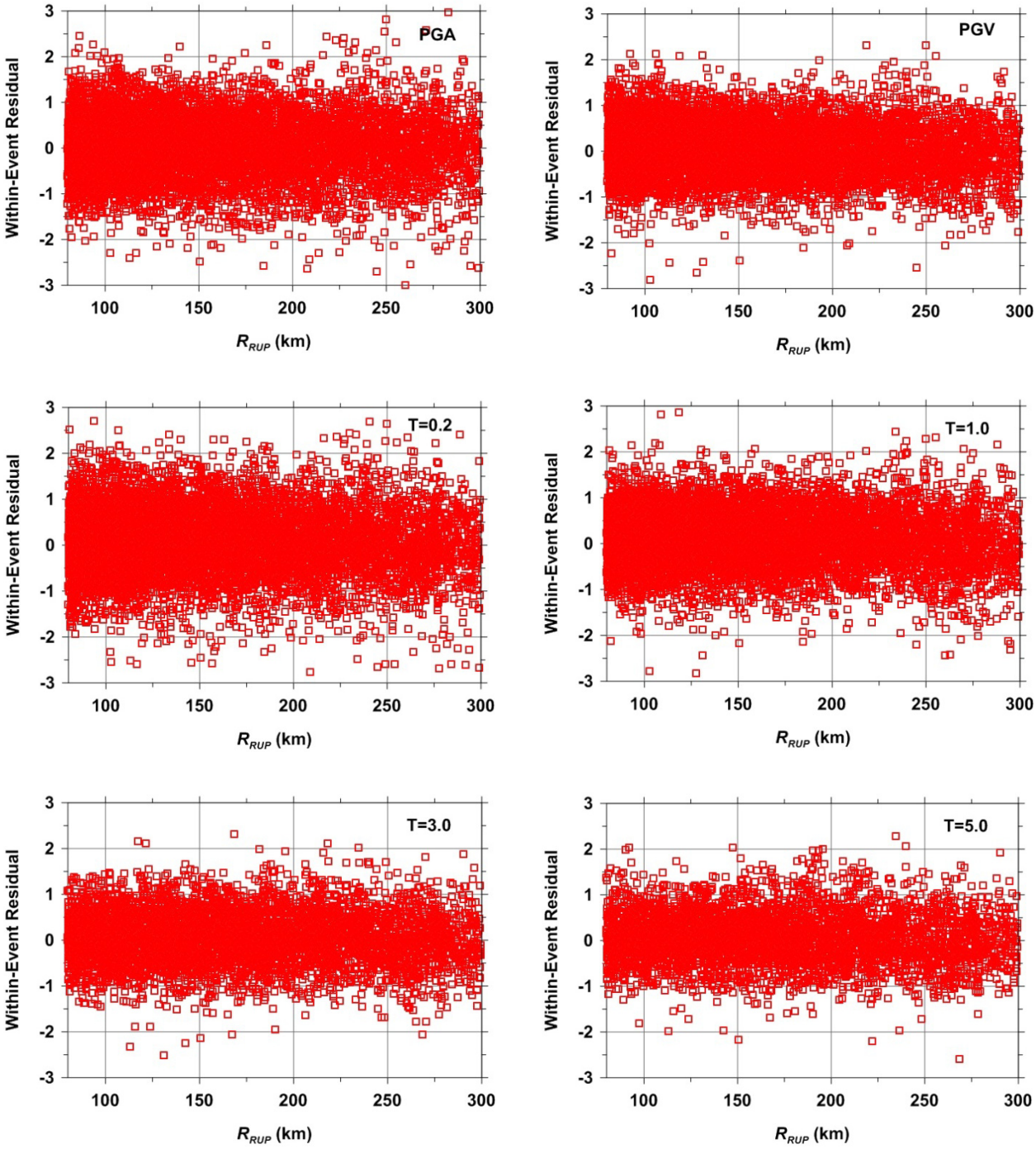

Figure 3.6(b) **Dependence of within-event residuals on rupture distance for distances ranging from 80 to 300 km.**

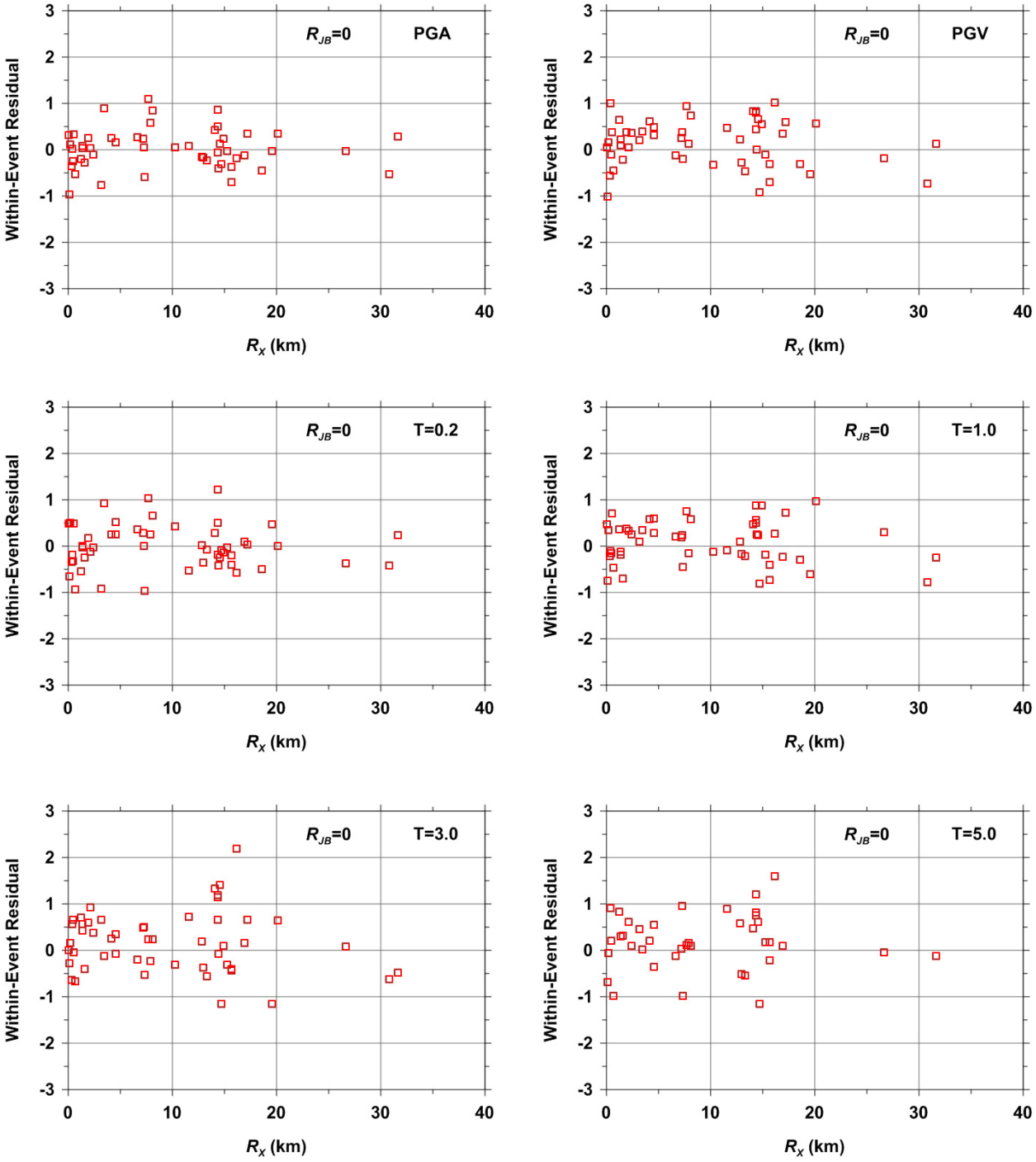

Figure 3.7 **Dependence of within-event residuals on horizontal distance for sites located over the rupture plane.**

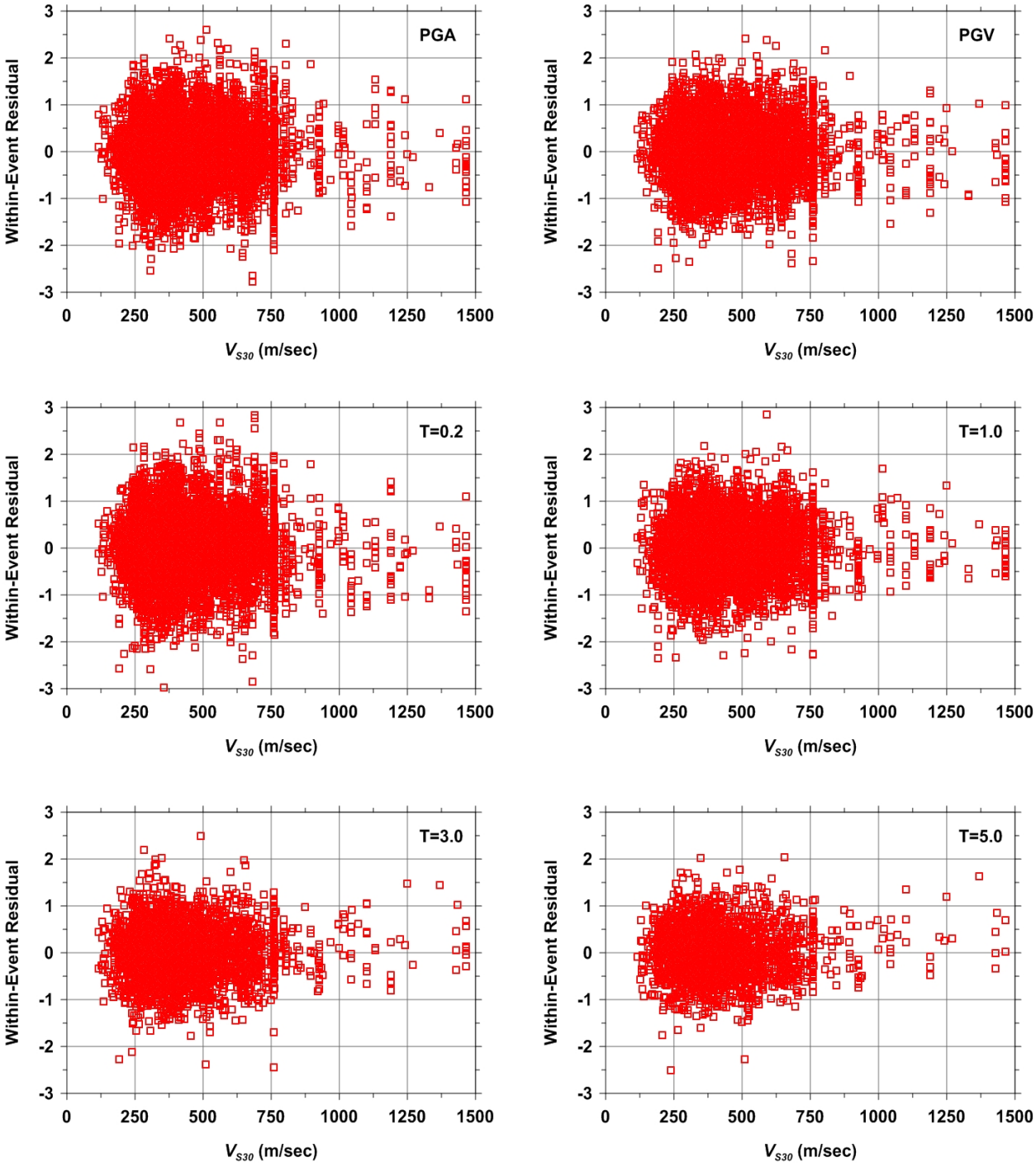

Figure 3.8 Dependence of within-event residuals on 30-m shear-wave velocity.

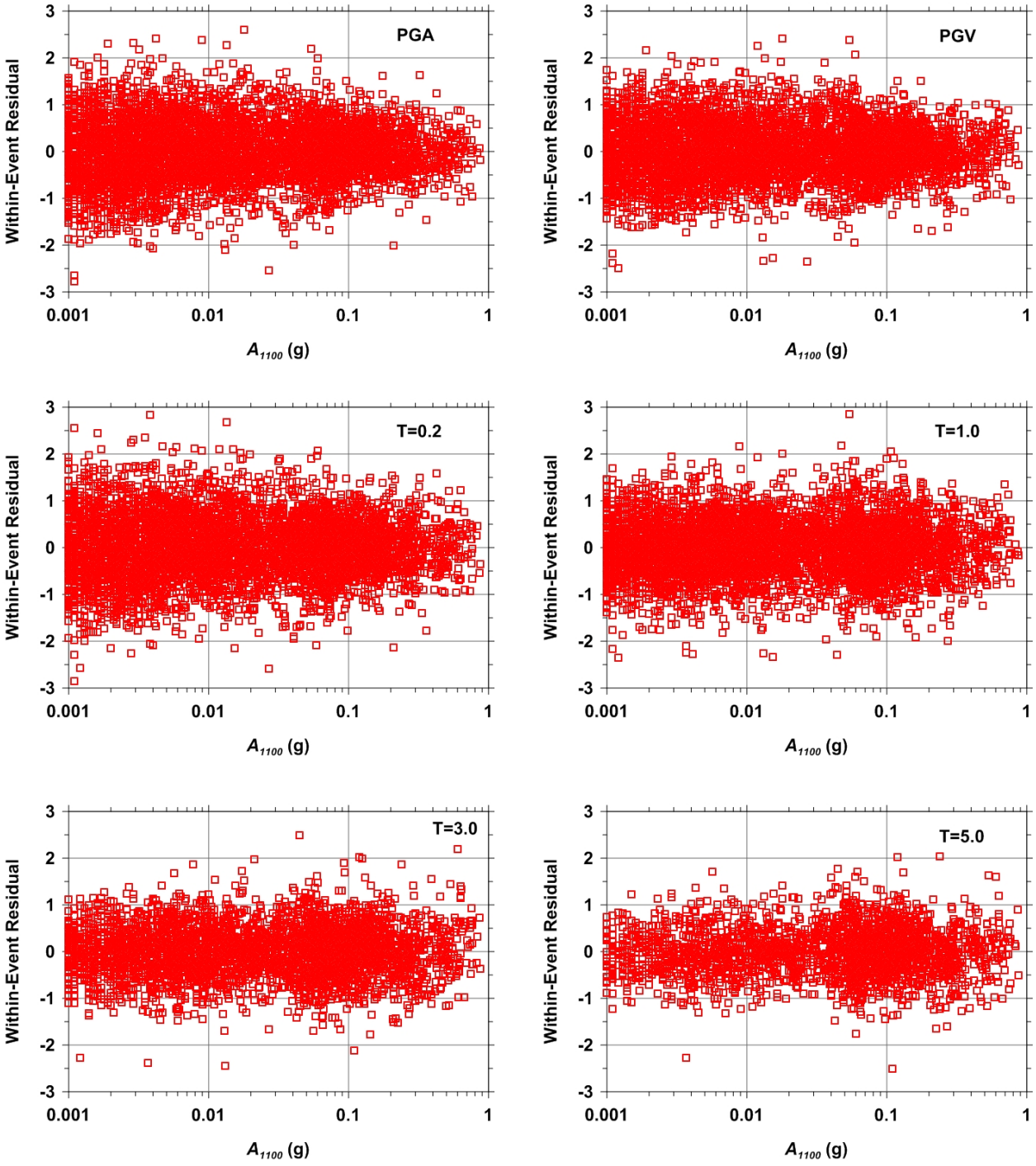

Figure 3.9 Dependence of within-event residuals on rock PGA.

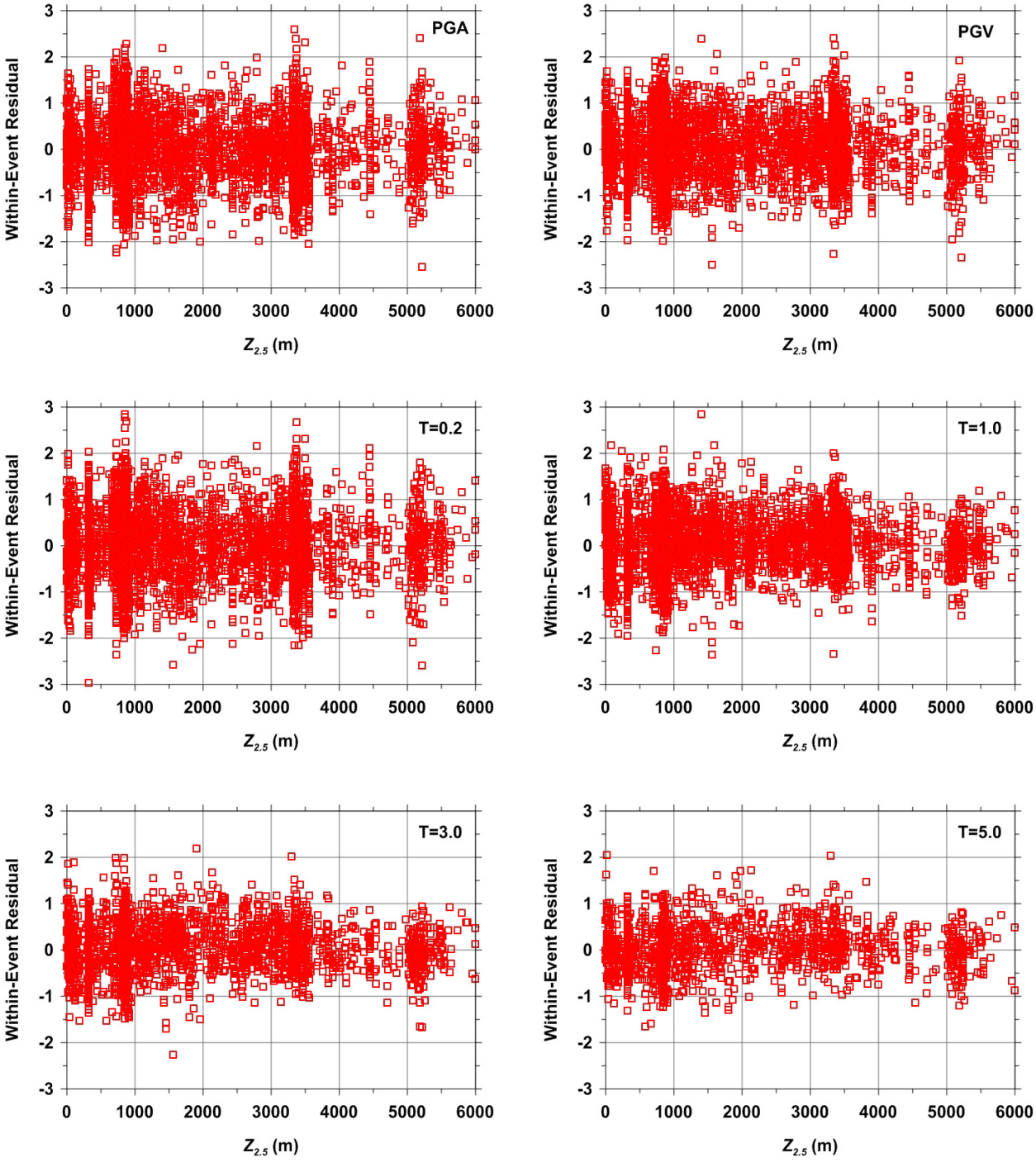

Figure 3.10 Dependence of within-event residuals on sediment (basin) depth.

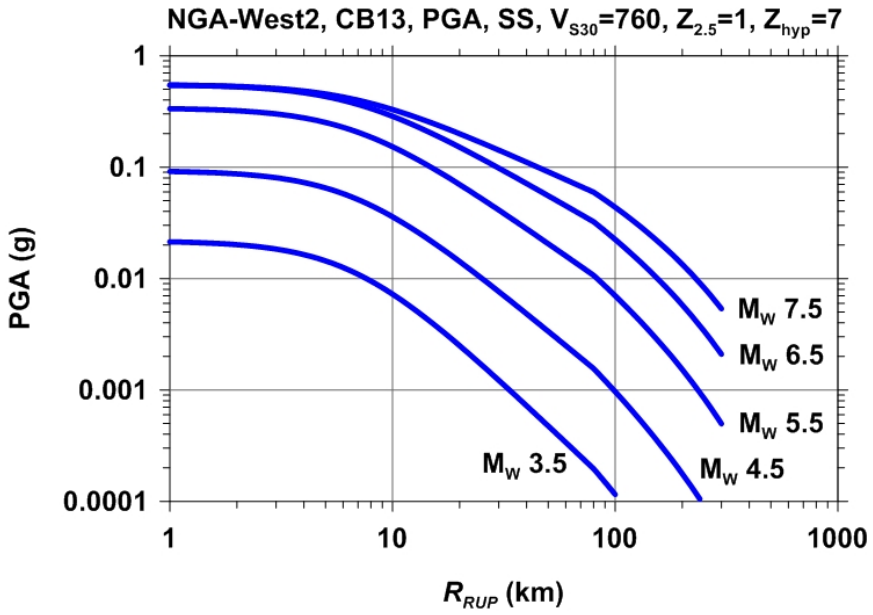

Figure 3.11 Scaling of PGA with distance for the CB13 model.

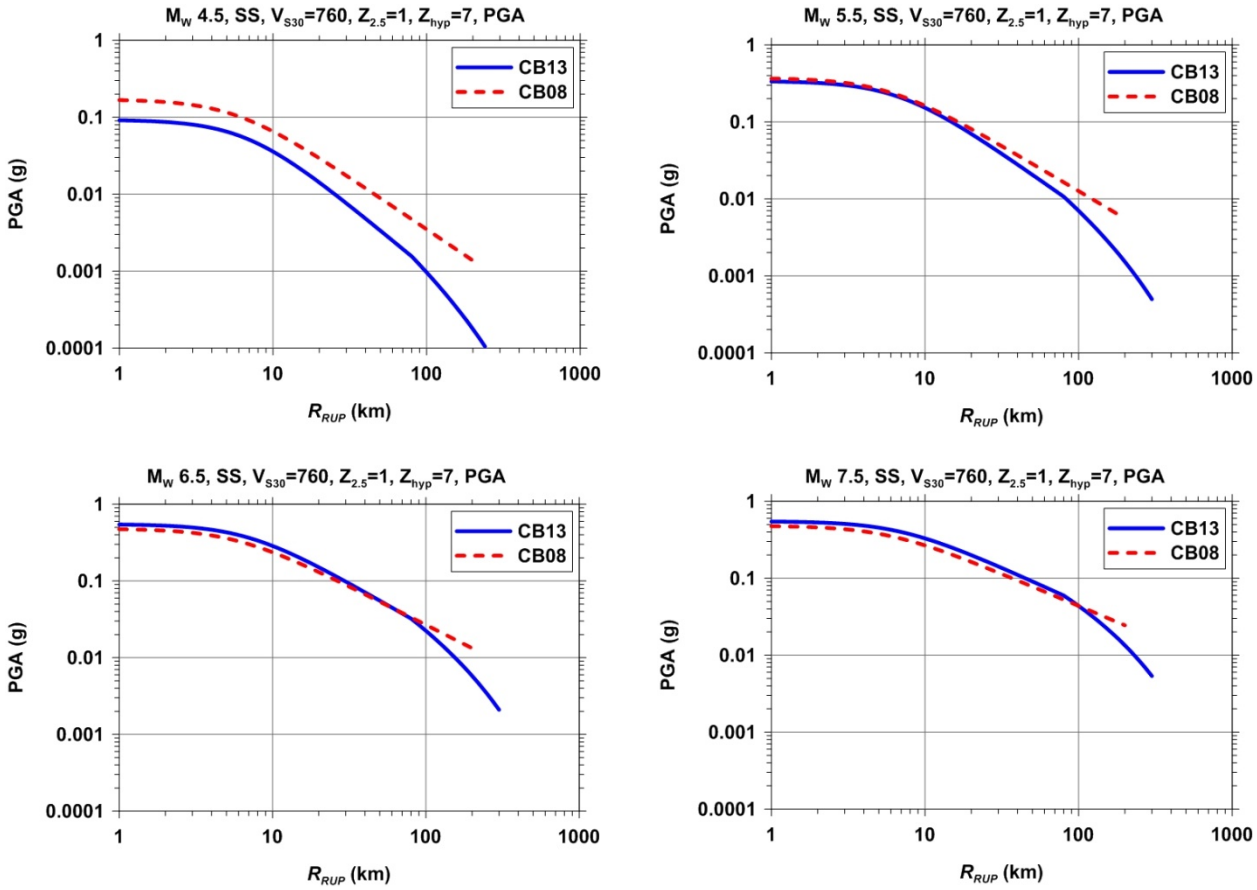

Figure 3.12 Scaling of PGA with distance for strike-slip faults comparing the CB08 and CB13 models.

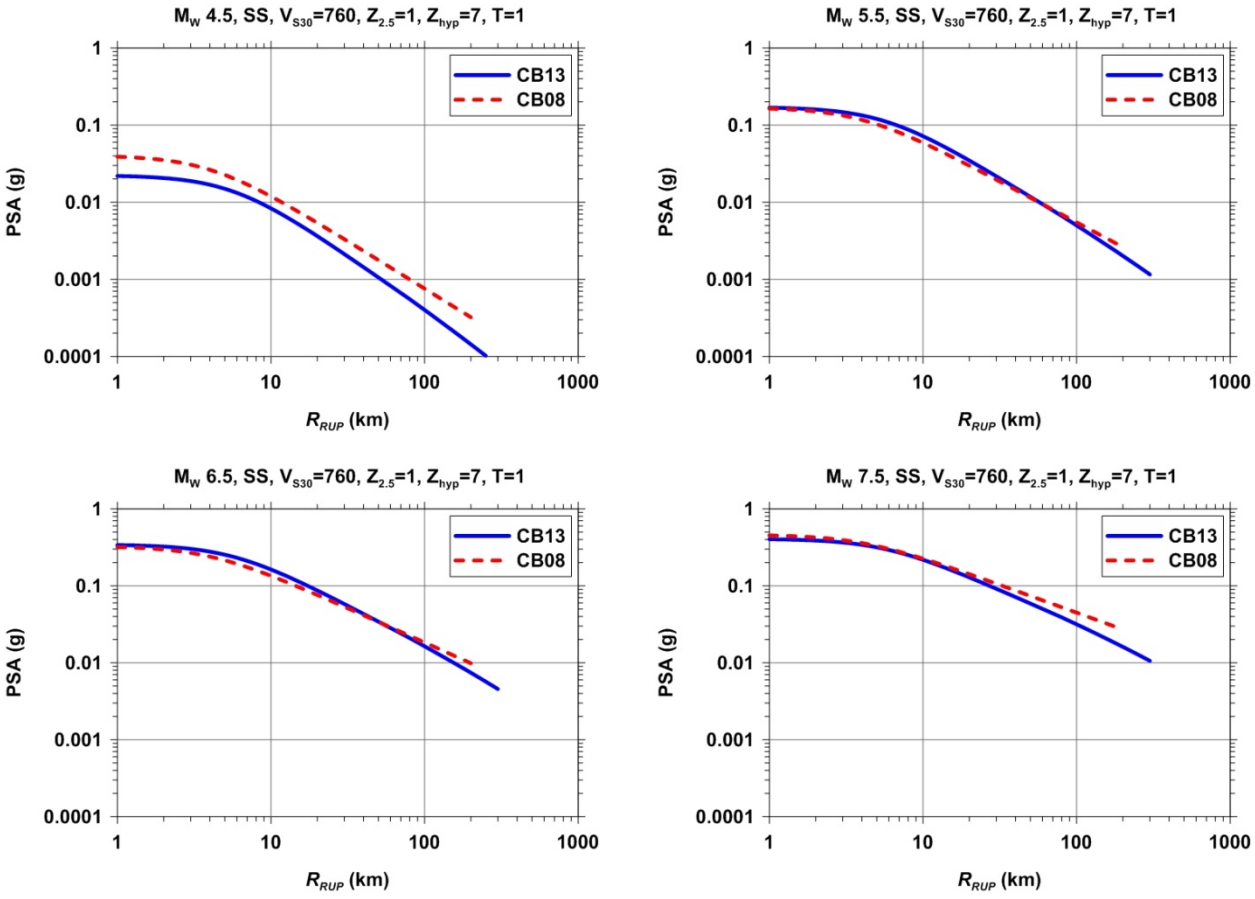

Figure 3.13 **Scaling of PSA (T = 1 sec) with distance for strike-slip faults comparing the CB08 and CB13 models.**

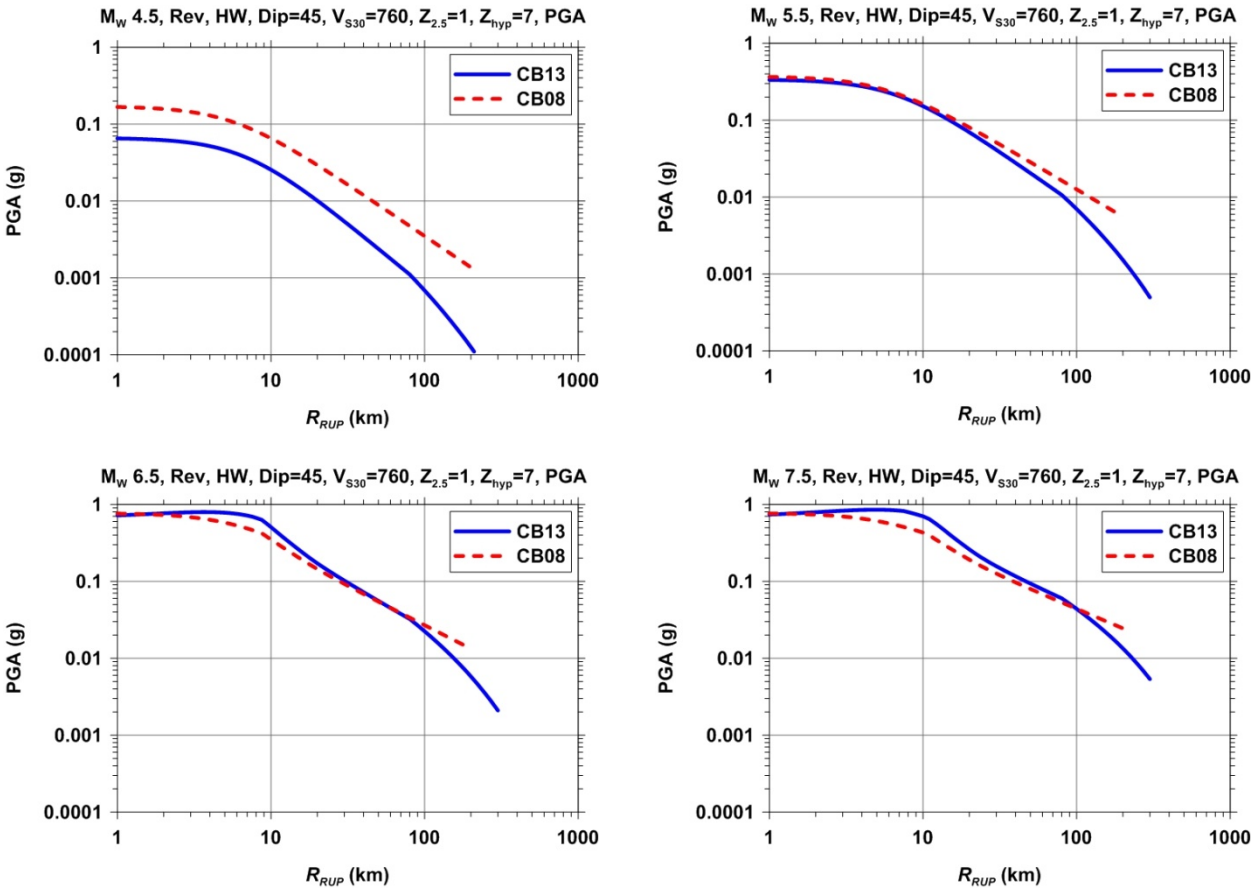

Figure 3.14 **Scaling of PGA with distance for reverse faults comparing the CB08 and CB13 models.**

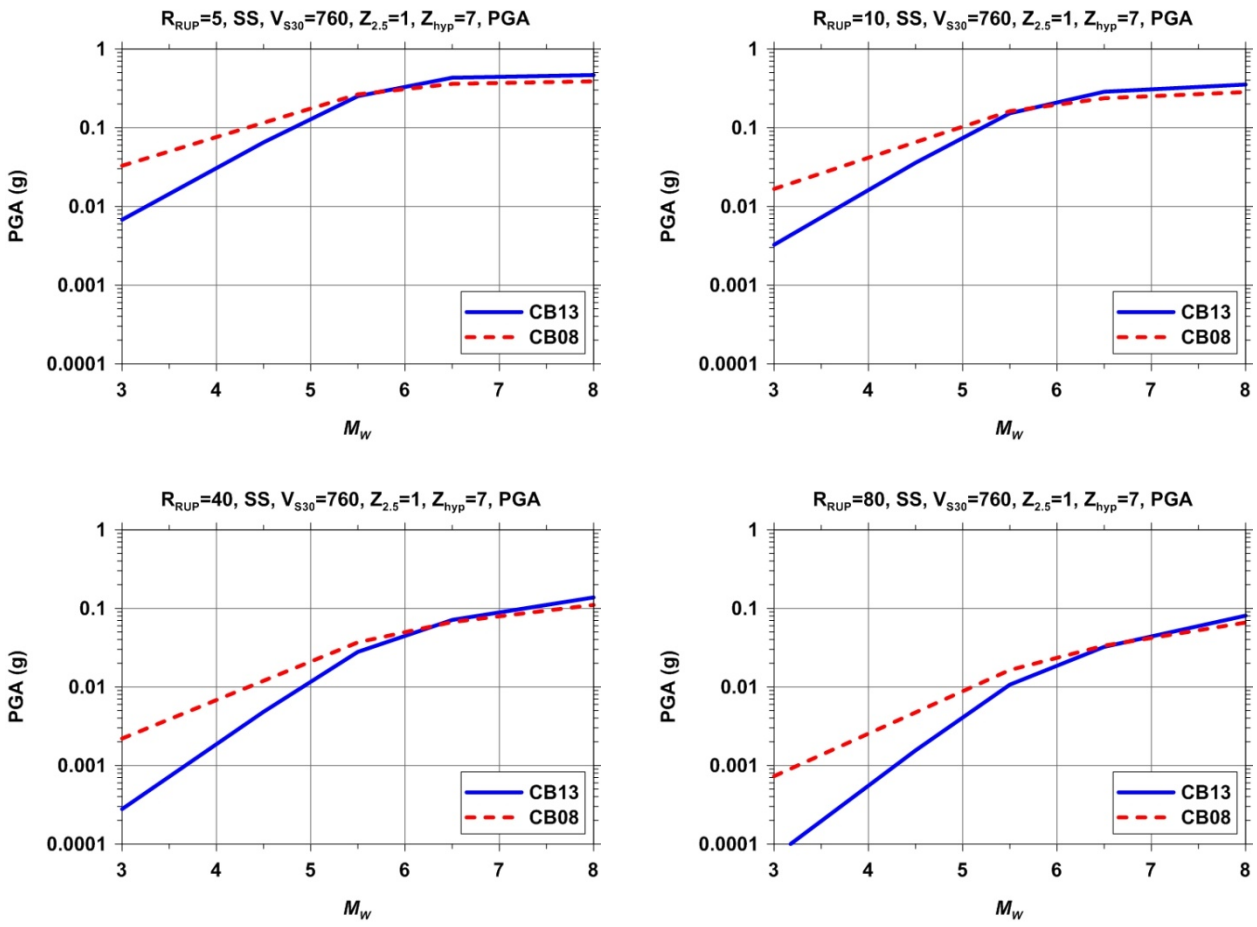

Figure 3.15 **Scaling of PGA with magnitude for strike-slip faults comparing the CB08 and CB13 models.**

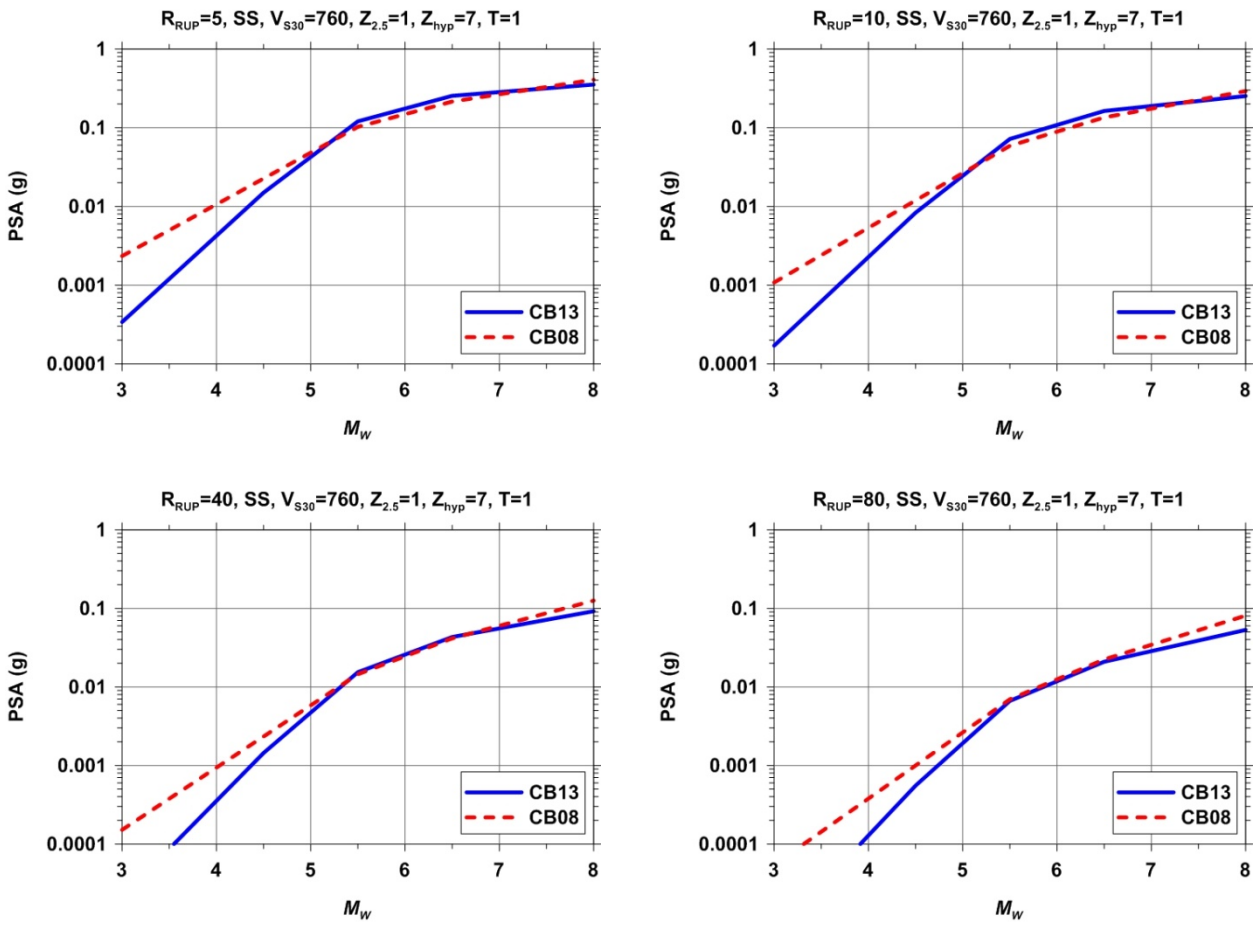

Figure 3.16 **Scaling of PSA (T = 1 sec) with magnitude for strike-slip faults comparing the CB08 and CB13 models.**

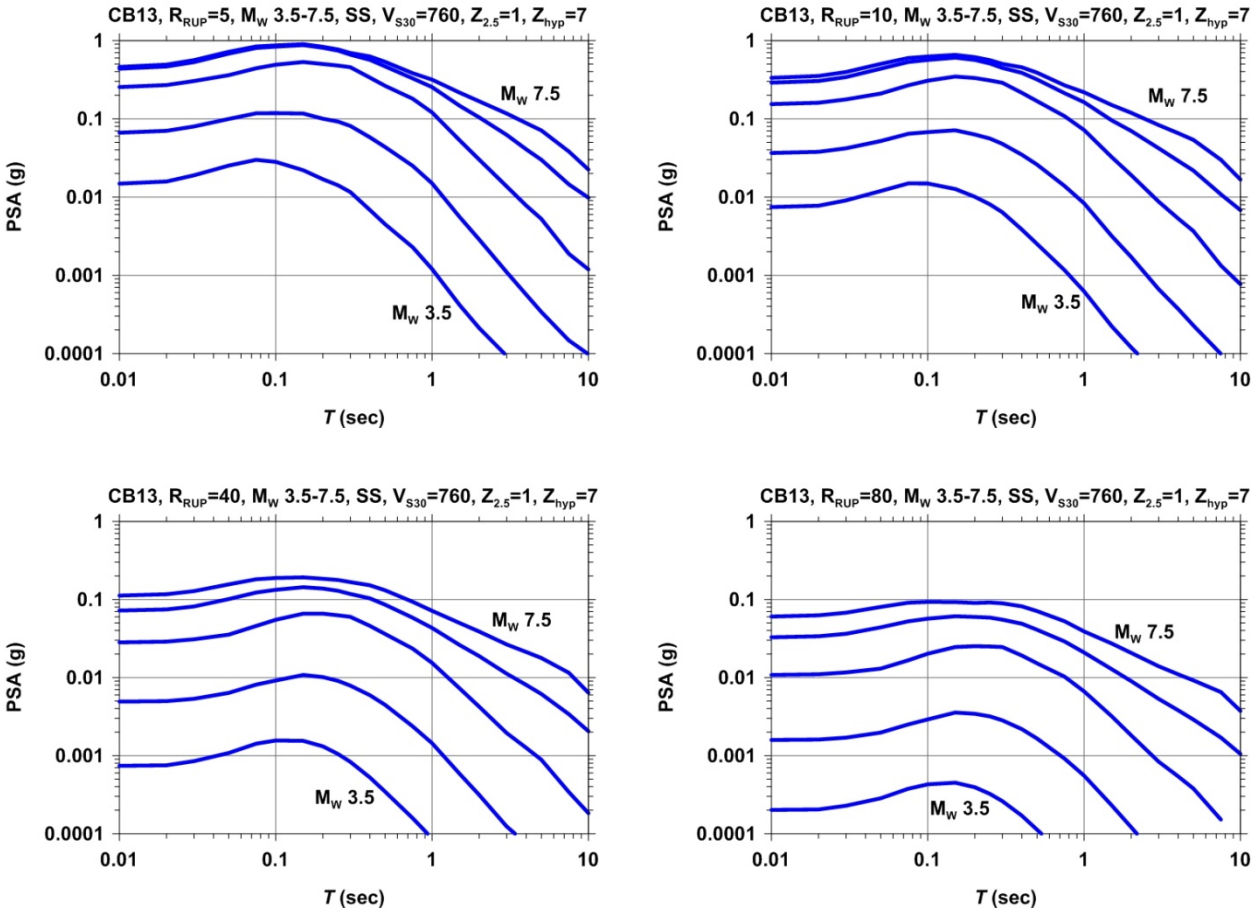

Figure 3.17 Scaling of PSA with magnitude (M3.5, 4.5, 5.5, 6.5 and 7.5) for the CB13 model.

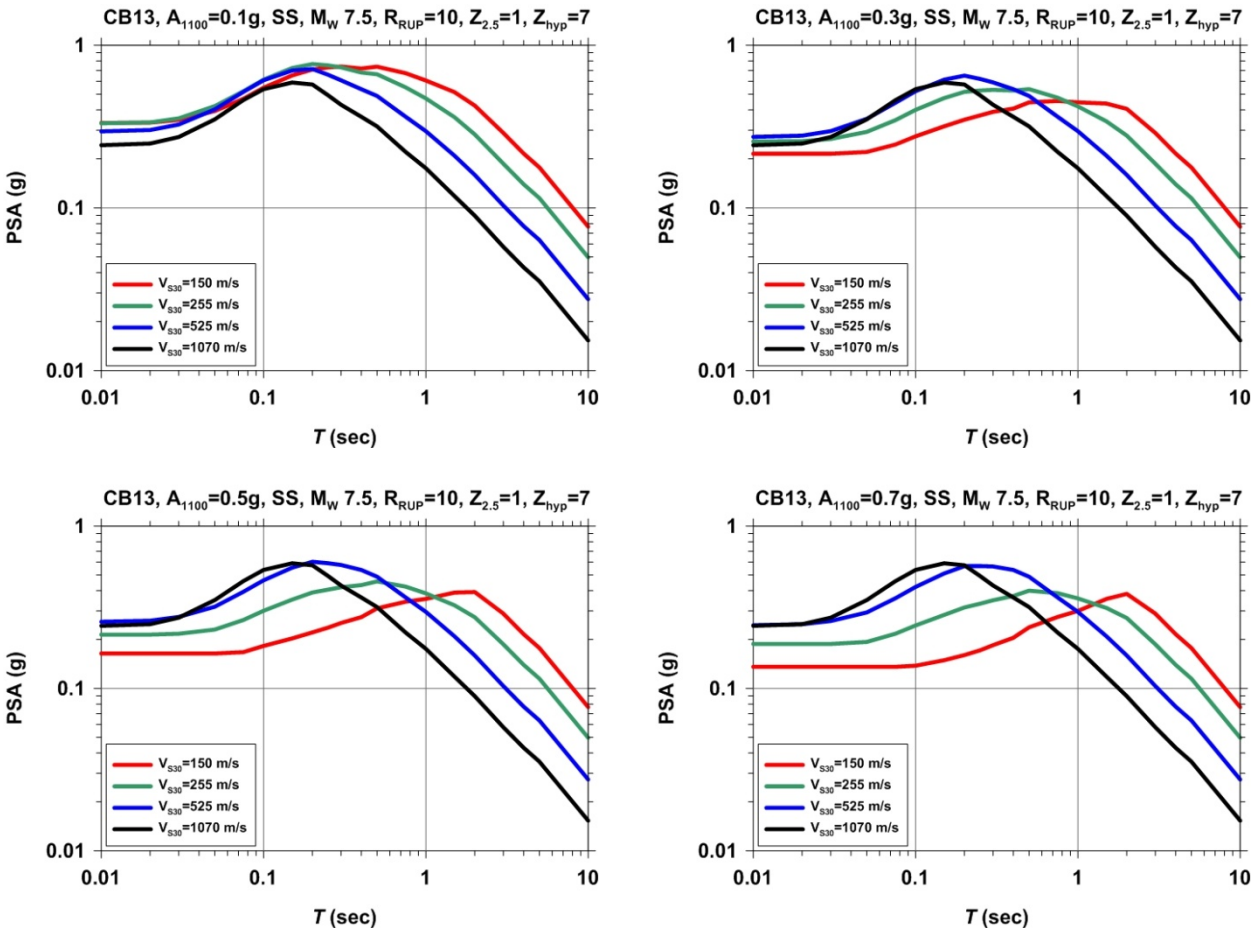

Figure 3.18 Scaling of PSA with site conditions and rock PGA for the CB13 model.

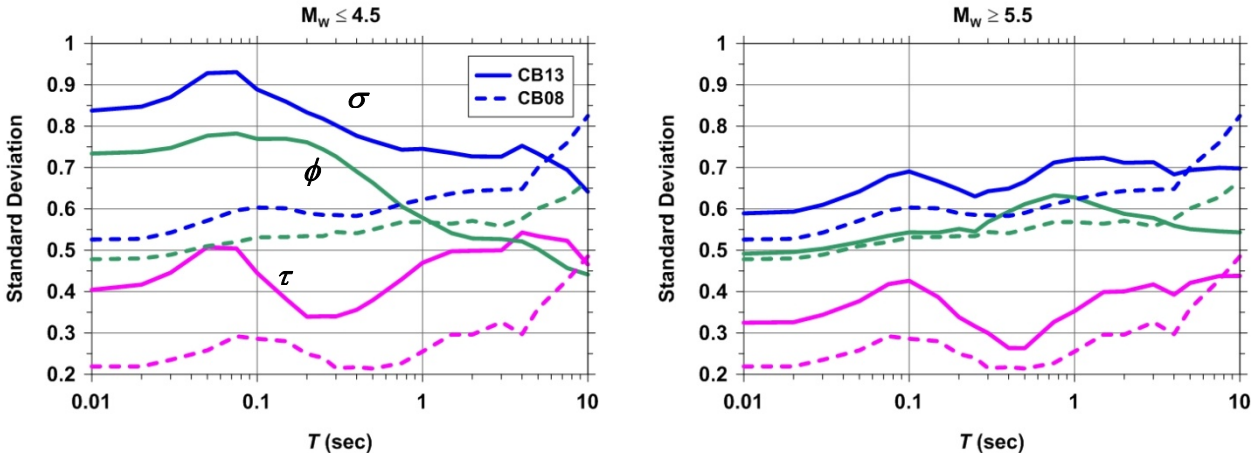

Figure 3.19 Aleatory standard deviations for τ (purple), ϕ (green) and σ (blue) comparing the CB08 and CB13 models.

4 Justification of Functional Forms

This chapter presents the justification for the functional forms of the predictor variable terms used to develop our median ground motion and aleatory uncertainty models. Sections include a discussion of the magnitude term, the geometric attenuation term, the style-of-faulting term, the hanging-wall term, the shallow site response term, the basin response term, the hypocentral depth term, the rupture dip term, and the anelastic attenuation term.

4.1 MAGNITUDE TERM

The quadrilinear functional form used to model f_{mag} was derived from an analysis of residuals. An additional linear scaling term for $\mathbf{M} < 4.5$ was needed to extend our previous trilinear scaling model down to $\mathbf{M} = 3$. The addition of the small-magnitude recordings to the NGA-West2 database together with this additional break in the magnitude scaling mitigated the over-prediction of small-magnitude ground motions that we observed in our NGA-West1 model as noted by Campbell (2008, 2011). This functional form models the observed decrease in the degree of magnitude scaling with increasing magnitude at short distances, commonly known as "magnitude saturation" (Campbell 1981), using a piecewise linear function rather than the more commonly used quadratic function. The piecewise linear scaling term for $\mathbf{M} > 6.5$ allows greater control of the large-magnitude scaling and, unlike the quadratic scaling model, decouples this scaling from that of smaller magnitudes allowing more flexibility in determining how ground motions scale with earthquake size. The stochastic simulations of Baltay and Hanks (2013a,b) confirmed that a piecewise linear model was able to fit the magnitude-scaling characteristics of ground motion just as well as the quadratic model over the magnitude range of interest in this study (Figure 4.1).

The regression analysis using the quadrilinear magnitude term predicted "oversaturation" (i.e., decreasing ground motion with increasing magnitude) for PGA and short-period ($T \leq 0.2$ sec) PSA for large magnitudes and short distances. This behavior, which had been noted in previous studies including our NGA-West1 study but not considered to be reliable, was still evident even after adding many more $\mathbf{M} > 6.5$ earthquakes, including the 2008 ($\mathbf{M}7.9$) Wenchuan earthquake. Although some seismologists believe that such a reduction in short-period ground motion is possible for very large earthquakes (e.g., Schmedes and Archuleta 2007; Tom Hanks, personal communication; Dave Boore, personal communication), this behavior was not allowed in our model as discussed further below.

Other functional forms were either found to be too difficult to constrain empirically (e.g., the hyperbolic tangent function used by Campbell 1997, 2000, 2001) or could not be reliably extrapolated to magnitudes as large as $\mathbf{M} = 8.5$ (e.g., the quadratic function used by many other investigators) as required by the PEER NGA-West2 Project. It is interesting to note that in our pre-NGA models (Campbell and Bozorgnia 2003a, 2003b, 2003c, 2004) we found it necessary to force magnitude saturation at all spectral periods in order to make the regression analysis converge. In our NGA-West1 (Campbell and Bozorgnia 2008) and NGA-West2 models this constraint was not necessary nor was it warranted at moderate-to-long periods.

During the review process of the NGA-West1 models, one of the reviewers was concerned that many of the large earthquakes in the PEER database had ground motions that were biased low because of a potentially biased distribution of recordings with respect to the tectonic domain, the source-site azimuth, and the location of large asperities on the rupture plane. This reviewer did, however, support the notion that short-period ground motion should "saturate" with magnitude near the fault. The concept of magnitude saturation was later verified by Frankel (2009) using broadband ground motion simulations of extended fault sources. Halldorsson and Papageorgiou (2005) also found a breakdown in self-similar magnitude scaling of high-frequency ground motion from worldwide crustal "interplate" earthquakes at $\mathbf{M} > 6.3$ that caused them to add a parameter to significantly decrease high-frequency magnitude scaling at large magnitudes in their specific barrier model. They attributed this deviation to a decrease in "effective" source area and/or irregularities in the rupture kinematics (i.e., a source effect). This supports the Hanks and Bakun (2002) finding that the rupture area of shallow continental earthquakes is less dependent on magnitude at $\mathbf{M} > 6.7$, which they attributed to a breakdown in self-similar magnitude scaling after coseismic rupture extends the full width of the seismogenic zone. This is also consistent with the *L* (length) rupture model of Scholz (1982). Douglas (2002) also found empirical evidence in support of the *L*-model's inferred near-source magnitude-scaling characteristics for PGA and PGV. Baltay and Hanks (2013a,b) found that they had to allow magnitude saturation at $\mathbf{M} > 6.6$ for PGA and $\mathbf{M} > 6.9$ for PGV when fitting stochastic simulations to NGA-West2 recordings within 20 km of the rupture plane. Schmedes and Archuleta (2007) used kinematic ground motion simulations of a strike-slip fault with a large aspect ratio (length/width ratio) to show that PGV increases to a maximum at a critical distance along the fault and then decreases to an asymptotic level beyond this distance that is related to the rupture width. Di Toro et al. (2006) gave a possible physical reason for a breakdown in self similarity. They concluded from investigations of exhumed faults and from laboratory experiments in granitoids (tonalities) that dynamic shear resistance becomes low at 10 km depths when coseismic slip exceeds around one meter due to friction-induced melting on the fault surface. According to Wells and Coppersmith (1994), one meter of displacement corresponds to an earthquake of approximately $\mathbf{M} = 6.7 - 6.9$.

These observations could possibly be interpreted as possible evidence for oversaturation of ground motion with magnitude. However, considering the weak statistical evidence for oversaturation in our analyses and the general support of the U.S. Geological Survey (USGS) and other seismologists and engineers that short-period ground motion can saturate but not necessarily oversaturate, we conservatively decided to constrain f_{mag} to remain constant (i.e., saturate but not oversaturate) at $\mathbf{M} > 6.5$ and $R_{RUP} = 0$ when oversaturation was indicated by the

regression analysis. This constraint is equivalent to setting $c_4 = -c_1 - c_2 - c_3 - c_6 \ln(c_7)$ in Equation (3.2).

Using a simple seismological model, Jack Boatwright (written communication, 2005) showed that the far-field magnitude-scaling coefficient of $\log \mathrm{PGA}$ and $\log \mathrm{PSA}$ at short periods for earthquakes of $\mathbf{M} > 6.7$ should be less than about $0.38\,\Delta\mathbf{M}$. In this magnitude range PGA and PSA can be expected to saturate with magnitude at close distances. The large-magnitude scaling in our model increases with distance due to the positive value of c_6. Nonetheless, after converting our large-magnitude scaling coefficient c_4 from a natural to a common logarithm we get PGA and short-period magnitude-scaling coefficients that are less than Boatwright's limit out to a distance of at least 200 km.

Baltay and Hanks (2013a,b) show that the magnitude-scaling characteristics of PGA and PGV inferred from the PEER NGA-West2 database for recordings within 20 km of the rupture plane are consistent with the magnitude-scaling characteristics of a Brune (1970, 1971) single-corner point-source (SCPS) stochastic simulation model with constant stress parameter from $\mathbf{M} = 3$ to a specified magnitude where saturation is observed. They found this saturation to occur at about $\mathbf{M} = 6.6$ for PGA and $\mathbf{M} = 6.9$ for PGV. The stress parameter was assumed to be independent of magnitude at 53 bars for both PGA and PGV. Site amplification was estimated from the quarter-wavelength method using the western United States crustal model of Boore and Joyner (1997) with a site shear-wave velocity of $V_{S30} = 620$ m/sec and a site attenuation parameter (Anderson and Hough 1984; Hough et al. 1988; Anderson 1991) of $\kappa_0 = 0.04$ sec. The magnitude at which magnitude saturation occurs is consistent with the threshold of 6.5 at which saturation occurs in our model. Baltay and Hanks (2013a,b) also show that their near-source magnitude scaling can be approximated by a piecewise linear model with breakpoints at $\mathbf{M} = 3.3$, 4.5 and at either 6.6 (PGA) or 6.9 (PGV). Although we have another breakpoint at $\mathbf{M} = 5.5$, which is required at further distances and longer periods, our predicted PGA near-source magnitude scaling from $\mathbf{M} = 4.5 - 5.5$ and $\mathbf{M} = 5.5 - 6.5$ is similar to that predicted by Baltay and Hanks (Figure 4.1).

4.2 GEOMETRIC ATTENUATION TERM

Our source-to-site distance term f_{dis} incorporates magnitude-dependent apparent geometric attenuation through the model coefficient c_6. This coefficient is well constrained empirically and varies from about 0.14 at long periods to 0.25 at short periods. In order to isolate the effects of geometric attenuation and avoid a trade-off with apparent anelastic attenuation, we first performed the regression analyses using recordings with $R_{RUP} \leq 80$ km. This analysis showed that geometric attenuation was regionally independent out to this distance, which greatly simplified the regression analyses.

Jack Boatwright (written communication, 2005) used a simple seismological model to show that the magnitude-dependent geometric attenuation coefficient c_6 should be less than 0.17 for $\log \mathrm{PGA}$ and $\log \mathrm{PSA}$. Our range of values bracket this estimate. However, because our estimates are so well constrained empirically, we chose not to set $c_6 = 0.17$ in our NGA-West2

model like we did in our NGA-West1 model. The geometric attenuation of PGA and PSA predicted by f_{dis} includes the effects of duration as well as geometric spreading and whatever anelastic attenuation there is at $R_{RUP} \leq 80$ km. Because the attenuation within this distance range behaves similar to geometric attenuation (i.e., it decays as r^{-n}), we refer to it as apparent geometric attenuation or simply geometric attenuation. We predict stronger overall geometric attenuation rates than either our NGA-West1 model or the theoretical values of –1 for a point source and –0.5 for an infinitely long fault predicted by Boatwright's simple seismological model. For **M**=5 we get values that systematically range from about –2.0 to –1.7 for **M**=3, –1.6 to –1.3 for **M**=5, and –0.9 to –0.8 for **M**=8 from short periods to long periods. As expected, our values are consistently higher than the theoretical values obtained from simple seismological theory. Frankel (2009) used broadband ground motion simulations of extended fault sources to show that the distance decay of PSA from simulations was consistent with the NGA-West1 models for magnitudes of 6.5 and 7.5 and distances ranging from about 2 to 100 km.

4.3 STYLE-OF-FAULTING TERM

The functional form used to model f_{flt} was determined from an analysis of residuals. In our NGA-West1 model we used Z_{TOR} to represent whether or not coseismic rupture extended to the surface. This predictor variable was found to be important for modeling reverse faults. Ground motions were found to be significantly higher for reverse faults when rupture did not propagate to the surface regardless of whether this rupture was on a blind thrust fault or on a fault with previous surface rupture. When rupture broke to the surface or to very shallow depths, ground motions for reverse faults were found to be comparable on average to those for strike-slip faults. Some strike-slip ruptures with partial or weak surface expression also appeared to have higher-than-average ground motions (e.g., 1995 Kobe, Japan, earthquake) but there were many counter examples in the database. Some of these discrepancies could have been due to the ambiguity in identifying coseismic surface rupture for strike-slip events. As a result, we decided that an additional study or additional data would be needed in order to resolve these discrepancies before it was possible to consider Z_{TOR} as a predictor variable for strike-slip faulting.

Somerville and Pitarka (2006) give both empirical and theoretical evidence to support their conclusions that ground motions from earthquakes that break the ground surface are weaker than those from buried events. Dynamic rupture simulations show that if a weak zone exists at shallow depths, rupture of the shallow part of the fault will be controlled by velocity strengthening with larger slip-weakening distance, larger fracture energy, larger energy absorption from the crack tip, lower rupture velocity, and lower slip velocity than at greater depths on the fault. These properties lead to lower ground motions for surface and shallow faulting than for buried faulting. The field and laboratory results of Di Toro et al. (2006) also indicate that this phenomenon might extend to intermediate crustal depths as well due to melting on the fault surface during large coseismic slip. If this is true we would expect this phenomenon to occur for all earthquakes of large enough slip (about one meter according to Di Toro et al. 2006). However, this phenomenon is interrelated with magnitude-scaling effects so it might be that the presence of a weak shallow layer adds to this effect for surface-rupturing earthquakes.

After adding hypocentral depth Z_{HYP} as a predictor variable, we found that we no longer needed to make a simple distinction between surface rupture and buried rupture. As before, we found that there is no significant difference between strike-slip and reverse mechanisms at short periods. With the addition of more normal mechanism earthquakes the normal-faulting factor is now statistically significant at a factor of about –25% at short periods decreasing to no difference at mid-to-long periods similar to the findings of Ambraseys et al. (2005). However, as in our NGA-West1 model this factor becomes very large (in a negative sense) at periods greater than about 5 sec. We are concerned that these long-period effects are due to systematic differences in sediment depth, although these depths are not known, since many of these events occurred in a geological and tectonic environment that might be associated with shallow depths to hard rock (e.g., Italy and Greece). Our concern is corroborated by Ambraseys et al. (2005), who found that strike-slip and normal mechanism ground motions from similar regions in Europe and the Middle East had similar spectral amplitudes at moderate-to-long periods. Therefore, we constrained c_9 to be zero for $T \geq 3$ sec.

In our NGA-West2 model we found that the style-of-faulting effects observed for large-magnitude earthquakes were not observed for small-magnitude events. Therefore, we included the term $f_{flt,M}$ to phase out these effects at small magnitudes. The reason for the lack of style-of-faulting effects for small-magnitude earthquakes could be due to the greater uncertainty in the focal mechanisms of such small events that smears out any mechanism effects. It is intriguing to note that even though we did not find mechanism effects for small magnitudes, we did find a strong dependence on rupture dip which might be acting as a proxy for mechanism effects (see Section 4.8). Further studies will be required to determine whether there is a seismological reason for these observations.

4.4 HANGING-WALL TERM

The functional form used to model f_{hng} was a modified version of the model developed by Donahue and Abrahamson (2013) from ground motion simulations. This model incorporates rupture width, W, rupture dip, δ, and horizontal distance from the top edge of the rupture plane, R_X. Our analysis of residuals showed that although this model worked well over the rupture plane it predicted hanging-wall effects that were too strong off the rupture plane. Therefore, we included the term $f_{hng,R}$ to model the distance-dependence of f_{hng}. This term, which was also used in our NGA-West1 model, has the additional effect of smoothing out the transition between the hanging wall and the footwall that avoids an abrupt drop in predicted ground motion as the site crosses the fault trace. In its preliminary review of the NGA-West1 models for PEER, the USGS pointed out that there is very little data to support an abrupt drop from the hanging wall to the footwall over what can amount to a distance of only a few meters, and that providing a smooth transition from the hanging wall to the footwall would allow for some uncertainty in the location of the actual fault trace. We also included the terms $f_{hng,M}$ and $f_{hng,Z}$ in Equation (3.7) that are not in the Donahue and Abrahamson (2013) model in order to phase out hanging-wall effects at small magnitudes and large rupture depths where the

simulations or residuals indicated that these effects are either negligible or cannot be resolved from the data.

Similar to our NGA-West1 model, we have included hanging-wall effects for strike-slip and normal faults in our current model. Although the statistical evidence for hanging-wall effects for normal faults is weak because of a lack of recordings, it is consistent with the large amplitudes recorded over the rupture plane of the 2009 L'Aquila earthquake. Furthermore, Jim Brune (personal communication, 2006) noted that hanging-wall effects similar to those for reverse faults have been observed in foam rubber modeling of normal mechanism earthquakes in laboratory experiments and is consistent with the limited amount of precarious rock observations on the hanging wall of normal faults with documented historical and Holocene rupture in the Basin and Range Province of the United States. In a study of broadband simulations in the Basin and Range, Collins et al. (2006) found a hanging-wall factor for normal faults that is similar to the one we found empirically for reverse faults. It should be noted that, unlike a reverse fault, the hanging wall of a normal fault will typically lie beneath the range front valley where the majority of the population and infrastructure is located (e.g., Reno, Nevada, and Salt Lake City, Utah). Although most strike-slip earthquakes have rupture planes that dip too steeply to produce strong hanging-wall effects, those that do have observed ground motions that are empirically consistent with our predicted hanging-wall effects.

4.5 SHALLOW SITE RESPONSE TERM

The linear part of the functional form used to model f_{site} is similar to that originally proposed by Boore et al. (1994) and Borcherdt (1994) and later adopted by Boore et al. (1997), Choi and Stewart (2005), and the NGA-West1 models among others. One difference from our NGA-West1 model is that we no longer hold the site term to be constant for $V_{S30} = 1100$ m/sec when 30-m shear-wave velocities are greater than this value. Although, we recommend that the model not be used for $V_{S30} > 1500$ m/sec, which represents the boundary between NEHRP A and NEHRP B site categories (BSSC 2009). Extrapolation of the model to larger velocities is not constrained by data. Furthermore, as the site conditions get very hard, it is likely that the site attenuation parameter κ_0 becomes small enough that the trend of lower amplification with increasing V_{S30} might begin to flatten or even trend upwards.

We retain the same theoretical nonlinear soil term that we used to develop our NGA-West1 shallow site response term since the empirical data were insufficient to constrain the complex nonlinear behavior of the softer soils. After including the linear part of f_{site} in the model, the residuals clearly exhibited a bias when plotted against rock PGA, A_{1100}, consistent with the nonlinear behavior of PGA and PSA at shorter periods. However, because of the relatively small number of recordings, the residuals alone cannot be used to determine how this behavior varies with V_{S30}, ground motion amplitude, and spectral period. The nonlinear site-response model developed by Walling et al. (2008) based on one-dimensional (1D) equivalent-linear site-response simulations conducted by Silva (2005) was used to constrain the functional form and the nonlinear model coefficients k_1, k_2, n and c in Equation (3.18). This approach is supported by Kwok and Stewart (2006), who found that theoretical site factors from 1D

equivalent-linear site-response analyses were able to capture the average effects of soil nonlinearity when used in conjunction with empirical ground motion models to estimate a reference rock spectrum.

The linear behavior of our current model was calibrated by empirically fitting the model coefficients c_{11} through c_{13} in the regression analysis. The first of these coefficients applies to all recording sites except for those in Japan. We found that the linear V_{S30} scaling for sites in Japan was different than for sites outside of Japan, which come primarily from California. We also found that the V_{S30} scaling in Japan was especially different for softer sites defined as $V_{S30} < 200$ m/sec than for harder sites. The way that f_{site} is defined means that the scaling in Japan represents the difference between Japan and non-Japan regions, so that the coefficients are additive, meaning that the total model coefficient for the harder sites in Japan is equal to $c_{11} + c_{13}$ and that for the softer sites in Japan is equal to $c_{11} + c_{12} + c_{13}$. There might be differences in other regions as noted by Ancheta et al. (2013) and Stewart et al. (2013). However, there are an insufficient number of either earthquakes, recordings, or shear-wave velocities in our selected database to evaluate and model such effects.

Walling et al. (2008) developed two sets of nonlinear model coefficients: one set representing dynamic soil properties (i.e., strain-dependent shear modulus reduction and damping curves) developed by EPRI (1993), and another set representing dynamic soil properties developed by Silva et al. (1999), which these latter authors refer to as the Peninsular Range or PEN curves. Neither our residuals nor the empirical site factors compiled by Power et al. (2004) could distinguish between these two alternative models, although a slightly lower aleatory standard deviation favored the PEN model. We selected the PEN model because it represents a wider range of regional site conditions than the EPRI model (Silva, personal communication, 2005).

As part of the NGA-West2 Project, Kamai et al. (2013) revised the nonlinear site-response model of Walling et al. (2008) using the same 1-D simulations by Silva (2005) augmented by additional simulations for soft sites. We evaluated this model and found that the residuals for soft sites plotted against rock PGA was slightly better fit using the Walling et al. (2008) model. Therefore, we chose not to use the Kamai et al. (2013) model at this time. One of the advantages of the Kamai et al. (2013) model is that it uses rock PSA as the reference ground motion instead of rock PGA, thus eliminating the need for including the correlation between PSA and PGA in Equations (3.29) and (3.30). We will pursue this approach in a future study.

4.6 BASIN RESPONSE TERM

The functional form used to model f_{sed} has two parts: (1) a term to model 3D basin effects for $Z_{2.5} > 3$ km and (2) a term to model shallow sediment effects for $Z_{2.5} < 1$ km. This is the same functional form used in our NGA-West1 model. We modeled the functional form of the 3D basin term from numerical simulations conducted by Day et al. (2008). We modeled the shallow sediment term based on an analysis of residuals. The residuals after including the shallow site response term f_{site} clearly indicated that long-period ground motion increased with sediment

depth up to around $Z_{2.5} = 1$ km, leveled off, then increased again at $Z_{2.5} = 3$ km. We surmise that the observed decrease in long-period ground motion for sites with shallow sediment depths might be the result of relatively lower long-period site-amplification effects compared to sites with deep sediment depths and the same values of V_{S30}. We found that the data were sufficient to empirically constrain this trend.

The trend for $Z_{2.5} > 3$ km, which is due presumably to 3D basin effects, was based on too few data to empirically determine how these effects could be extrapolated with sediment depth and spectral period. Instead, this trend was constrained using the sediment-depth model developed by Day et al. (2008) from theoretical ground motion simulations of the 3D response of the Los Angeles, San Gabriel, and San Fernando basins in southern California. These authors also found that ground motions scaled strongly with depth between depths of 1.0 and 3.0 km, whereas we did not find any trend in the residuals over this depth range. We believe that this scaling is apparently accounted for by other predictor variables in our model (most likely V_{S30}). For example, it is below a depth of 3 km that we found a strong correlation between $Z_{2.5}$ and V_{S30} in the PEER database. It is also possible that the ground motion simulations are dominated by 1D effects at depths shallower than about 3 km that are adequately modeled by f_{site}. Because there is no basin-response adjustment between depths of 1 and 3 km, this depth range represents the default, which means that the results are centered on this depth range.

The Day et al. (2008) model was developed for spectral periods of 2.0 sec and greater, but these authors developed relationships for their model coefficients that allowed us to extrapolate them to shorter periods. In order to remove any bias that this extrapolation might cause, we included an additional model coefficient c_{16} in Equation (3.20) to empirically adjust the theoretical model coefficient k_3 (the a_2 coefficient of Day et al. 2008). This additional coefficient was found to increase from about 0.4 for PGA and short-period PSA to around 0.8 for PSA at longer periods, although this value decreases again to around 0.6 to 0.7 at long periods. Because the Day et al. (2008) model was applied only at large sediment depths, their first term (involving their a_1 coefficient) was found to be negligible and was dropped from our basin response term. The small but finite value of c_{16} at short periods causes our model to predict some (albeit weak) amplification at these periods. Although counter-intuitive to many seismologists' expectations, these results are generally consistent with the empirical results of Campbell (1997, 2000, 2001), Field (2000), and our NGA-West1 model, although Campbell did not find any significant amplification at spectral periods less than 0.5 sec.

We found that the shallow basin response term was different for sites in Japan than for sites outside of Japan. The model coefficient c_{14} for non-Japan recording sites is based primarily on California sites because of a lack of sediment-depth information for other regions. A different coefficient was found for recording sites in Japan. Since this coefficient is additive, the total Japan coefficient is equal to $c_{14} + c_{15}$. The deep basin response term was found to be similar in Japan and California.

Tom Shantz (personal communication, 2009) found that $Z_{2.5}$ was a better predictor than the depth to the 1 km/sec shear-wave velocity horizon ($Z_{1.0}$) to characterize basin depths in

California because geological and geophysical data could be used more easily to estimate this depth. Art Frankel (personal communication, 2013) found that ground motion simulations of 3D basin effects in the Seattle basin were better correlated with $Z_{2.5}$ than with $Z_{1.0}$ because of the very shallow depth to the 1 km/sec velocity horizon (glacial till). This adds support to our choice of $Z_{2.5}$ to represent sediment-depth and basin-response effects.

4.7 HYPOCENTRAL DEPTH TERM

In our NGA-West1 model, we incorporated source depth by allowing reverse-mechanism events to have higher ground motions for $Z_{TOR} > 1$ km that gradually diminishes to no effect for surface faulting. The small-magnitude recordings in the NGA-West2 database clearly show that there is a strong increase in ground motion with hypocentral depth for $Z_{HYP} > 7$ km that is captured in a new term, f_{hyp}. We explored the use of Z_{TOR} to model the depth-dependence of ground motion, but found that it left a residual trend with hypocentral depth at large magnitudes where the two depths can be very different. We surmise that even if the top of the ruptre is shallow a relatively deep hypocentral depth implies a higher average stress drop and correspondingly higher ground motion. Because of the similarity of Z_{HYP} and Z_{TOR} for small-magnitude earthquakes, both predictor variables modeled this trend equally as good. In order to remove the trend at large magnitudes we chose to use Z_{HYP} instead of Z_{TOR} to model earthquake depth effects. We found that this dependence was stronger for small-magnitude earthquakes than for large-magnitude earthquakes, which we accounted for by using a different model coefficient for the former (c_{17}) than for the latter (c_{18}). The deepest events in our database have hypocentral depths of about 20 km, so the effect is capped at this depth in Equation (3.22).

4.8 RUPTURE DIP TERM

Although we found that recordings from small-magnitude earthquakes did not show a dependency on focal mechanism, they did show a strong dependence on the dip of the rupture plane, δ, for small-magnitude earthquakes. This is captured with a new rupture dip term f_{dip} and model coefficient c_{19}. This effect becomes negligible at large magnitudes. This means that style-of-faulting effects are found only at large magnitudes, whereas rupture dip effects are found only at small magnitudes.

4.9 ANELASTIC ATTENUATION TERM

An initial review of ground motions recorded at larger distances indicated that there is a strong regional dependence of attenuation beyond the 80 km distance used to develop our near-source NGA-West2 model. This implies that there is a regional dependence to the apparent anelastic attenuation we observe. Like geometric attenuation, we call the nonlinear decay of ground motion at large distances apparent anelastic attenuation or simply anelastic attenuation because it

behaves in a similar manner (i.e., it decays as $e^{-\gamma r}$). We have modeled this decay with a new anelastic attenuation term f_{atn} and model coefficients c_{20} and Δc_{20}. Although probabilistic seismic hazard is typically dominated by sources that are located within 80 km of the site of interest, we included this term for completeness and for estimating ground motion at those sites that are located in lower seismicity regions and might be impacted by distant large earthquakes. We fit the anelastic attenuation term by holding all of the other coefficients constant and using the far-source database ($80 < R_{RUP} \leq 500$ km) to derive the anelastic attenuation coefficients using random-effects regression.

We used an analysis of residuals together with iterative random-effects regression to determine which regions had both a sufficient number of far-source recordings to derive a reliable anelastic attenuation coefficient and a significant difference in this coefficient. This analysis indicated that California, Taiwan, the Middle East, and other similar active tectonic regions could be used to represent a typical anelastic attenuation or average Q region. Japan and Italy were found to exhibit relatively high anelastic attenuation, representing a relatively lower value of Q and a negative value of Δc_{20}. Eastern China (i.e., the Wenchuan earthquake region) was found to exhibit relatively low anelastic attenuation represented by a relatively higher value of Q and a postive value of Δc_{20}. The quality factor Q, or more appropriately $1/Q$, is a term used by seismologists to quantify anelastic attenuation (Lay and Wallace 1995). Parts of eastern China are characterized as a SCR, which explains the relatively lower rate of attenuation, however it was the decision of the NGA-West2 working group responsible for reviewing finite-fault models that the Wenchuan earthquake could be considered representative of an active tectonic domain based on its source characteristics and its location on the boundary between active and stable tectonic regions. The regional differences in attenuation observed in our analysis are consistent with previous seismological and ground motion studies.

4.10 ALEATORY VARIABILITY TERM

In our NGA-West1 model, we included an alternative formulation to the calculation of aleatory variability to that used in our pre-NGA models. The more complicated functional form of this formulation takes into account the soil nonlinearity effects embodied in Equation (3.18) that predicts that as the value of A_{1100} (the median estimate of rock PGA) increases, the corresponding value of f_{site} decreases for soils with $V_{S30} < k_1$ (i.e., softer soils). The self-compensating effects of this nonlinearity impacts the within-event standard deviation by reducing the variability in the site-amplification factor at high values of A_{1100} modeled by the first-order second-moment approximations of τ and ϕ given by Equations (3.29) and (3.30). This approximation was first introduced by Bazzurro and Cornell (2004a) for the case in which PSA is used as the reference rock ground motion and later extended by Stewart and Goulet (2006) to our case in which PGA is used as the reference rock ground motion. These effects are especially significant for NEHRP site categories D and E (BSSC 2009).

In our NGA-West1 model we only included nonlinear site effects in the estimate of ϕ based on a common understanding at the time that between-event terms are not significantly affected by soil nonlinearity e.g., Kwok and Stewart 2006; J. Stewart, personal communication,

2007). Their argument is that the between-event residual is a source term and represents the average source effects that apply to all sites and not just to the site response of an individual site. On the other hand, Abrahamson and Silva (2008) included nonlinear site effects in both ϕ and τ for reasons that were later justified by Al Atik and Abrahamson (2010). These latter authors argue that both ϕ and τ are impacted by nonlinear response because, with the incorporation of nonlinear site response in the median ground motion model, the interpretation of the between-event term is revised to represent the average residual for rock site conditions (i.e., linear site response). Therefore, for application of the GMPE to soil sites the standard deviation of the rock source terms need to be modified to be applicable to nonlinear site conditions. For this reason we now include nonlinear site response effects in both ϕ and τ. Note that even if we were to assume that τ was not subject to soil nonlinearity effects, this assumption would have a relatively small impact on the total standard deviation because of the dominance of the within-event standard deviation.

Another key element in our nonlinear formulation of aleatory variability is the selection of an appropriate value for $\phi_{\ln AF}$, the aleatory variability associated with site response. Although this value can be impacted by many factors, site-response studies using both empirical methods (e.g., Baturay and Stewart 2003) and theoretical methods (e.g., Silva et al. 1999, 2000; Silva 2005; Bazzurro and Cornell 2004b, 2005) suggest that a period-independent value of $\phi_{\ln AF} \approx 0.3$ is a reasonable value for deep soil sites, at least once 3D basin response effects have been removed as is the case in our model. Walt Silva (personal communication, 2007) also recommends $\phi_{\ln AF} \approx 0.3$ for all spectral periods based on the 1-D equvalent-linear site-response analyses of Silva (2005). This variability is expected to decrease as sites become harder (Silva et al. 1999, 2000), but since such sites do not respond nonlinearly, the value of ϕ is not sensitive to the value of $\phi_{\ln AF}$.

Baturay and Stewart (2003), Stewart et al. (2003), and Choi and Stewart (2005) also found a dependence of the within-event standard deviation on V_{S30}. They found that softer sites tend to have lower standard deviations than stiffer sites. Since these authors did not include ground motion amplitude as a parameter in their aleatory variability model, the difference in standard deviations that they found is likely due, at least in part, to the nonlinear site effects embodied in Equations (3.29) to (3.31). We investigated this in our NGA-West1 study by binning our within-event residuals into V_{S30} ranges corresponding to NEHRP site categories C ($V_{S30} = 360 - 760$ m/sec) and D ($V_{S30} = 180 - 360$ m/sec) and performing a hypothesis test to see if the differences in the mean residuals for PGA and PSA at periods of 0.2, 1, and 3 sec were statistically significant. We found that the mean residuals for each of the velocity bins were not significantly different from zero (i.e., they were unbiased) at the 95% confidence level, and that the residual standard deviations of the two bins differed by less than 6%. Based on these results, we concluded that the within-event standard deviations for our model is not dependent on V_{S30} once nonlinear site effects are taken into account. Therefore, we did not find it necessary to make the standard deviations of the linear ground motion predictions dependent on the value of V_{S30}.

We did find both a slight positive bias in the mean residuals and a larger difference in the residual standard deviations between bins in our NGA-West1 study when we included only those

sites with measured values of V_{S30}. The differences in the standard deviations were generally consistent with the results of Choi and Stewart (2005) who only used sites with measured values of V_{S30}. The bias in the mean residuals suggested that ground motion amplitudes might be under-predicted by our NGA-West1 model by as much as 10% at some spectral periods. We concluded that further study was needed before we would recommend adjusting our model for possible differences in the predicted amplitudes of ground motion between sites with estimated and measured values of V_{S30}, particularly since there is likely to be a correlation between sites with measured 30-m shear-wave velocities and recordings with relatively high levels of ground motion due to the engineering significance of such recordings. Because the percentage of recording sites with measured values of V_{S30} is about the same in the NGA-West2 database, we did not believe that we needed to repeat this study and accepted our previous conclusions.

We did not find within-event and between-event standard deviations to be a significant function of magnitude in our NGA-West1 study, whereas we do in our current study. These observations are not as contradictory as they would first appear. We observe an increase in aleatory variability in our current study for earthquakes with $\mathbf{M} < 5.5$ that fully phases in at $\mathbf{M} \leq 4.5$. Previously, we only had a few earthquakes in this magnitude range, which precluded us from determining whether there was a significant magnitude-dependent standard deviation. These later findings were consistent with those of Choi and Stewart (2005) who, in a careful investigation of the residuals of several empirical GMPEs, did not find compelling evidence for either a magnitude-dependent or distant-dependent between-event or within-event standard deviation once the dependence on V_{S30} was taken into account. However, those GMPEs were developed from earthquakes with $\mathbf{M} \geq 5.0$ near the magnitude threshold at which our increase in aleatory variability begins.

We found that standard deviations generally increase at $R_{RUP} > 80$ km. This is especially noticeable for $\mathbf{M} < 5.5$. The increase in the between-event standard deviation is not considered important because we do not consider the large distant data to be suitable for estimating τ. The within-earthquake standard deviation for the small-magnitude events is not very different from that found for the near-source data ($R_{RUP} \leq 80$ km). This is likely because it is derived from recordings from a single region (California). This suggests that the larger value of ϕ for the larger magnitudes might be caused by epistemic uncertainty rather than aleatory variability. Therefore, the standard deviations listed in Table 3.3 can be used at $R_{RUP} \leq 300$ km, corresponding to the distance range over which we consider our GMPE to be valid. Epistemic uncertainty at these large distances will be captured through the use of multiple GMPEs.

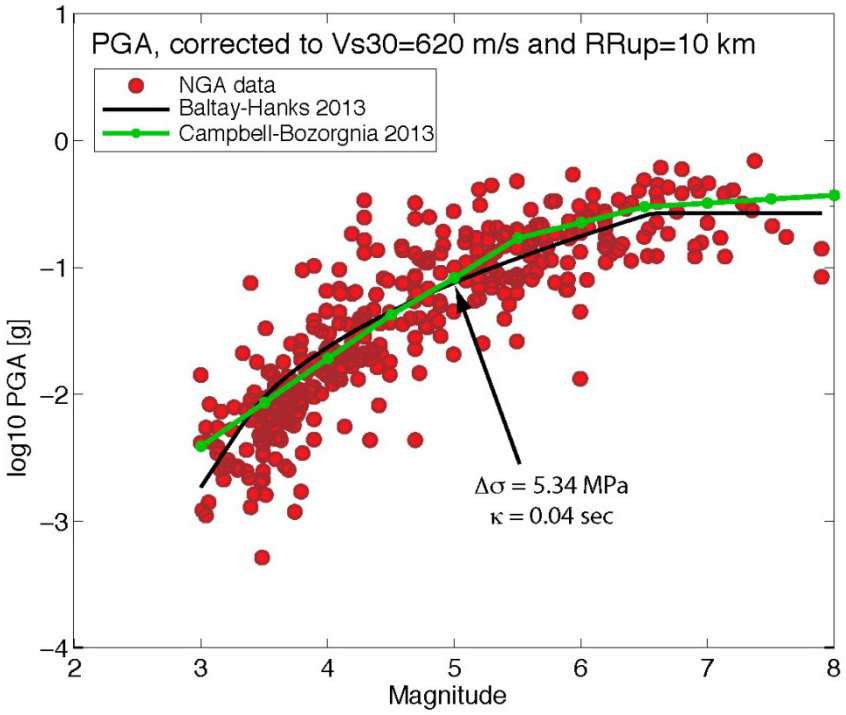

Figure 4.1 **Comparison of stochastic model of Baltay and Hanks (2013a,b) with the CB13 model.**

5 User Guidance

Because of the relatively complex nature of the functional forms that comprise our NGA-West2 ground motion model, and because of the inclusion of many new predictor variables, this chapter presents guidelines to users on how one might evaluate the model for engineering applications. Covered topics include general limits of applicability, calculating PGA on rock, accounting for unknown predictor variables, estimating epistemic uncertainty, and use in PSHA.

5.1 GENERAL LIMITS OF APPLICABILITY

Generally speaking, our ground motion model is considered to be valid for shallow continental earthquakes occurring worldwide in active tectonic regimes for which the following conditions apply:

- Minimum magnitudes of $\mathbf{M} \geq 3.3$
- Maximum magnitude limits of $\mathbf{M} \leq 8.5$ for strike-slip faults, $\mathbf{M} \leq 8.0$ for reverse faults, and $\mathbf{M} \leq 7.5$ for normal faults
- Distances of $R_{RUP} = 0 - 300$ km
- Shear-wave velocities of $V_{S30} = 150 - 1500$ m/sec (NEHRP site categories B, C, D, and E)
- Sediment depths of $Z_{2.5} = 0 - 10$ km
- Depths to top of rupture of $Z_{TOR} = 0 - 20$ km
- Hypocentral depths of $Z_{HYP} = 0 - 20$ km
- Rupture dips of $\delta = 15 - 90°$.

The model is not uniformly valid over the entire range of predictor variables listed above. Statistical prediction errors are smallest for values of predictor variables near their mean and increase as these values diverge from this mean (e.g., see Campbell 2004). These errors can become very large when the model is extrapolated beyond the data limits of the predictor variable and should be used with caution under such conditions. The applicable range of some predictor variables have been extended beyond the limits of the data when the model has been constrained theoretically. Additional details are given in the following sections.

5.1.1 Magnitude

The upper magnitude limits for strike-slip and reverse faults are dictated by the requirements of the PEER NGA-West2 Project. The largest magnitudes for each of these style-of-faulting categories are 0.1–0.6 magnitude units smaller than these limits. Although not a requirement by the PEER NGA-West2 Project, we have recommended a similar extrapolation for normal faults. We believe that such an extrapolation can be justified because of the careful selection of an appropriate magnitude-scaling term that includes magnitude saturation. Nonetheless, any extrapolation is associated with additional epistemic uncertainty (see Section 5.4). Figure 4.1 indicates that although we have data down to $\mathbf{M}=3$, we tend to overestimate PGA for the smallest events where simple seismological theory would predict that magnitude should scale as $-1.5\mathbf{M}$ (Baltay and Hanks 2013a,b). As a result, we consider our GMPE to be most reliable for earthquakes of $\mathbf{M}\geq 3.3$ or 0.3 magnitude units above the smallest magnitude used in the analysis.

5.1.2 Source-to-Site Distance

The PEER NGA-West2 Project required that the GMPE be valid to a minimum distance of 200 km. The rate of attenuation out to 80 km where geometric attenuation dominates is well constrained for all magnitudes. The rate of attenuation at larger distances where anelastic attenuation becomes important is constrained by events for which a significant number of large distance recordings are available (primarily California and Japan). Although we used recordings out to 500 km to constrain the anelastic attenuation term, we consider the GMPE to be most valid at $R_{RUP}\leq 300$ km, beyond which the number of recordings dimishes rapidly. It should be noted that such distant earthquakes rarely have a material impact on PSHA results.

5.1.3 Shear-Wave Velocity

Even though our selected NGA-West2 database included a limited number of recording sites with $V_{S30}<180$ m/sec, such soft-soil sites or even sites with somewhat higher shear-wave velocities might have other unusual site conditions (e.g., shallow Bay Mud over rock) that make site effects more complicated than our simple nonlinear site response term would predict. For that reason, we caution the use of our GMPE for NEHRP site category E and F sites (BSSC 2009). Furthermore, the 1D equivalent-linear site-response simulations that were used to derive the nonlinear soil model become less reliable at shear strains in excess of about 1%. However, if neither of these conditions exists, our nonlinear soil model might be generally valid at $V_{S30}<180$ m/sec because of its theoretical basis and its lack of any significant bias in the within-event residuals (Figure 3.8). Otherwise, we recommend that a site-specific site-response analysis be conducted. There is only one recording site in our database that would be classified as NEHRP site category A, which is insufficient to determine whether the model can be extrapolated beyond $V_{S30}>1500$ m/sec. There is still a tendency for our GMPE to underestimate ground motions for spectral periods greater than 1 sec for NEHRP site category B sites, which might indicate that site attenuation or kappa effects need to be considered for these hard rock sites. This will be a topic of a future study. The shallow site-response term included in our model is intended to

provide an approximate empirical estimate of site response for general site classifications. We strongly recommend that a site-response analysis be conducted for site-specific studies.

5.1.4 Sediment Depth

The sediment depth limit used in the 3D basin response simulations that formed the basis for our sediment depth term at $Z_{2.5} > 3$ km was about 6 km. However, the model might be valid beyond this depth limit (up to about 10 km) because of its theoretical basis. It is possible, although improbable, that the value of V_{S30} could be inconsistent with the value of $Z_{2.5}$ for very shallow sediment depths. There are two cases where this might occur: (1) when V_{S30} is extrapolated to values exceeding 2500 m/sec, in which case $Z_{2.5} = 0$; and (2) when $Z_{2.5}$ becomes very small, in which case V_{S30} must be large enough to adequately represent the top 30 m of the site profile. The first case should never occur based on our recommendation that the model should not be extrapolated beyond $V_{S30} = 1500$ m/sec. For small values of both V_{S30} and $Z_{2.5}$, it is possible that a site resonance condition will occur, which is not predicted by our model. In this case we strongly recommended that a site-specific site-response analysis be conducted.

5.1.5 Hypocentral Depth

The 20 km limit for hypocentral depth is based on an analysis of residuals that showed that the between-event residuals were generally unbiased down to this depth (Figure 3.2). Therefore, until we can acquire additional deep earthquake data to better constrain this possible depth dependence, we recommend that our ground motion model not be used for hypocentral depths or depths to the top of rupture greater than about 20 km. This depth limit constrains the modeled earthquakes to occur in the shallow lithosphere, which was a requirement of the PEER NGA-West2 Project.

5.1.6 Rupture Dip

The dip of the rupture plane is used in the hanging-wall term for large-magnitude earthquakes and in the rupture dip term for small-magnitude earthquakes. The relatively wide range of rupture dips for which we consider our GMPE to be valid is selected to represent the range of values in our selected NGA-West2 database over which the between-event residuals are unbiased (Figure 3.4).

5.1.7 Tectonic Domain

Even if an earthquake is relatively shallow, there can be some uncertainty in deciding whether it is located within the continental lithosphere. “Continental” means that the earthquake must occur within continental crust rather than oceanic crust. Earthquakes that occur on land or on the continental shelf and have focal depths of less than about 25 km can generally be considered to occur within the shallow continental lithosphere. There is also some uncertainty in deciding if a region can be considered an active tectonic region. A general rule of thumb is that it can be

classified as active if it is not otherwise identified as a SCR (e.g., Johnston 1996); Campbell 2004), although regional studies should be used to confirm this.

5.1.8 Source Directivity

It was our original intent to include a source directivity term in our NGA-West2 GMPE based on the work of the PEER Directivity Working Group (Spudich et al. 2013). However, the four teams that composed this working group produced directivity models that varied significantly for reverse and/or faults with complicated rupture plane geometry. The NGA project decided to continue the investigation of the working group to understand the cause of these differences. As a result, we decided not to include any of the directivity models in our NGA-West2 model until such time that the directivity models become more mature.

5.2 ESTIMATING ROCK PGA

It might appear at first that the shallow site response term is non-unique because it requires an estimate of median rock PGA, A_{1100}. However, in no case does the model coefficient k_1, the threshold value of V_{S30} at which f_{site} becomes linear, exceed the 1100 m/sec value used to define rock PGA. Therefore, rock PGA can be calculated using only the second (linear) term in Equation (3.18) that is independent of A_{1100}. This estimate of rock PGA can then be substituted back into f_{site} for purposes of calculating ground motion, including PGA, when $V_{S30} < k_1$. Consistent with the way that our aleatory variability model was developed, the median estimate of rock PGA should be used for this purpose even if this estimate is for a level of aleatory variability larger or smaller than the median.

5.3 ESTIMATING UNKNOWN PREDICTOR VARIABLES

There will be instances in which the user will not know the value of one or more of the predictor variables. Simply substituting a default value for a predictor variable can lead to biased results and an underestimation of variability. The more rigorous approach is to estimate or assume reasonable estimates for the mean values of these variables, assign them subjective weights, and model them as additional epistemic uncertainty (e.g., using a logic tree). If a predictor variable is estimated from a model rather than from data, it also might be associated with additional aleatory variability. The determination of whether estimates of predictor variables are subject to aleatory variability or epistemic uncertainty is beyond the scope of this report and is left to the user. However, some guidance on the selection and estimation of unknown or uncertain predictor variables is provided in Kaklamanos et al. (2011) and in the following sections. However, note that some of the relationships given in Kaklamanos et al. (2011), which are based on the NGA-West1 datbabase, are superseded by the NGA-West2 database and should be used with caution.

5.3.1 Magnitude and Distance

If **M** or R_{RUP} are unknown, these predictor variables can be estimated from other magnitude and distance measures (e.g., Scherbaum et al. 2004). However, it is preferable to directly include in the seismic hazard analysis one or more 3D models of the potential rupture planes of the relevant seismic sources in order to properly account for epistemic and aleatory uncertainty in the estimated distances and, for reverse faults, to take into account potential hanging-wall effects. A convenient method for pre-calculating the mean values of R_{JB}, R_{RUP}, and the hanging-wall factor for randomly oriented virtual faults used to model diffuse seismicity was used in the National Seismic Hazard Mapping Program (NSHMP) and documented in Petersen et al. (2008). Although this method only estimates the mean distances and hanging-wall effects for a randomly oriented fault, it could be easily modified to estimate the uncertainty in these estimates.

5.3.2 Shear-Wave Velocity

If V_{S30} is unknown, it can be estimated from the definition of the NEHRP site categories (BSSC 2009; Campbell 2004; Bozorgnia and Campbell 2004) or from surface geological units, geotechnical site categories, ground slope, geomorphology, or elevation based on proxy relationships given in Ancheta et al. (2013). If NEHRP site categories are used, we recommend that either the boundary values or the geometric mean of the boundary values of V_{S30} be used because of the logarithmic relationship between site amplification and V_{S30}. Our recommended values of V_{S30} for NEHRP site categories E, DE, D, CD, C, BC and B are 150, 180, 255, 360, 525, 760 and 1070 m/sec, respectively.

5.3.3 Style-of-Faulting and Rupture Dip

If style-of-faulting or rupture dip is unknown, weights should be assigned to alternative estimates of the predictor variables F_{RV}, F_{NM}, and δ based on the orientation and dip of the proposed rupture plane and its relationship to the regional tectonic stress domain. If a single estimate of rupture dip is desired, values of 50° for reverse and normal faults and 90° for strike-slip faults are generally reasonable assumptions.

5.3.4 Depth to Top of Rupture and Hypocentral Depth

If the depth to the top of coseismic rupture (Z_{TOR}) is unknown, its aleatory distribution can be estimated probabilistically using the approach of Youngs et al. (2003). If that approach is considered to be too complicated, a simpler empirical approach can be used in which the likelihood of surface rupture is probabilistically estimated using the logistic regression model of Wells and Coppersmith (1993). In this approach, the probability of principal surface rupture is estimated from the equation

$$P(\text{slip}) = \frac{\exp(f_{slip})}{1+\exp(f_{slip})} \tag{6.1}$$

where

$$f_{slip} = -12.51 + 2.053\mathbf{M} \tag{6.2}$$

This probability can then be used to weight two alternative logic-tree branches that define whether or not surface rupture occurs. For the branch where surface rupture is assumed to occur, the user should set $Z_{TOR} = 0$ in Equation (3.15). For the branch where the top of rupture is assumed to be buried the user should set one or more hypothesized values of Z_{TOR} in this equation. If the more rigorous approach of Youngs et al. (2003) is used, a distribution of Z_{TOR} values will be simulated and $f_{hng,Z}$ should be determined accordingly.

If the value of hypocentral depth (Z_{HYP}) is unknown, but the geometry and depth of the rupture plane is known, it can be estimated from the equations

$$\ln \Delta Z = \min\left(f_{\Delta Z,\mathbf{M}} + f_{\Delta Z,\delta}, \ln[0.9(Z_{BOR} - Z_{TOR})]\right) \tag{6.3}$$

$$f_{\Delta Z,\mathbf{M}} = \begin{cases} -4.317 + 0.984\mathbf{M}; & \mathbf{M} < 6.75 \\ 2.325; & \mathbf{M} \geq 6.75 \end{cases} \tag{6.4}$$

$$f_{\Delta Z,\delta} = \begin{cases} 0.0445(\delta - 40); & \delta \leq 40 \\ 0; & \delta > 40 \end{cases} \tag{6.5}$$

which were developed from the metadata in the NGA-West2 database (Figure 5.1), where $\Delta Z = Z_{HYP} - Z_{TOR}$ (km), Z_{BOR} (km) is the depth to the bottom of the rupture plane, and ΔZ (km) is constrained to be no greater than 90% of the difference between the top and bottom depths of the rupture plane. The limit at $\mathbf{M} \geq 6.75$ corresponds to $\Delta Z = 10.2$ km. The standard deviation of $\ln \Delta Z$ and the r-square value of the regression (a measure of the goodness of fit) are 0.40 and 0.89, respectively. Plots of the residuals of the regression are given in Figure 5.2. If Z_{HYP} is known but Z_{TOR} is unknown, Z_{TOR} can be estimated from the above equations.

Although we strongly recommend that Equations (6.3) to (6.5) be used to estimate Z_{HYP} Z_{HYP} or Z_{TOR}, if these equations are found to be too difficult to use, a simpler option may be to assume that the hypocenter is located in the middle of the known or hypothesized rupture plane. If the depth to the top of the rupture plane is unknown, under this assumption Z_{TOR} (km) can be estimated from Z_{HYP} (km) and the width and dip of the rupture plane from the equation

$$Z_{TOR} = Z_{HYP} - 0.5W\sin(\delta) \tag{6.6}$$

where δ (°) is rupture dip and W (km) is rupture width. If W is unknown, it can be estimated from the equation

$$W = \min\left(\sqrt{(\mathbf{M} - 4.07)/0.98}, (Z_{BOT} - Z_{TOR})/\sin(\delta)\right) \tag{6.7}$$

where Z_{BOT} (km) is the depth to the bottom of the seismogenic crust. The first term in Equation (6.7) is based on the rupture area relationship of Wells and Coppersmith (1994) assuming a 1:1

aspect ratio. The second term is the maximum width of the rupture plane, assuming that rupture does not extend below the depth to the bottom of the seismogenic crust.

If the user does not know anything about the rupture plane or is unable to estimate one, the value of hypocentral depth can be taken as 9.0 km, which is an average of the mean and median values of Z_{HYP} in our combined near-source and far-source databases. However, the standard deviation of this estimate is a relatively large 3.8 km.

5.3.5 Sediment Depth

For sites located in southern California, central California or Japan, $Z_{2.5}$ can be estimated from the same community velocity models that were used to estimate $Z_{2.5}$ for the recording sites in the PEER NGA-West2 database (Ancheta et al. 2013). Alternatively, we suggest that the depth to crystalline basement rock beneath the site, if it is known or can be estimated, can be used as a proxy for $Z_{2.5}$. Otherwise, $Z_{2.5}$ can be estimated from V_{S30} using data from the NGA-West2 database. This is only possible for California and Japan where there are estimates or measured values of both $Z_{2.5}$ and V_{S30}. We used our combined near-source and far-source databases to develop the relationships between these two parameters so that they would be consistent with the values used to develop our GMPE. A recording station was used only once in the analysis so as not to bias the results towards stations with multiple recordings.

The relationship between $Z_{2.5}$ (km) and V_{S30} (m/sec) for the combined Califronia and Japan database is given by the equation

$$\ln Z_{2.5} = 6.510 - 1.181 \ln V_{S30} \tag{6.8}$$

which has a r-square value of 0.100 and a standard deviation of 1.447. The relationship for California is given by the equation

$$\ln Z_{2.5} = 7.089 - 1.144 \ln V_{S30} \tag{6.9}$$

which has a r-square value of 0.131 and a standard deviation of 1.026. The relationship for Japan is given by the equation

$$\ln Z_{2.5} = 5.359 - 1.102 \ln V_{S30} \tag{6.10}$$

which has a r-square value of 0.112 and a standard deviation of 1.403. Although the coefficients in these equations are statistically significant at the 95% confidence level, the correlation between $Z_{2.5}$ (km) and V_{S30} is relatively poor as evidenced by the relatively small r-square values and relatively large standard deviations. As a result, the user should exercise caution when using these relationships. Equations (6.8), (6.9) and (6.10) give estimates of $Z_{2.5}$ corresponding to 0.27, 0.61 and 0.14 km, respectively, for $V_{S30} = 760$ m/sec.

We used the same combined near-source and far-source database to develop relationships between $Z_{2.5}$ (km) and $Z_{1.0}$ (km), which can be used when this latter depth is known. The relationship for the combined California and Japan database is given by the equation

$$Z_{2.5} = 0.748 + 2.128 Z_{1.0} \tag{6.11}$$

which has a r-square value of 0.307 and a standard deviation of 1.264. The relationship for California is given by the equation

$$Z_{2.5} = 1.392 + 1.798 Z_{1.0} \tag{6.12}$$

which has a r-square value of 0.162 and a standard deviation of 1.562. The relationship for Japan is given by the equation

$$Z_{2.5} = 0.408 + 1.745 Z_{1.0} \tag{6.13}$$

which has a r-square value of 0.473 and a standard deviation of 0.696. Again, the coefficients in these equations are statistically significant, but the correlation between $Z_{2.5}$ and $Z_{1.0}$ is relatively poor. As a result, the user should exercise caution when using these relationships.

If none of the above guidance can be used, sediment depth is the only predictor variable that can be assigned a default value, unless it is known or expected to be either less than 1 km or greater than 3 km deep. If sediment-depth effects are not expected to be important, then V_{S30} can serve as a reasonable representative of both shallow and deep site response by setting $Z_{2.5} = 2$ km, or for that matter to any value between 1 and 3 km, where this predictor variable has no effect on the predicted ground motion. If sediment depth effects are expected to be important, then reasonable alternative values for $Z_{2.5}$ and their associated weights should be used to evaluate epistemic uncertainty in the value of this predictor variable.

5.4 ESTIMATING EPISTEMIC UNCERTAINTY

Although magnitude saturation of short-period ground motion at short distances limits the median predicted value of near-source ground motion at large magnitudes, these predictions are based on a limited number of recordings. As a result, there is additional epistemic uncertainty in the near-source median predictions that might not be adequately captured by the use of multiple GMPEs. There is also additional epistemic uncertainty associated with the modeling space that is not well constrained by the recordings. A preliminary comparison of the NGA-West2 models indicates that there are ranges of magnitude and distance, and probably other predictor variables, where there is very little variability between the GMPEs. We believe that such implied "agreement" is not representative of a lack of uncertainty but rather an artifact of using a limited number of models that have been developed with developer collaboration using a consistent database. We recommend that a minimum estimate of epistemic uncertainty be incorporated using the epistemic uncertainty model developed by Al Atik and Youngs (2013) as part of the PEER NGA-West2 Project.

5.5 ESTIMATING SPECTRAL DISPLACEMENT AND PGD

A surge in the design and construction of high-rise condominium buildings and base-isolated structures in recent years has brought about a renewed interest in the prediction of long-period

spectral displacement and in some cases PGD. Both of these IMs have been largely ignored by the developers of ground motion models in the past or, if not ignored, have not been properly constrained either empirically or theoretically. It is for this reason that the PEER NGA-West1 and NGA-West2 Projects required the developers to provide models for PSA out to spectral periods of 10 sec. Many of the developers of the NGA-West1 models attempted to constrain long-period PSA using simple seismological theory, but there was a great deal of uncertainty between these models. With the addition of a significant number of new digital recordings, the long-period spectral ordinates are much better constrained and no additional constraints were applied in our NGA-West2 model. There is still a considerable amount of uncertainty associated with these predictions, and the behavior of spectral displacement at long periods does not necessarily agree with simple seismological theory. Therefore, the user should use caution when evaluating the GMPEs for very long periods, e.g., $T > 5$ sec where the number of recordings begins to dimish rapidly with increasing spectral period (Ancheta et al. 2013). A preliminary GMPE for PGD was developed by Campbell and Bozornia (2008) for evaluation purposes.

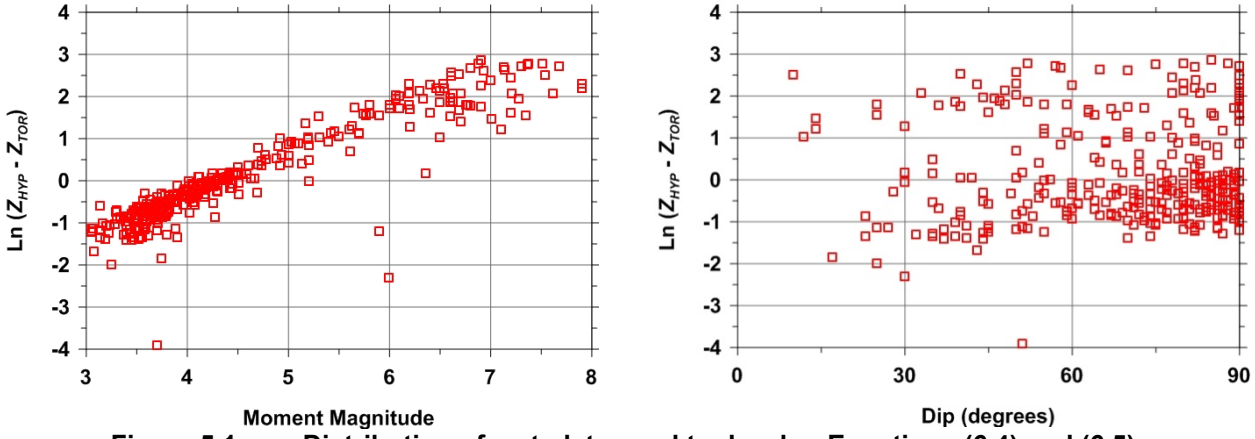

Figure 5.1 Distribution of metadata used to develop Equations (6.4) and (6.5).

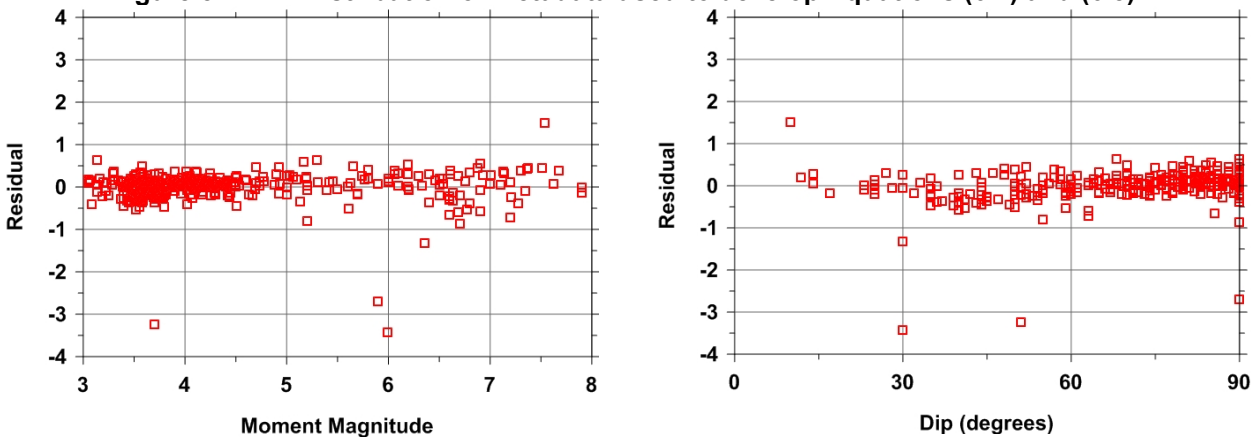

Figure 5.2 Dependence of residuals of Equations (6.4) and (6.5) with magnitude and rupture dip.

REFERENCES

Abrahamson N.A., Silva W.J. (2007). Abrahamson-Silva NGA ground motion relations for the geometric mean horizontal component of peak and spectral ground motion parameters, *Report PEER 2007/03*, Pacific Earthquake Engineering Research Center, University of California, Berkeley, CA.

———. (2008). Summary of the Abrahamson & Silva NGA ground-motion relations, *Earthq. Spectra* 24: 67–97.

Abrahamson N.A., Youngs R.R. (1992). A stable algorithm for regression analyses using the random effects model, *Bull. Seismol. Soc. Am.,* 100**:** 1288–92.

Al Atik, L., Abrahamson, N. (2010). Nonlinear site response effects on the standard deviations of predicted ground motions, *Bull. Seismo. Soc. Am,* 82**:** 505–10.

Al Atik L., Youngs R.R. (2013). Epistemic uncertainty for NGA-West2 models, *Report PEER 2013/11*, Pacific Earthquake Engineering Research Center, University of California, Berkeley, CA.

Ambraseys N.N., Douglas J., Sarma S.K., Smit P.M. (2005). Equations for the estimation of strong ground motions from shallow crustal earthquakes using data from Europe and the Middle East: Horizontal peak ground acceleration and spectral acceleration, *Bull. Earthq. Eng.* 3: 1–53.

Ancheta T.D., Bozorgnia Y., Darragh R., Silva W.J., Chiou B., Stewart J.P., Boore D.M., Graves R.W., Abrahamson N.A., Campbell K.W., Idriss I.M., Youngs R.R., Atkinson G.A. (2012). PEER NGA-West2 database: A database of ground motions recorded in shallow crustal earthquakes in active tectonic regions, *Proceedings, 15th World Conference on Earthquake Engineering*, Paper No. 5599, Lisbon, Portugal.

Ancheta T.D., Darragh R., Stewart J.P., Seyhan E., Silva W.J., Chiou B.S.J., Wooddell K.E., Graves R.W, Kotke A.R., Boore D.M., Kashida T., Donahue J.L. (2013). PEER NGA-West2 database, *Report PEER 2013/03*, Pacific Earthquake Engineering Research Center, University of California, Berkeley, CA.

Anderson J.G. (1991). A preliminary description model for the distance dependence of the spectral decay parameter in southern California, *Bull. Seismol. Soc. Am*., 81: 2186–93.

Anderson J.G., Hough S.E. (1984). A model for the shape of the Fourier amplitude spectrum of acceleration at high frequencies, *Bull. Seismol. Soc. Am*., 74: 1969–1993.

Baker J.W., Cornell C.A. (2006). Which spectral acceleration are you using? *Earthq. Spectra* 22**:** 293–312.

Baker J.W., Shahi S. (2013). NGA-West 2 Models for Ground-Motion Directionality, *Report PEER 2013/10*, Pacific Earthquake Engineering Research Center, University of California, Berkeley, CA.

Baltay A.S., Hanks T.C. (2013a). Magnitude dependence of PGA and PGV in NGA-West2 data, abstract, *Seismol. Res. Lett.,* 84: 302.

———. (2013b). Understanding the magnitude dependence of PGA and PGV in NGA-West2 data, *Bull. Seismol. Soc. Am.,* 103: submitted for publication.

Baturay M.B., Stewart J.P. (2003). Uncertainty and bias in ground-motion estimates from ground response analyses, *Bull. Seismol. Soc. Am.,* 93**:** 2025–42.

Bazzurro P., Cornell C.A. (2004a). Nonlinear soil-site effects in probabilistic seismic-hazard analysis, *Bull. Seismol. Soc. Am.,* 94**:** 2110–23.

———. (2004b). Ground motion amplification in nonlinear soil sites with uncertain properties, *Bull. Seismo. Soc. Am.,* 94**:** 2090–2109.

———. (2005). *Erratum to* Ground motion amplification in nonlinear soil sites with uncertain properties, *Bull. Seismol. Soc. Am.,* 95**:** 2027.

Boore D.M. (2005). *Erratum to* Equations for estimating horizontal response spectra and peak acceleration from western North American earthquakes: A summary of recent work, *Seismol. Res. Lett.,* 76**:** 368–69.

——— (2010). Orientation-independent, nongeometric-mean measures of seismic intensity from two horizontal components of motion, *Bull. Seismol. Soc. Am.,* 100: 1830–35.

Boore D.M., Atkinson G.M. (2007). Boore-Atkinson NGA ground motion relations for the geometric mean horizontal component of peak and spectral ground motion parameters, *Report PEER 2007/01*, Pacific Earthquake Engineering Research Center, University of California, Berkeley, CA.

——— (2008). Ground-motion prediction equations for the average horizontal component of PGA, PGV, and 5%-damped PSA at spectral periods between 0.01 s and 10.0 s, *Earthq. Spectra,* 24: 99–138.

Boore D.M., Joyner W.B. (1997). Site amplification for generic rock sites, *Bull. Seismol. Soc. Am.,* 87: 327–41.

Boore D.M., Joyner W.B., Fumal T.E. (1993). Estimation of response spectra and peak accelerations from western North American earthquakes: An interim report, U.S. Geological Survey, *USGS Geological Survey Open-File Report. 93-509*.

——— (1994). Estimation of response spectra and peak accelerations from western North American earthquakes: An interim report, part 2, U.S. Geological Survey, *USGS Open-File Report 94-127*.

——— (1997). Equations for estimating horizontal response spectra and peak acceleration from western North American earthquakes: A summary of recent work, *Seismol. Res. Lett.,* 68**:** 128–53.

Boore D.M., Watson-Lamprey J., Abrahamson N.A. (2006). Orientation-independent measures of ground motion, *Bull. Seismol. Soc. Am.,* 96**:** 1502–11.

Borcherdt R.D. (1994). Estimates of site-dependent response spectra for design (methodology and justification), *Earthq. Spectra,* 10**:** 617–53.

Bozorgnia Y., Campbell K.W. (2004). Engineering characterization of ground motion, In: *Earthquake Engineering: From Engineering Seismology to Performance-Based Engineering,* Bozorgnia, Y., Bertero, V.V. (eds.), Chapter 5, pp. 1–74. Boca Raton, FL: CRC Press.

Bozorgnia Y., Hachem M.M., Campbell K.W. (2006). Attenuation of inelastic and damage spectra. *Proceedings, 8th National Conference on Earthquake Engineering*, Earthquake Engineering Research Institute, CD-ROM, Paper No. 1127, San Francisco, CA.

———. (2010). Ground motion prediction equation ("attenuation relationship") for inelastic response spectra, *Earthq. Spectra,* 26: 1–23.

Bozorgnia Y., Abrahamson N.A., Campbell K.W., Rowshandal B., Shantz T. (2012). NGA-West2: A comprehensive research program to update ground motion predictions equations for shallow crustal earthquakes in active tectonic regions, *Proceedings, 15th World Conference on Earthquake Engineering*, Paper No. 2572, Lisbon, Portugal.

Brune J. (1970). Tectonic stress and the spectra of seismic shear waves, *J. Geophys. Res.,* 75: 4997–5009.

——— (1971). *Correction to* Tectonic stress and the spectra of seismic shear waves, *J. Geophys. Res.,* 76**:** 5002.

BSSC (2009). NEHRP recommended seismic provisions for new buildings and other structures (*FEMA P-750*), 2009 edition, Report prepared for the Federal Emergency Management Agency (FEMA). Washington, D.C.: Building Seismic Safety Council, National Institute of Building Sciences.

Campbell K.W. (1981). Near-source attenuation of peak horizontal acceleration, *Bull. Seismol. Soc. Am.,* 71**:** 2039–70.

——— (1997). Empirical near-source attenuation relationships for horizontal and vertical components of peak ground acceleration, peak ground velocity, and pseudo-absolute acceleration response spectra, *Seismol. Res. Lett.,* 68**:** 154–79.

——— (2000). *Erratum to* Empirical near-source attenuation relationships for horizontal and vertical components of peak ground acceleration, peak ground velocity, and pseudo-absolute acceleration response spectra, *Seismol. Res. Lett.,* 71**:** 352–54.

——— (2001). *Erratum to* Empirical near-source attenuation relationships for horizontal and vertical components of peak ground acceleration, peak ground velocity, and pseudo-absolute acceleration response spectra, *Seismol. Res. Lett.,* 72**:** 474.

——— (2004). Engineering models of strong ground motion, In: *Earthquake Engineering Handbook,* Chen, W.F., Scawthorn, C. (eds.), Chapter 5, pp. 1–76. Boca Raton, Florida: CRC Press.

——— (2008). Hybrid empirical ground motion model for PGA and 5% damped linear elastic response spectra from shallow crustal earthquakes in stable continental regions: Example for eastern North America, *Proceedings, 14th World Conference on Earthquake Engineering*, Paper No. S03-001, Beijing, China.

——— (2011). Ground motion simulation using the hybrid empirical method: Issues and insights, In: *Earthquake Data in Engineering Seismology*, Akkar, S., Gülkan, P., van Eck, T. (eds.), Geotechnical, Geological, and Earthquake Engineering 14, Chapter 7, pp. 81–95. Berlin: Springer.

Campbell K.W., Bozorgnia Y. (1994). Near-source attenuation of peak horizontal acceleration from worldwide accelerograms recorded from 1957 to 1933, *Proceedings, 5th U.S. National Conference on Earthquake Engineering,* Earthquake Engineering Research Institute, Vol. III, pp. 283–92, Chicago, IL.

——— (2003a). Updated near-source ground motion (attenuation) relations for the horizontal and vertical components of peak ground acceleration and acceleration response spectra, *Bull. Seismol. Soc. Am.,* 93**:** 314–31.

——— (2003b). *Erratum to* Updated near-source ground motion (attenuation) relations for the horizontal and vertical components of peak ground acceleration and acceleration response spectra, *Bull. Seismol. Soc. Am.,* 93**:** 1872.

——— 2003c. *Erratum to* Updated near-source ground motion (attenuation) relations for the horizontal and vertical components of peak ground acceleration and acceleration response spectra, *Bull. Seismol. Soc. Am.,* 93**:** 1413.

——— (2004). *Erratum to* Updated near-source ground motion (attenuation) relations for the horizontal and vertical components of peak ground acceleration and acceleration response spectra, *Bull. Seismol. Soc. Am.,* 94**:** 2417.

——— (2007). Campbell-Bozorgnia NGA ground motion relations for the geometric mean horizontal component of peak and spectral ground motion parameters, *Report PEER 2007/02*, Pacific Earthquake Engineering Research Center, University of California, Berkeley, CA.
——— (2008). NGA ground motion model for the geometric mean horizontal component of PGA, PGV, PGD and 5% damped linear-elastic response spectra for periods ranging from 0.01 and 10.0 s, *Earthq. Spectra,* 24: 139–71.
——— (2010). A ground motion prediction equation for the horizontal component of cumulative absolute velocity (CAV) based on the PEER-NGA strong motion database, *Earthq. Spectra,* 26: 635–50.
——— (2011a). A ground motion prediction equation for JMA instrumental seismic intensity for shallow crustal earthquakes in active tectonic regimes, *Earthq. Eng. Struct. Dyn.,* 40: 413–27.
——— (2011b). Predictive equations for the standardized version of cumulative absolute velocity as adapted for use in the shutdown of U.S. nuclear power plants, *Nucl. Eng. Des.,* 241: 2558–69.
——— (2012a). A comparison of ground motion prediction equations for Arias intensity and cumulative absolute velocity developed using a consistent database and functional form, *Earthq. Spectra,* 28: 931–41.
——— (2012b). Cumulative absolute velocity (CAV) and seismic intensity based on the PEER-NGA database, *Earthq. Spectra* 28: 457–85.
Chiou B.S.-J., Youngs R.R. (2008a). An NGA model for the average horizontal component of peak ground motion and response spectra, *Earthq. Spectra,* 24: 173–215.
——— (2008b). NGA model for average horizontal component of peak ground motion and response spectra, *Report PEER 2008/09*, Pacific Earthquake Engineering Research Center, University of California, Berkeley, CA.
Choi Y., Stewart J.P. (2005). Nonlinear site amplification as function of 30 m shear wave velocity, *Earthq. Spectra,* 21**:** 1–30.
Collins N., Graves. R.W., Ichinose G., Somerville P. (2006). Ground motion attenuation relations for the Intermountain West*, Final report prepared for the U.S. Geological Survey, Award No. 05HQGR0031*, URS Corporation, Pasadena, CA.
Day S.M., Graves R., Bielak J., Dreger. D., Larsen S., Olsen. K.B., Pitarka A., Ramirez-Guzman L. (2006). Model for basin effects on long-period response spectra in southern California, *Earthq. Spectra,* 24: 257–77.
Di Toro G., Hirose T., Nielsen S., Pennacchioni G., Shimamoto T. (2006). Natural and experimental evidence of melt lubrication of faults during earthquakes, *Science*, 311**:** 647–49.
Donahue J., Abrahamson N.A. (2013). Hanging-wall scaling using finite-fault simulations, *Report PEER 2013/14*, Pacific Earthquake Engineering Research Center, University of California, Berkeley, CA.
Douglas J. (2002). Note on scaling of peak ground acceleration and peak ground velocity with magnitude, *Geophys. J. Int.,* 148: 336–39.
EPRI (1993). Methods and guidelines for estimating earthquake ground motion in eastern North America: Guidelines for determining design basis ground motions, Electric Power Research Institute, *Report EPRI TR-102293*, Vol. 1, Palo Alto, CA.
Field E.H. (2000). A modified ground-motion attenuation relationship for southern California that accounts for detailed site classification and a basin-depth effect, *Bull. Seismol. Soc. Am.,* 90**:** S209–21.
Frankel A.D. (2009). A constant stress-drop model for producing broadband synthetic seismograms: Comparison with the next generation attenuation relationships, *Bull. Seismol. Soc Am.,* 99**:** 664–80.
Halldorsson B., Papgeorgiou A.S. (2005). Calibration of the specific barrier model to earthquakes of different tectonic regions, *Bull. Seismol. Soc. Am.* 95**:** 1276–1300.
Hanks T.C., Bakun W.H. (2002). A bilinear source-scaling model for **M**–log *A* observations of continental earthquakes, *Bull. Seismol. Soc. Am.,* 92**:** 1841–46.
Hough S.E., Anderson J.G., Brune J., Vernon III F., Berger J., Fletcher J., Haar L., Hanks T., Baker L. (1988). Attenuation near Anza, California, *Bull. Seismol. Soc. Am.,* 78**:** 672–91.
Idriss I.M. (2008). An NGA empirical model for estimating the horizontal spectral values generated by shallow crustal earthquakes, *Earthq. Spectra,* 24: 217–42.
Johnston A.C. (1996). Seismic moment assessment of earthquakes in stable continental regions—I. Instrumental seismicity, *Geophys. J. Int.,* 124**:** 381–414.
Joyner W.B., Boore D.M. (1993). Methods for regression analysis of strong-motion data, *Bull. Seismol. Soc. Am.,* 83**:** 469–87.
Kaklamanos J., Baise L.G., Boore D.M. (2011). Estimating unknown input parameters when implementing the NGA ground-motion prediction equations in engineering practice, *Earthq. Spectra,* 27: 1219–35.

Kamai R., Abrahamson N.A., Silva W.J. (2013). Nonlinear horizontal site response for the NGA-West2 project, *Report PEER 2013/12*, Pacific Earthquake Engineering Research Center, University of California, Berkeley, CA.

Kwok A.O., Stewart J.P. (2006). Evaluation of the effectiveness of theoretical 1D amplification factors for earthquake ground-motion prediction, *Bull. Seismol. Soc. Am.,* 96**:** 1422–36.

Lay T., Wallace T.C. (1995). *Modern Global Seismology*. San Diego: Academic Press.

Lee W.H K., Shin T.C., Kuo. K.W., Chen. K.C., Wu C.F. (2001). Data files from "CWB free-field strong-motion data from the 21 September Chi-Chi, Taiwan, earthquake," *Bull. Seismol. Soc. Am.* 91**:** 1390.

Petersen M.D., Frankel A.D., Harmsen S.C., Mueller C.S., Haller K.M., Wheeler R.L., Wesson R.L., Zeng Y., Boyd O.S., Perkins D.M., Luco N., Field E.H., Wills C.J., Rukstales K.S. (2008). Documentation for the 2008 update of the United States national seismic hazard maps, U.S. Geological Survey, *USGS Open-File Report 2008-1128*.

Power M., Borcherdt R., Stewart J.P. (2004). Site amplification factors from empirical studies, *Report of NGA Working Group #5*, Pacific Earthquake Engineering Research Center, University of California, Berkeley, CA.

Power M., Chiou B., Abrahamson N.A., Bozorgnia Y., Shantz T., Roblee C. (2006). An overview of the NGA project, *Earthq. Spectra,* 24: 3–21.

Rezaeian S., Bozorgnia Y., Idriss I.M., Campbell K., Abrahamson N.A., Silva W.J. (2012). Spectral damping scaling factors for shallow crustal earthquakes in active tectonic regions, *Report PEER 2012/01*, Pacific Earthquake Engineering Research Center, University of California, Berkeley, CA.

Rezaeian S., Bozorgnia Y., Idriss I.M., Abrahamson N.A., Campbell K.W., Silva W.J. (2013). Damping scaling factors for elastic response spectra for shallow crustal earthquakes in active tectonic regions: "Average" horizontal component, *Earthq. Spectra,* 29: in press.

Scherbaum F., Schmedes J., Cotton F. (2004). On the conversion of source-to-site distance measures for extended earthquake source models, *Bull. Seismol. Soc. Am.,* 94**:** 1053–69.

Scholz C.H. (1982). Scaling laws for large earthquakes: Consequences for physical models, *Bull. Seismol. Soc. Am.,* 72**:** 1–14.

Schmedes J., Archuleta R.J. (2007). Oversaturation of peak ground velocity along strike slip faults, abstract, *Seismol. Res. Lett.,* 78**:** 272.

Silva W.J. (2005). Site response simulations for the NGA project, Pacific Engineering and Analysis, El Cerrito, CA, *Report prepared for the Pacific Earthquake Engineering Research Center*, University of California, Berkeley, CA.

Silva W.J., Li S., Darragh R.B., Gregor N. (1999). Surface geology based strong motion amplification factors for the San Francisco Bay and Los Angeles Areas*,* Pacific Engineering and Analysis, El Cerrito, CA, *Report prepared for the Pacific Earthquake Engineering Research Center*, *Task 5B*, University of California, Berkeley, CA.

Silva W.J., Darragh R.B., Gregor N., Martin N., Abrahamson N.A., Kircher C. (2000). Reassessment of site coefficients and near-fault factors for building code provisions, *Final report to U.S. Geological Survey, Award No. 98HQGR1010*, Pacific Engineering and Analysis, El Cerrito, CA

Somerville P., Pitarka A. (2006). Differences in earthquake source and ground motion characteristics between surface and buried earthquakes, *Proceedings., 8th National Conference on Earthquake Engineering,* Earthquake Engineering Research Institute, CD-ROM, Paper No. 977. Oakland, CA.

Spudich, P., Bayless J., Rowshandel B., Baker J.W., Shahi S., Choiu B.S.-J., Somerville P. (2013). Final report of the NGA-West2 directivity working group, *Report PEER 2013/09*, Pacific Earthquake Engineering Research Center, University of California, Berkeley, CA.

Stewart J.P., Goulet C.A. (2006). Comment on "Nonlinear soil-site effects in probabilistic seismic-hazard analysis by Paolo Bazzuro and C. Allin Cornell," *Bull. Seismol. Soc. Am.,* 96: 745–47.

Stewart J.P., Seyhan E. (2013). Semi-empirical nonlinear site amplification and its application in NEHRP site factors, *Report PEER 2013/13*, Pacific Earthquake Engineering Research Center, University of California, Berkeley, CA.

Stewart J.P., Liu A.H., Choi Y. (2003). Amplification factors for spectral acceleration in tectonically active regions, *Bull. Seismol. Soc. Am.,* 93: 332–52.

Stewart J.P., Seyhan E., Boore D.M., Campbell K.W., Erdik M., Silva W.J., Di Alessandro C., Bozorgnia Y. (2012). Site effects in parametric ground motion models for the GEM-PEER global GMPEs project, *Proceedings, 15th World Conference on Earthquake Engineering*, Paper No. 2554, Lisbon, Portugal.

Walling M., Silva W.J., Abrahamson N.A. (2008). Non-linear site amplification factors for constraining the NGA models, *Earthq. Spectra* 24: 243–55.

Wells D.L., Coppersmith K.J. (1993). Likelihood of surface rupture as a function of magnitude, abstract, *Seismol. Res. Lett.,* 64**:** 54.

———. (1994). New empirical relationships among magnitude, rupture length, rupture width, rupture area, and surface displacement, *Bull. Seismol. Soc. Am.*, 84**:** 974–1002.

Wooddell K.E., Abrahamson N.A. (2012). New earthquake classification scheme for mainshocks and aftershocks in the NGA-West2 ground motion prediction equations (GMPEs), *Proceedings, 15th World Conference on Earthquake Engineering*, Paper No. 3872, Lisbon, Portugal.

Youngs, R. R., Arabasz W.J., Anderson R.E., Ramelli A.R., Ake J.P., Slemmons D.B., McCalpin J.P., Doser D.I., Fridrich C.F., Swan F.H., Rogers A.M., Yount J.C., Anderson L.W., Smith K.D., Bruhn R.L., Knuepfer P.L.K., Smith R.B., dePolo C.M., O'Leary D.W., Coppersmith K.J., Pezzopane S.K., Schwartz D.P., Whitney J.W., Olig S.S., Toro G.R. (2003). A methodology for probabilistic fault displacement hazard analysis (PFSHA), *Earthq. Spectra,* 19**:** 191–219.

Appendix A: Electronic List of Selected Earthquakes and Recordings in the Near-Source Database

http://peer.berkeley.edu/publications/peer_reports/reports_2013/reports_2013.html

Appendix B: Electronic List of Selected Earthquakes and Recordings in the Far-Source Database

http://peer.berkeley.edu/publications/peer_reports/reports_2013/reports_2013.html

PEER REPORTS

PEER reports are available as a free PDF download from http://peer.berkeley.edu/publications/peer_reports_complete.html. Printed hard copies of PEER reports can be ordered directly from our printer by following the instructions at http://peer.berkeley.edu/publications/peer_reports.html. For other related questions about the PEER Report Series, contact the Pacific Earthquake Engineering Research Center, 325 Davis Hall mail code 1792, Berkeley, CA 94720. Tel.: (510) 642-3437; Fax: (510) 665-1655; Email: peer_editor@berkeley.edu

PEER 2013/06 *NGA-West2 Campbell-Bozorgnia Ground Motion Model for the Horizontal Components of PGA, PGV, and 5%-Damped Elastic Pseudo-Acceleration Response Spectra for Periods Ranging from 0.01 to 10 sec.* Kenneth W. Campbell and Yousef Bozorgnia. May 2013.

PEER 2013/05 *NGA-West2 Equations for Predicting Response Spectral Accelerations for Shallow Crustal Earthquakes.* David M. Boore, Jonathan P. Stewart, Emel Seyhan, Gail M. Atkinson. May 2013.

PEER 2013/04 *Update of the AS08 Ground-Motion Prediction Equations Based on the NGA-West2 Data Set.* Norman SA. Abrahamson, Walter J. Silva, and Ronnie Kamai. May 2013.

PEER 2013/03 *PEER NGA-West2 Database.* Timothy D. Ancheta, Robert B. Darragh, Jonathan P. Stewart, Emel Seyhan, Walter J. Silva, Brian S.J. Chiou, Katie E. Wooddell, Robert W. Graves, Albert R. Kottke, David M. Boore, Tadahiro Kishida, and Jennifer L. Donahue. May 2013.

PEER 2013/02 *Hybrid Simulation of the Seismic Response of Squat Reinforced Concrete Shear Walls.* Catherine A. Whyte and Bozidar Stojadinovic. May 2013.

PEER 2013/01 *Housing Recovery in Chile: A Qualitative Mid-program Review.* Mary C. Comerio. February 2013.

PEER 2012/08 *Guidelines for Estimation of Shear Wave Velocity.* Bernard R. Wair, Jason T. DeJong, and Thomas Shantz. December 2012.

PEER 2012/07 *Earthquake Engineering for Resilient Communities: 2012 PEER Internship Program Research Report Collection.* Heidi Tremayne (Editor), Stephen A. Mahin (Editor), Collin Anderson, Dustin Cook, Michael Erceg, Carlos Esparza, Jose Jimenez, Dorian Krausz, Andrew Lo, Stephanie Lopez, Nicole McCurdy, Paul Shipman, Alexander Strum, Eduardo Vega. December 2012.

PEER 2012/06 *Fragilities for Precarious Rocks at Yucca Mountain.* Matthew D. Purvance, Rasool Anooshehpoor, and James N. Brune. December 2012.

PEER 2012/05 *Development of Simplified Analysis Procedure for Piles in Laterally Spreading Layered Soils.* Christopher R. McGann, Pedro Arduino, and Peter Mackenzie–Helnwein. December 2012.

PEER 2012/04 *Unbonded Pre-Tensioned Columns for Bridges in Seismic Regions.* Phillip M. Davis, Todd M. Janes, Marc O. Eberhard, and John F. Stanton. December 2012.

PEER 2012/03 *Experimental and Analytical Studies on Reinforced Concrete Buildings with Seismically Vulnerable Beam-Column Joints.* Sangjoon Park and Khalid M. Mosalam. October 2012.

PEER 2012/02 *Seismic Performance of Reinforced Concrete Bridges Allowed to Uplift during Multi-Directional Excitation.* Andres Oscar Espinoza and Stephen A. Mahin. July 2012.

PEER 2012/01 *Spectral Damping Scaling Factors for Shallow Crustal Earthquakes in Active Tectonic Regions.* Sanaz Rezaeian, Yousef Bozorgnia, I. M. Idriss, Kenneth Campbell, Norman Abrahamson, and Walter Silva. July 2012.

PEER 2011/10 *Earthquake Engineering for Resilient Communities: 2011 PEER Internship Program Research Report Collection.* Eds. Heidi Faison and Stephen A. Mahin. December 2011.

PEER 2011/09 *Calibration of Semi-Stochastic Procedure for Simulating High-Frequency Ground Motions.* Jonathan P. Stewart, Emel Seyhan, and Robert W. Graves. December 2011.

PEER 2011/08 *Water Supply in regard to Fire Following Earthquake.* Charles Scawthorn. November 2011.

PEER 2011/07 *Seismic Risk Management in Urban Areas. Proceedings of a U.S.-Iran-Turkey Seismic Workshop.* September 2011.

PEER 2011/06 *The Use of Base Isolation Systems to Achieve Complex Seismic Performance Objectives.* Troy A. Morgan and Stephen A. Mahin. July 2011.

PEER 2011/05 *Case Studies of the Seismic Performance of Tall Buildings Designed by Alternative Means.* Task 12 Report for the Tall Buildings Initiative. Jack Moehle, Yousef Bozorgnia, Nirmal Jayaram, Pierson Jones, Mohsen Rahnama, Nilesh Shome, Zeynep Tuna, John Wallace, Tony Yang, and Farzin Zareian. July 2011.

PEER 2011/04 *Recommended Design Practice for Pile Foundations in Laterally Spreading Ground.* Scott A. Ashford, Ross W. Boulanger, and Scott J. Brandenberg. June 2011.

PEER 2011/03 *New Ground Motion Selection Procedures and Selected Motions for the PEER Transportation Research Program.* Jack W. Baker, Ting Lin, Shrey K. Shahi, and Nirmal Jayaram. March 2011.

PEER 2011/02 *A Bayesian Network Methodology for Infrastructure Seismic Risk Assessment and Decision Support.* Michelle T. Bensi, Armen Der Kiureghian, and Daniel Straub. March 2011.

PEER 2011/01 *Demand Fragility Surfaces for Bridges in Liquefied and Laterally Spreading Ground.* Scott J. Brandenberg, Jian Zhang, Pirooz Kashighandi, Yili Huo, and Minxing Zhao. March 2011.

PEER 2010/05 *Guidelines for Performance-Based Seismic Design of Tall Buildings.* Developed by the Tall Buildings Initiative. November 2010.

PEER 2010/04 *Application Guide for the Design of Flexible and Rigid Bus Connections between Substation Equipment Subjected to Earthquakes.* Jean-Bernard Dastous and Armen Der Kiureghian. September 2010.

PEER 2010/03 *Shear Wave Velocity as a Statistical Function of Standard Penetration Test Resistance and Vertical Effective Stress at Caltrans Bridge Sites.* Scott J. Brandenberg, Naresh Bellana, and Thomas Shantz. June 2010.

PEER 2010/02 *Stochastic Modeling and Simulation of Ground Motions for Performance-Based Earthquake Engineering.* Sanaz Rezaeian and Armen Der Kiureghian. June 2010.

PEER 2010/01 *Structural Response and Cost Characterization of Bridge Construction Using Seismic Performance Enhancement Strategies.* Ady Aviram, Božidar Stojadinović, Gustavo J. Parra-Montesinos, and Kevin R. Mackie. March 2010.

PEER 2009/03 *The Integration of Experimental and Simulation Data in the Study of Reinforced Concrete Bridge Systems Including Soil-Foundation-Structure Interaction.* Matthew Dryden and Gregory L. Fenves. November 2009.

PEER 2009/02 *Improving Earthquake Mitigation through Innovations and Applications in Seismic Science, Engineering, Communication, and Response. Proceedings of a U.S.-Iran Seismic Workshop.* October 2009.

PEER 2009/01 *Evaluation of Ground Motion Selection and Modification Methods: Predicting Median Interstory Drift Response of Buildings.* Curt B. Haselton, Ed. June 2009.

PEER 2008/10 *Technical Manual for Strata.* Albert R. Kottke and Ellen M. Rathje. February 2009.

PEER 2008/09 *NGA Model for Average Horizontal Component of Peak Ground Motion and Response Spectra.* Brian S.-J. Chiou and Robert R. Youngs. November 2008.

PEER 2008/08 *Toward Earthquake-Resistant Design of Concentrically Braced Steel Structures.* Patxi Uriz and Stephen A. Mahin. November 2008.

PEER 2008/07 *Using OpenSees for Performance-Based Evaluation of Bridges on Liquefiable Soils.* Stephen L. Kramer, Pedro Arduino, and HyungSuk Shin. November 2008.

PEER 2008/06 *Shaking Table Tests and Numerical Investigation of Self-Centering Reinforced Concrete Bridge Columns.* Hyung IL Jeong, Junichi Sakai, and Stephen A. Mahin. September 2008.

PEER 2008/05 *Performance-Based Earthquake Engineering Design Evaluation Procedure for Bridge Foundations Undergoing Liquefaction-Induced Lateral Ground Displacement.* Christian A. Ledezma and Jonathan D. Bray. August 2008.

PEER 2008/04 *Benchmarking of Nonlinear Geotechnical Ground Response Analysis Procedures.* Jonathan P. Stewart, Annie On-Lei Kwok, Yousseff M. A. Hashash, Neven Matasovic, Robert Pyke, Zhiliang Wang, and Zhaohui Yang. August 2008.

PEER 2008/03 *Guidelines for Nonlinear Analysis of Bridge Structures in California.* Ady Aviram, Kevin R. Mackie, and Božidar Stojadinović. August 2008.

PEER 2008/02 *Treatment of Uncertainties in Seismic-Risk Analysis of Transportation Systems.* Evangelos Stergiou and Anne S. Kiremidjian. July 2008.

PEER 2008/01 *Seismic Performance Objectives for Tall Buildings.* William T. Holmes, Charles Kircher, William Petak, and Nabih Youssef. August 2008.

PEER 2007/12 *An Assessment to Benchmark the Seismic Performance of a Code-Conforming Reinforced Concrete Moment-Frame Building.* Curt Haselton, Christine A. Goulet, Judith Mitrani-Reiser, James L. Beck, Gregory G. Deierlein, Keith A. Porter, Jonathan P. Stewart, and Ertugrul Taciroglu. August 2008.

PEER 2007/11 *Bar Buckling in Reinforced Concrete Bridge Columns.* Wayne A. Brown, Dawn E. Lehman, and John F. Stanton. February 2008.

PEER 2007/10 *Computational Modeling of Progressive Collapse in Reinforced Concrete Frame Structures.* Mohamed M. Talaat and Khalid M. Mosalam. May 2008.

PEER 2007/09 *Integrated Probabilistic Performance-Based Evaluation of Benchmark Reinforced Concrete Bridges.* Kevin R. Mackie, John-Michael Wong, and Božidar Stojadinović. January 2008.

PEER 2007/08 *Assessing Seismic Collapse Safety of Modern Reinforced Concrete Moment-Frame Buildings.* Curt B. Haselton and Gregory G. Deierlein. February 2008.

PEER 2007/07 *Performance Modeling Strategies for Modern Reinforced Concrete Bridge Columns.* Michael P. Berry and Marc O. Eberhard. April 2008.

PEER 2007/06 *Development of Improved Procedures for Seismic Design of Buried and Partially Buried Structures.* Linda Al Atik and Nicholas Sitar. June 2007.

PEER 2007/05 *Uncertainty and Correlation in Seismic Risk Assessment of Transportation Systems.* Renee G. Lee and Anne S. Kiremidjian. July 2007.

PEER 2007/04 *Numerical Models for Analysis and Performance-Based Design of Shallow Foundations Subjected to Seismic Loading.* Sivapalan Gajan, Tara C. Hutchinson, Bruce L. Kutter, Prishati Raychowdhury, José A. Ugalde, and Jonathan P. Stewart. May 2008.

PEER 2007/03 *Beam-Column Element Model Calibrated for Predicting Flexural Response Leading to Global Collapse of RC Frame Buildings.* Curt B. Haselton, Abbie B. Liel, Sarah Taylor Lange, and Gregory G. Deierlein. May 2008.

PEER 2007/02 *Campbell-Bozorgnia NGA Ground Motion Relations for the Geometric Mean Horizontal Component of Peak and Spectral Ground Motion Parameters.* Kenneth W. Campbell and Yousef Bozorgnia. May 2007.

PEER 2007/01 *Boore-Atkinson NGA Ground Motion Relations for the Geometric Mean Horizontal Component of Peak and Spectral Ground Motion Parameters.* David M. Boore and Gail M. Atkinson. May. May 2007.

PEER 2006/12 *Societal Implications of Performance-Based Earthquake Engineering.* Peter J. May. May 2007.

PEER 2006/11 *Probabilistic Seismic Demand Analysis Using Advanced Ground Motion Intensity Measures, Attenuation Relationships, and Near-Fault Effects.* Polsak Tothong and C. Allin Cornell. March 2007.

PEER 2006/10 *Application of the PEER PBEE Methodology to the I-880 Viaduct.* Sashi Kunnath. February 2007.

PEER 2006/09 *Quantifying Economic Losses from Travel Forgone Following a Large Metropolitan Earthquake.* James Moore, Sungbin Cho, Yue Yue Fan, and Stuart Werner. November 2006.

PEER 2006/08 *Vector-Valued Ground Motion Intensity Measures for Probabilistic Seismic Demand Analysis.* Jack W. Baker and C. Allin Cornell. October 2006.

PEER 2006/07 *Analytical Modeling of Reinforced Concrete Walls for Predicting Flexural and Coupled–Shear-Flexural Responses.* Kutay Orakcal, Leonardo M. Massone, and John W. Wallace. October 2006.

PEER 2006/06 *Nonlinear Analysis of a Soil-Drilled Pier System under Static and Dynamic Axial Loading.* Gang Wang and Nicholas Sitar. November 2006.

PEER 2006/05 *Advanced Seismic Assessment Guidelines.* Paolo Bazzurro, C. Allin Cornell, Charles Menun, Maziar Motahari, and Nicolas Luco. September 2006.

PEER 2006/04 *Probabilistic Seismic Evaluation of Reinforced Concrete Structural Components and Systems.* Tae Hyung Lee and Khalid M. Mosalam. August 2006.

PEER 2006/03 *Performance of Lifelines Subjected to Lateral Spreading.* Scott A. Ashford and Teerawut Juirnarongrit. July 2006.

PEER 2006/02 *Pacific Earthquake Engineering Research Center Highway Demonstration Project.* Anne Kiremidjian, James Moore, Yue Yue Fan, Nesrin Basoz, Ozgur Yazali, and Meredith Williams. April 2006.

PEER 2006/01 *Bracing Berkeley. A Guide to Seismic Safety on the UC Berkeley Campus.* Mary C. Comerio, Stephen Tobriner, and Ariane Fehrenkamp. January 2006.

PEER 2005/16 *Seismic Response and Reliability of Electrical Substation Equipment and Systems.* Junho Song, Armen Der Kiureghian, and Jerome L. Sackman. April 2006.

PEER 2005/15 *CPT-Based Probabilistic Assessment of Seismic Soil Liquefaction Initiation.* R. E. S. Moss, R. B. Seed, R. E. Kayen, J. P. Stewart, and A. Der Kiureghian. April 2006.

PEER 2005/14 *Workshop on Modeling of Nonlinear Cyclic Load-Deformation Behavior of Shallow Foundations.* Bruce L. Kutter, Geoffrey Martin, Tara Hutchinson, Chad Harden, Sivapalan Gajan, and Justin Phalen. March 2006.

PEER 2005/13 *Stochastic Characterization and Decision Bases under Time-Dependent Aftershock Risk in Performance-Based Earthquake Engineering.* Gee Liek Yeo and C. Allin Cornell. July 2005.

PEER 2005/12 *PEER Testbed Study on a Laboratory Building: Exercising Seismic Performance Assessment.* Mary C. Comerio, editor. November 2005.

PEER 2005/11 *Van Nuys Hotel Building Testbed Report: Exercising Seismic Performance Assessment.* Helmut Krawinkler, editor. October 2005.

PEER 2005/10 *First NEES/E-Defense Workshop on Collapse Simulation of Reinforced Concrete Building Structures.* September 2005.

PEER 2005/09 *Test Applications of Advanced Seismic Assessment Guidelines.* Joe Maffei, Karl Telleen, Danya Mohr, William Holmes, and Yuki Nakayama. August 2006.

PEER 2005/08 *Damage Accumulation in Lightly Confined Reinforced Concrete Bridge Columns.* R. Tyler Ranf, Jared M. Nelson, Zach Price, Marc O. Eberhard, and John F. Stanton. April 2006.

PEER 2005/07 *Experimental and Analytical Studies on the Seismic Response of Freestanding and Anchored Laboratory Equipment.* Dimitrios Konstantinidis and Nicos Makris. January 2005.

PEER 2005/06 *Global Collapse of Frame Structures under Seismic Excitations*. Luis F. Ibarra and Helmut Krawinkler. September 2005.

PEER 2005//05 *Performance Characterization of Bench- and Shelf-Mounted Equipment.* Samit Ray Chaudhuri and Tara C. Hutchinson. May 2006.

PEER 2005/04 *Numerical Modeling of the Nonlinear Cyclic Response of Shallow Foundations.* Chad Harden, Tara Hutchinson, Geoffrey R. Martin, and Bruce L. Kutter. August 2005.

PEER 2005/03 *A Taxonomy of Building Components for Performance-Based Earthquake Engineering.* Keith A. Porter. September 2005.

PEER 2005/02 *Fragility Basis for California Highway Overpass Bridge Seismic Decision Making*. Kevin R. Mackie and Božidar Stojadinović. June 2005.

PEER 2005/01 *Empirical Characterization of Site Conditions on Strong Ground Motion.* Jonathan P. Stewart, Yoojoong Choi, and Robert W. Graves. June 2005.

PEER 2004/09 *Electrical Substation Equipment Interaction: Experimental Rigid Conductor Studies.* Christopher Stearns and André Filiatrault. February 2005.

PEER 2004/08 *Seismic Qualification and Fragility Testing of Line Break 550-kV Disconnect Switches.* Shakhzod M. Takhirov, Gregory L. Fenves, and Eric Fujisaki. January 2005.

PEER 2004/07 *Ground Motions for Earthquake Simulator Qualification of Electrical Substation Equipment.* Shakhzod M. Takhirov, Gregory L. Fenves, Eric Fujisaki, and Don Clyde. January 2005.

PEER 2004/06 *Performance-Based Regulation and Regulatory Regimes.* Peter J. May and Chris Koski. September 2004.

PEER 2004/05 *Performance-Based Seismic Design Concepts and Implementation: Proceedings of an International Workshop.* Peter Fajfar and Helmut Krawinkler, editors. September 2004.

PEER 2004/04 *Seismic Performance of an Instrumented Tilt-up Wall Building.* James C. Anderson and Vitelmo V. Bertero. July 2004.

PEER 2004/03 *Evaluation and Application of Concrete Tilt-up Assessment Methodologies.* Timothy Graf and James O. Malley. October 2004.

PEER 2004/02 *Analytical Investigations of New Methods for Reducing Residual Displacements of Reinforced Concrete Bridge Columns.* Junichi Sakai and Stephen A. Mahin. August 2004.

PEER 2004/01 *Seismic Performance of Masonry Buildings and Design Implications.* Kerri Anne Taeko Tokoro, James C. Anderson, and Vitelmo V. Bertero. February 2004.

PEER 2003/18 *Performance Models for Flexural Damage in Reinforced Concrete Columns.* Michael Berry and Marc Eberhard. August 2003.

PEER 2003/17 *Predicting Earthquake Damage in Older Reinforced Concrete Beam-Column Joints.* Catherine Pagni and Laura Lowes. October 2004.

PEER 2003/16 *Seismic Demands for Performance-Based Design of Bridges.* Kevin Mackie and Božidar Stojadinović. August 2003.

PEER 2003/15 *Seismic Demands for Nondeteriorating Frame Structures and Their Dependence on Ground Motions.* Ricardo Antonio Medina and Helmut Krawinkler. May 2004.

PEER 2003/14 *Finite Element Reliability and Sensitivity Methods for Performance-Based Earthquake Engineering.* Terje Haukaas and Armen Der Kiureghian. April 2004.

PEER 2003/13 *Effects of Connection Hysteretic Degradation on the Seismic Behavior of Steel Moment-Resisting Frames.* Janise E. Rodgers and Stephen A. Mahin. March 2004.

PEER 2003/12 *Implementation Manual for the Seismic Protection of Laboratory Contents: Format and Case Studies.* William T. Holmes and Mary C. Comerio. October 2003.

PEER 2003/11 *Fifth U.S.-Japan Workshop on Performance-Based Earthquake Engineering Methodology for Reinforced Concrete Building Structures.* February 2004.

PEER 2003/10 *A Beam-Column Joint Model for Simulating the Earthquake Response of Reinforced Concrete Frames.* Laura N. Lowes, Nilanjan Mitra, and Arash Altoontash. February 2004.

PEER 2003/09 *Sequencing Repairs after an Earthquake: An Economic Approach.* Marco Casari and Simon J. Wilkie. April 2004.

PEER 2003/08 *A Technical Framework for Probability-Based Demand and Capacity Factor Design (DCFD) Seismic Formats*. Fatemeh Jalayer and C. Allin Cornell. November 2003.

PEER 2003/07 *Uncertainty Specification and Propagation for Loss Estimation Using FOSM Methods.* Jack W. Baker and C. Allin Cornell. September 2003.

PEER 2003/06 *Performance of Circular Reinforced Concrete Bridge Columns under Bidirectional Earthquake Loading*. Mahmoud M. Hachem, Stephen A. Mahin, and Jack P. Moehle. February 2003.

PEER 2003/05 *Response Assessment for Building-Specific Loss Estimation.* Eduardo Miranda and Shahram Taghavi. September 2003.

PEER 2003/04 *Experimental Assessment of Columns with Short Lap Splices Subjected to Cyclic Loads*. Murat Melek, John W. Wallace, and Joel Conte. April 2003.

PEER 2003/03 *Probabilistic Response Assessment for Building-Specific Loss Estimation.* Eduardo Miranda and Hesameddin Aslani. September 2003.

PEER 2003/02 *Software Framework for Collaborative Development of Nonlinear Dynamic Analysis Program.* Jun Peng and Kincho H. Law. September 2003.

PEER 2003/01 *Shake Table Tests and Analytical Studies on the Gravity Load Collapse of Reinforced Concrete Frames*. Kenneth John Elwood and Jack P. Moehle. November 2003.

PEER 2002/24 *Performance of Beam to Column Bridge Joints Subjected to a Large Velocity Pulse.* Natalie Gibson, André Filiatrault, and Scott A. Ashford. April 2002.

PEER 2002/23 *Effects of Large Velocity Pulses on Reinforced Concrete Bridge Columns.* Greg L. Orozco and Scott A. Ashford. April 2002.

PEER 2002/22 *Characterization of Large Velocity Pulses for Laboratory Testing.* Kenneth E. Cox and Scott A. Ashford. April 2002.

PEER 2002/21 *Fourth U.S.-Japan Workshop on Performance-Based Earthquake Engineering Methodology for Reinforced Concrete Building Structures*. December 2002.

PEER 2002/20 *Barriers to Adoption and Implementation of PBEE Innovations.* Peter J. May. August 2002.

PEER 2002/19 *Economic-Engineered Integrated Models for Earthquakes: Socioeconomic Impacts.* Peter Gordon, James E. Moore II, and Harry W. Richardson. July 2002.

PEER 2002/18 *Assessment of Reinforced Concrete Building Exterior Joints with Substandard Details.* Chris P. Pantelides, Jon Hansen, Justin Nadauld, and Lawrence D. Reaveley. May 2002.

PEER 2002/17 *Structural Characterization and Seismic Response Analysis of a Highway Overcrossing Equipped with Elastomeric Bearings and Fluid Dampers: A Case Study.* Nicos Makris and Jian Zhang. November 2002.

PEER 2002/16 *Estimation of Uncertainty in Geotechnical Properties for Performance-Based Earthquake Engineering.* Allen L. Jones, Steven L. Kramer, and Pedro Arduino. December 2002.

PEER 2002/15 *Seismic Behavior of Bridge Columns Subjected to Various Loading Patterns.* Asadollah Esmaeily-Gh. and Yan Xiao. December 2002.

PEER 2002/14 *Inelastic Seismic Response of Extended Pile Shaft Supported Bridge Structures.* T.C. Hutchinson, R.W. Boulanger, Y.H. Chai, and I.M. Idriss. December 2002.

PEER 2002/13 *Probabilistic Models and Fragility Estimates for Bridge Components and Systems.* Paolo Gardoni, Armen Der Kiureghian, and Khalid M. Mosalam. June 2002.

PEER 2002/12 *Effects of Fault Dip and Slip Rake on Near-Source Ground Motions: Why Chi-Chi Was a Relatively Mild M7.6 Earthquake.* Brad T. Aagaard, John F. Hall, and Thomas H. Heaton. December 2002.

PEER 2002/11 *Analytical and Experimental Study of Fiber-Reinforced Strip Isolators*. James M. Kelly and Shakhzod M. Takhirov. September 2002.

PEER 2002/10 *Centrifuge Modeling of Settlement and Lateral Spreading with Comparisons to Numerical Analyses***.** Sivapalan Gajan and Bruce L. Kutter. January 2003.

PEER 2002/09 *Documentation and Analysis of Field Case Histories of Seismic Compression during the 1994 Northridge, California, Earthquake.* Jonathan P. Stewart, Patrick M. Smith, Daniel H. Whang, and Jonathan D. Bray. October 2002.

PEER 2002/08 *Component Testing, Stability Analysis and Characterization of Buckling-Restrained Unbonded Braces™.* Cameron Black, Nicos Makris, and Ian Aiken. September 2002.

PEER 2002/07 *Seismic Performance of Pile-Wharf Connections.* Charles W. Roeder, Robert Graff, Jennifer Soderstrom, and Jun Han Yoo. December 2001.

PEER 2002/06 *The Use of Benefit-Cost Analysis for Evaluation of Performance-Based Earthquake Engineering Decisions*. Richard O. Zerbe and Anthony Falit-Baiamonte. September 2001.

PEER 2002/05 *Guidelines, Specifications, and Seismic Performance Characterization of Nonstructural Building Components and Equipment*. André Filiatrault, Constantin Christopoulos, and Christopher Stearns. September 2001.

PEER 2002/04 *Consortium of Organizations for Strong-Motion Observation Systems and the Pacific Earthquake Engineering Research Center Lifelines Program: Invited Workshop on Archiving and Web Dissemination of Geotechnical Data, 4–5 October 2001*. September 2002.

PEER 2002/03 *Investigation of Sensitivity of Building Loss Estimates to Major Uncertain Variables for the Van Nuys Testbed.* Keith A. Porter, James L. Beck, and Rustem V. Shaikhutdinov. August 2002.

PEER 2002/02 *The Third U.S.-Japan Workshop on Performance-Based Earthquake Engineering Methodology for Reinforced Concrete Building Structures*. July 2002.

PEER 2002/01 *Nonstructural Loss Estimation: The UC Berkeley Case Study.* Mary C. Comerio and John C. Stallmeyer. December 2001.

PEER 2001/16 *Statistics of SDF-System Estimate of Roof Displacement for Pushover Analysis of Buildings.* Anil K. Chopra, Rakesh K. Goel, and Chatpan Chintanapakdee. December 2001.

PEER 2001/15 *Damage to Bridges during the 2001 Nisqually Earthquake.* R. Tyler Ranf, Marc O. Eberhard, and Michael P. Berry. November 2001.

PEER 2001/14 *Rocking Response of Equipment Anchored to a Base Foundation.* Nicos Makris and Cameron J. Black. September 2001.

PEER 2001/13 *Modeling Soil Liquefaction Hazards for Performance-Based Earthquake Engineering.* Steven L. Kramer and Ahmed-W. Elgamal. February 2001.

PEER 2001/12 *Development of Geotechnical Capabilities in OpenSees.* Boris Jeremić. September 2001.

PEER 2001/11 *Analytical and Experimental Study of Fiber-Reinforced Elastomeric Isolators*. James M. Kelly and Shakhzod M. Takhirov. September 2001.

PEER 2001/10 *Amplification Factors for Spectral Acceleration in Active Regions.* Jonathan P. Stewart, Andrew H. Liu, Yoojoong Choi, and Mehmet B. Baturay. December 2001.

PEER 2001/09 *Ground Motion Evaluation Procedures for Performance-Based Design.* Jonathan P. Stewart, Shyh-Jeng Chiou, Jonathan D. Bray, Robert W. Graves, Paul G. Somerville, and Norman A. Abrahamson. September 2001.

PEER 2001/08 *Experimental and Computational Evaluation of Reinforced Concrete Bridge Beam-Column Connections for Seismic Performance*. Clay J. Naito, Jack P. Moehle, and Khalid M. Mosalam. November 2001.

PEER 2001/07 *The Rocking Spectrum and the Shortcomings of Design Guidelines.* Nicos Makris and Dimitrios Konstantinidis. August 2001.

PEER 2001/06 *Development of an Electrical Substation Equipment Performance Database for Evaluation of Equipment Fragilities*. Thalia Agnanos. April 1999.

PEER 2001/05 *Stiffness Analysis of Fiber-Reinforced Elastomeric Isolators.* Hsiang-Chuan Tsai and James M. Kelly. May 2001.

PEER 2001/04 *Organizational and Societal Considerations for Performance-Based Earthquake Engineering.* Peter J. May. April 2001.

PEER 2001/03 *A Modal Pushover Analysis Procedure to Estimate Seismic Demands for Buildings: Theory and Preliminary Evaluation.* Anil K. Chopra and Rakesh K. Goel. January 2001.

PEER 2001/02 *Seismic Response Analysis of Highway Overcrossings Including Soil-Structure Interaction.* Jian Zhang and Nicos Makris. March 2001.

PEER 2001/01 *Experimental Study of Large Seismic Steel Beam-to-Column Connections.* Egor P. Popov and Shakhzod M. Takhirov. November 2000.

PEER 2000/10 *The Second U.S.-Japan Workshop on Performance-Based Earthquake Engineering Methodology for Reinforced Concrete Building Structures.* March 2000.

PEER 2000/09 *Structural Engineering Reconnaissance of the August 17, 1999 Earthquake: Kocaeli (Izmit), Turkey.* Halil Sezen, Kenneth J. Elwood, Andrew S. Whittaker, Khalid Mosalam, John J. Wallace, and John F. Stanton. December 2000.

PEER 2000/08 *Behavior of Reinforced Concrete Bridge Columns Having Varying Aspect Ratios and Varying Lengths of Confinement.* Anthony J. Calderone, Dawn E. Lehman, and Jack P. Moehle. January 2001.

PEER 2000/07 *Cover-Plate and Flange-Plate Reinforced Steel Moment-Resisting Connections.* Taejin Kim, Andrew S. Whittaker, Amir S. Gilani, Vitelmo V. Bertero, and Shakhzod M. Takhirov. September 2000.

PEER 2000/06 *Seismic Evaluation and Analysis of 230-kV Disconnect Switches.* Amir S. J. Gilani, Andrew S. Whittaker, Gregory L. Fenves, Chun-Hao Chen, Henry Ho, and Eric Fujisaki. July 2000.

PEER 2000/05 *Performance-Based Evaluation of Exterior Reinforced Concrete Building Joints for Seismic Excitation.* Chandra Clyde, Chris P. Pantelides, and Lawrence D. Reaveley. July 2000.

PEER 2000/04 *An Evaluation of Seismic Energy Demand: An Attenuation Approach.* Chung-Che Chou and Chia-Ming Uang. July 1999.

PEER 2000/03 *Framing Earthquake Retrofitting Decisions: The Case of Hillside Homes in Los Angeles.* Detlof von Winterfeldt, Nels Roselund, and Alicia Kitsuse. March 2000.

PEER 2000/02 *U.S.-Japan Workshop on the Effects of Near-Field Earthquake Shaking.* Andrew Whittaker, ed. July 2000.

PEER 2000/01 *Further Studies on Seismic Interaction in Interconnected Electrical Substation Equipment.* Armen Der Kiureghian, Kee-Jeung Hong, and Jerome L. Sackman. November 1999.

PEER 1999/14 *Seismic Evaluation and Retrofit of 230-kV Porcelain Transformer Bushings*. Amir S. Gilani, Andrew S. Whittaker, Gregory L. Fenves, and Eric Fujisaki. December 1999.

PEER 1999/13 *Building Vulnerability Studies: Modeling and Evaluation of Tilt-up and Steel Reinforced Concrete Buildings.* John W. Wallace, Jonathan P. Stewart, and Andrew S. Whittaker, editors. December 1999.

PEER 1999/12 *Rehabilitation of Nonductile RC Frame Building Using Encasement Plates and Energy-Dissipating Devices.* Mehrdad Sasani, Vitelmo V. Bertero, James C. Anderson. December 1999.

PEER 1999/11 *Performance Evaluation Database for Concrete Bridge Components and Systems under Simulated Seismic Loads.* Yael D. Hose and Frieder Seible. November 1999.

PEER 1999/10 *U.S.-Japan Workshop on Performance-Based Earthquake Engineering Methodology for Reinforced Concrete Building Structures.* December 1999.

PEER 1999/09 *Performance Improvement of Long Period Building Structures Subjected to Severe Pulse-Type Ground Motions*. James C. Anderson, Vitelmo V. Bertero, and Raul Bertero. October 1999.

PEER 1999/08 *Envelopes for Seismic Response Vectors.* Charles Menun and Armen Der Kiureghian. July 1999.

PEER 1999/07 *Documentation of Strengths and Weaknesses of Current Computer Analysis Methods for Seismic Performance of Reinforced Concrete Members.* William F. Cofer. November 1999.

PEER 1999/06 *Rocking Response and Overturning of Anchored Equipment under Seismic Excitations.* Nicos Makris and Jian Zhang. November 1999.

PEER 1999/05 *Seismic Evaluation of 550 kV Porcelain Transformer Bushings.* Amir S. Gilani, Andrew S. Whittaker, Gregory L. Fenves, and Eric Fujisaki. October 1999.

PEER 1999/04 *Adoption and Enforcement of Earthquake Risk-Reduction Measures.* Peter J. May, Raymond J. Burby, T. Jens Feeley, and Robert Wood.

PEER 1999/03 *Task 3 Characterization of Site Response General Site Categories.* Adrian Rodriguez-Marek, Jonathan D. Bray, and Norman Abrahamson. February 1999.

PEER 1999/02 *Capacity-Demand-Diagram Methods for Estimating Seismic Deformation of Inelastic Structures: SDF Systems*. Anil K. Chopra and Rakesh Goel. April 1999.

PEER 1999/01 *Interaction in Interconnected Electrical Substation Equipment Subjected to Earthquake Ground Motions.* Armen Der Kiureghian, Jerome L. Sackman, and Kee-Jeung Hong. February 1999.

PEER 1998/08 *Behavior and Failure Analysis of a Multiple-Frame Highway Bridge in the 1994 Northridge Earthquake.* Gregory L. Fenves and Michael Ellery. December 1998.

PEER 1998/07 *Empirical Evaluation of Inertial Soil-Structure Interaction Effects.* Jonathan P. Stewart, Raymond B. Seed, and Gregory L. Fenves. November 1998.

PEER 1998/06 *Effect of Damping Mechanisms on the Response of Seismic Isolated Structures.* Nicos Makris and Shih-Po Chang. November 1998.

PEER 1998/05 *Rocking Response and Overturning of Equipment under Horizontal Pulse-Type Motions.* Nicos Makris and Yiannis Roussos. October 1998.

PEER 1998/04 *Pacific Earthquake Engineering Research Invitational Workshop Proceedings, May 14–15, 1998: Defining the Links between Planning, Policy Analysis, Economics and Earthquake Engineering.* Mary Comerio and Peter Gordon. September 1998.

PEER 1998/03 *Repair/Upgrade Procedures for Welded Beam to Column Connections.* James C. Anderson and Xiaojing Duan. May 1998.

PEER 1998/02 *Seismic Evaluation of 196 kV Porcelain Transformer Bushings.* Amir S. Gilani, Juan W. Chavez, Gregory L. Fenves, and Andrew S. Whittaker. May 1998.

PEER 1998/01 *Seismic Performance of Well-Confined Concrete Bridge Columns.* Dawn E. Lehman and Jack P. Moehle. December 2000.

ONLINE PEER REPORTS

The following PEER reports are available by Internet only at http://peer.berkeley.edu/publications/peer_reports_complete.html.

PEER 2012/103 *Performance-Based Seismic Demand Assessment of Concentrically Braced Steel Frame Buildings.* Chui-Hsin Chen and Stephen A. Mahin. December 2012.

PEER 2012/102 *Procedure to Restart an Interrupted Hybrid Simulation: Addendum to PEER Report 2010/103.* Vesna Terzic and Bozidar Stojadinovic. October 2012.

PEER 2012/101 *Mechanics of Fiber Reinforced Bearings.* James M. Kelly and Andrea Calabrese. February 2012.

PEER 2011/107 *Nonlinear Site Response and Seismic Compression at Vertical Array Strongly Shaken by 2007 Niigata-ken Chuetsu-oki Earthquake.* Eric Yee, Jonathan P. Stewart, and Kohji Tokimatsu. December 2011.

PEER 2011/106 *Self Compacting Hybrid Fiber Reinforced Concrete Composites for Bridge Columns.* Pardeep Kumar, Gabriel Jen, William Trono, Marios Panagiotou, and Claudia Ostertag. September 2011.

PEER 2011/105 *Stochastic Dynamic Analysis of Bridges Subjected to Spacially Varying Ground Motions.* Katerina Konakli and Armen Der Kiureghian. August 2011.

PEER 2011/104 *Design and Instrumentation of the 2010 E-Defense Four-Story Reinforced Concrete and Post-Tensioned Concrete Buildings.* Takuya Nagae, Kenichi Tahara, Taizo Matsumori, Hitoshi Shiohara, Toshimi Kabeyasawa, Susumu Kono, Minehiro Nishiyama (Japanese Research Team) and John Wallace, Wassim Ghannoum, Jack Moehle, Richard Sause, Wesley Keller, Zeynep Tuna (U.S. Research Team). June 2011.

PEER 2011/103 *In-Situ Monitoring of the Force Output of Fluid Dampers: Experimental Investigation.* Dimitrios Konstantinidis, James M. Kelly, and Nicos Makris. April 2011.

PEER 2011/102 *Ground-motion prediction equations 1964 - 2010.* John Douglas. April 2011.

PEER 2011/101 *Report of the Eighth Planning Meeting of NEES/E-Defense Collaborative Research on Earthquake Engineering.* Convened by the Hyogo Earthquake Engineering Research Center (NIED), NEES Consortium, Inc. February 2011.

PEER 2010/111 *Modeling and Acceptance Criteria for Seismic Design and Analysis of Tall Buildings.* Task 7 Report for the Tall Buildings Initiative - Published jointly by the Applied Technology Council. October 2010.

PEER 2010/110 *Seismic Performance Assessment and Probabilistic Repair Cost Analysis of Precast Concrete Cladding Systems for Multistory Buildlings.* Jeffrey P. Hunt and Božidar Stojadinovic. November 2010.

PEER 2010/109 *Report of the Seventh Joint Planning Meeting of NEES/E-Defense Collaboration on Earthquake Engineering. Held at the E-Defense, Miki, and Shin-Kobe, Japan, September 18–19, 2009.* August 2010.

PEER 2010/108 *Probabilistic Tsunami Hazard in California.* Hong Kie Thio, Paul Somerville, and Jascha Polet, preparers. October 2010.

PEER 2010/107 *Performance and Reliability of Exposed Column Base Plate Connections for Steel Moment-Resisting Frames.* Ady Aviram, Božidar Stojadinovic, and Armen Der Kiureghian. August 2010.

PEER 2010/106 *Verification of Probabilistic Seismic Hazard Analysis Computer Programs.* Patricia Thomas, Ivan Wong, and Norman Abrahamson. May 2010.

PEER 2010/105 *Structural Engineering Reconnaissance of the April 6, 2009, Abruzzo, Italy, Earthquake, and Lessons Learned.* M. Selim Günay and Khalid M. Mosalam. April 2010.

PEER 2010/104 *Simulating the Inelastic Seismic Behavior of Steel Braced Frames, Including the Effects of Low-Cycle Fatigue.* Yuli Huang and Stephen A. Mahin. April 2010.

PEER 2010/103 *Post-Earthquake Traffic Capacity of Modern Bridges in California.* Vesna Terzic and Božidar Stojadinović. March 2010.

PEER 2010/102 *Analysis of Cumulative Absolute Velocity (CAV) and JMA Instrumental Seismic Intensity (I_{JMA}) Using the PEER–NGA Strong Motion Database.* Kenneth W. Campbell and Yousef Bozorgnia. February 2010.

PEER 2010/101 *Rocking Response of Bridges on Shallow Foundations.* Jose A. Ugalde, Bruce L. Kutter, and Boris Jeremic. April 2010.

PEER 2009/109 *Simulation and Performance-Based Earthquake Engineering Assessment of Self-Centering Post-Tensioned Concrete Bridge Systems.* Won K. Lee and Sarah L. Billington. December 2009.

PEER 2009/108 *PEER Lifelines Geotechnical Virtual Data Center.* J. Carl Stepp, Daniel J. Ponti, Loren L. Turner, Jennifer N. Swift, Sean Devlin, Yang Zhu, Jean Benoit, and John Bobbitt. September 2009.

PEER 2009/107 *Experimental and Computational Evaluation of Current and Innovative In-Span Hinge Details in Reinforced Concrete Box-Girder Bridges: Part 2: Post-Test Analysis and Design Recommendations.* Matias A. Hube and Khalid M. Mosalam. December 2009.

PEER 2009/106 *Shear Strength Models of Exterior Beam-Column Joints without Transverse Reinforcement.* Sangjoon Park and Khalid M. Mosalam. November 2009.

PEER 2009/105 *Reduced Uncertainty of Ground Motion Prediction Equations through Bayesian Variance Analysis.* Robb Eric S. Moss. November 2009.

PEER 2009/104 *Advanced Implementation of Hybrid Simulation.* Andreas H. Schellenberg, Stephen A. Mahin, Gregory L. Fenves. November 2009.

PEER 2009/103 *Performance Evaluation of Innovative Steel Braced Frames.* T. Y. Yang, Jack P. Moehle, and Božidar Stojadinovic. August 2009.

PEER 2009/102 *Reinvestigation of Liquefaction and Nonliquefaction Case Histories from the 1976 Tangshan Earthquake.* Robb Eric Moss, Robert E. Kayen, Liyuan Tong, Songyu Liu, Guojun Cai, and Jiaer Wu. August 2009.

PEER 2009/101 *Report of the First Joint Planning Meeting for the Second Phase of NEES/E-Defense Collaborative Research on Earthquake Engineering.* Stephen A. Mahin et al. July 2009.

PEER 2008/104 *Experimental and Analytical Study of the Seismic Performance of Retaining Structures.* Linda Al Atik and Nicholas Sitar. January 2009.

PEER 2008/103 *Experimental and Computational Evaluation of Current and Innovative In-Span Hinge Details in Reinforced Concrete Box-Girder Bridges. Part 1: Experimental Findings and Pre-Test Analysis.* Matias A. Hube and Khalid M. Mosalam. January 2009.

PEER 2008/102 *Modeling of Unreinforced Masonry Infill Walls Considering In-Plane and Out-of-Plane Interaction.* Stephen Kadysiewski and Khalid M. Mosalam. January 2009.

PEER 2008/101 *Seismic Performance Objectives for Tall Buildings.* William T. Holmes, Charles Kircher, William Petak, and Nabih Youssef. August 2008.

PEER 2007/101 *Generalized Hybrid Simulation Framework for Structural Systems Subjected to Seismic Loading.* Tarek Elkhoraibi and Khalid M. Mosalam. July 2007.

PEER 2007/100 *Seismic Evaluation of Reinforced Concrete Buildings Including Effects of Masonry Infill Walls.* Alidad Hashemi and Khalid M. Mosalam. July 2007.

The Pacific Earthquake Engineering Research Center (PEER) is a multi-institutional research and education center with headquarters at the University of California, Berkeley. Investigators from over 20 universities, several consulting companies, and researchers at various state and federal government agencies contribute to research programs focused on performance-based earthquake engineering.

These research programs aim to identify and reduce the risks from major earthquakes to life safety and to the economy by including research in a wide variety of disciplines including structural and geotechnical engineering, geology/seismology, lifelines, transportation, architecture, economics, risk management, and public policy.

PEER is supported by federal, state, local, and regional agencies, together with industry partners.

PEER Core Institutions:
University of California, Berkeley (Lead Institution)
California Institute of Technology
Oregon State University
Stanford University
University of California, Davis
University of California, Irvine
University of California, Los Angeles
University of California, San Diego
University of Southern California
University of Washington

PEER reports can be ordered at http://peer.berkeley.edu/publications/peer_reports.html or by contacting

Pacific Earthquake Engineering Research Center
University of California, Berkeley
325 Davis Hall, mail code 1792
Berkeley, CA 94720-1792
Tel: 510-642-3437
Fax: 510-642-1655
Email: peer_editor@berkeley.edu

ISSN 1547-0587X